University of Calgary

PRISM Repository **https://prism.ucalgary.ca**

The Vault Open Theses and Dissertations

2018-05-22

Using Flowband Modelling to Reconstruct Volume Change of Athabasca Glacier in the Canadian Rocky Mountains over the Last Millennium

Nath, Rituparna

Nath, R. (2018). Using Flowband Modelling to Reconstruct Volume Change of Athabasca Glacier in the Canadian Rocky Mountains over the Last Millennium (Master's thesis, University of Calgary, Calgary, Canada). Retrieved from https://prism.ucalgary.ca. doi:10.11575/PRISM/31942
http://hdl.handle.net/1880/106675
Downloaded from PRISM Repository, University of Calgary

UNIVERSITY OF CALGARY

Using Flowband Modelling to Reconstruct Volume Change of Athabasca Glacier in the Canadian Rocky Mountains over the Last Millennium

by

Rituparna Nath

A THESIS
SUBMITTED TO THE FACULTY OF GRADUATE STUDIES
IN PARTIAL FULFILMENT OF THE REQUIREMENTS FOR THE
DEGREE OF MASTER OF SCIENCE

GRADUATE PROGRAM IN GEOGRAPHY

CALGARY, ALBERTA

MAY, 2018

©Rituparna Nath, 2018

Abstract

Glaciers respond strongly to small climatic shifts, so records of historical glacier change can be used to reconstruct past climate. In turn, understanding glacier sensitivity to climate variability is important for regional water resource management and for projecting glacier response to ongoing climate change. We develop an enhanced flow-band model of glacier dynamics to simulate the past and future extent of glaciers in the Canadian Rocky Mountains, with the aim of coupling this model within larger scale regional climate models of glacier response to climate change. Longitudinal stress and valley shape factors are introduced to provide a more complete treatment of glacier dynamics. This presentation focuses on glacier volume reconstructions over the last millennium for Athabasca Glacier, Alberta, Canada, with a particular focus on glacier reconstructions in the Little Ice Age (LIA). Athabasca Glacier, located on the continental divide of the Canadian Rocky Mountains, is the second largest outlet of the Columbia Icefield. With the availability of SPOT 5 imagery, digital elevation models, and the ArcGIS Hydro tool, ice catchment properties, glacier width, and LIA moraines have been extracted using automated procedures. I model glacier thickness, volume, and mass change for different climate and glaciological parametrizations that give good reconstructions of LIA ice extent. Dated lateral and terminal moraines provide geological control on the LIA maximum glacier geometry. Mass balance modelling is based on observed temperature records from the region, along with the winter Pacific Decadal Oscillation index as a precipitation proxy. Reconstructions of glacier mass change inform estimates of meltwater runoff over the historical period, and model calibration from the LIA and 20th-century reconstructions will aid in future projections of the effects of climate change on glacier recession. Furthermore, the model developed will be effective for further future studies with ensembles of glaciers.

Acknowledgements

This work was supported by the Natural Sciences and Engineering Research council of Canada (NSERC) and Changing Cold Regions Network (CCRN).

I would like to thank you my advisor-cum-supervisor, Dr. Shawn Marshall, for providing me with the great opportunity to participate in the glaciology project and supporting me for every bit of the research. He taught me much about research, data assimilations, writing and also of the language of glaciology.

I would like to thank Dr. Gerald D. Osborn, one of my committee person, for every bit of knowledge building process about the research and the subject.

Thanks Myrka for being my committee person.

A special thanks to Dr. Brian Luckman, who helped me with his priceless advice about the tree ring based temperature reconstruction data.

I would like to thank my friend Suvajit for helping me with the understanding of the Matlab and working with it.

None the less, thanks to my loving and caring husband, Amitava for keeping me unending faith on me and for boosting my confidence every time I lose. Thanks Aniruddha (my son), for being a calm and cool kid.

Table of Content

Abstract ii
Acknowledgements iii
Table of Content iv
List of Figures vi
List of Tables x
Chapter 1: Introduction 1
1.1. Background 1
1.2. Scientific Rationale 2
1.3. Research Objective 5
1.4. Study Area 5
1.5. Thesis Organization 8
Chapter 2: Background and Literature Review 9
2. Introduction 9
2.1. Glaciers and Climate 9
2.1.1. Glacier Mass Balance 10
2.1.2. Surface Energy Balance and Feedback Mechanisms 12
2.2. Flow of a Glacier 13
2.2.1. Idealized Flow Patterns of a Valley Glacier 14
2.2.2. Stress and Strain 15
2.2.3. Internal Deformation 16
2.3. Numerical Glacier Modelling 17
2.4. Flowband Modelling and its Constitutive Equations 19
2.5. Flowline Modelling 20
2.5.1. Evolution of Flowline Modelling 20
2.5.2. Valley Geometry and Flowline Modelling 21
2.5.3. Conservation of Mass for Flowband Models 22
2.5.4. Ice Fluxes 23
2.5.5. Parameterization of Lateral Drag and Longitudinal Stress 24
2.5.6. Basal Sliding 25
2.6. Glacial Fluctuations 26
2.6.1. The Global Neoglacial Fluctuation 26
2.6.2. The Canadian Rockies Neoglacial Fluctuation 27
2.6.3. Neoglacial Fluctuation of Athabasca Glacier 27

Chapter 3: Methodology 29
3. Flowband Modelling for Glacier Volume Reconstruction 29
3.1. Datasets 29
3.1.1. Digital Elevation Model (DEM) 30
3.1.2. SPOT 5 Imagery 30
3.1.3. Sur[face Air Temperature and Precipitation 30
3.1.4. Peyto Glacier Mass Balance 33
3.1.5. Pacific Decadal Oscillation (PDO) 34
3.2. Glacier Model Inputs 38
3.2.1. Glacier Geometry 38
3.2.2. Central Flowline 38
3.2.3. Initial Ice Thickness 39
3.3. Data Preparation and Extraction 40
3.3.1. Deriving Glacier Boundaries 41
3.3.2. Central Flow Line (CFL) 49
3.4. Ice Thickness 55
Chapter 4: Results 56
4.1. Mass Balance Model 56
4.2. Multivariate Model of Regional Mass Balance 57
4.3 Climate Proxies for the Last Millennium 61
4.4. Ice Thickness 65
4.5. Creating an Initial Model 67
4.6. Transient Simulations of the Historical Athabasca Glacier Evolution 72
Chapter 5: Discussion and Recommendation 77
5.1. Summary of Research 77
5.2. Evaluation of the method 77
5.3. Evaluation of Results 78
5.4. Recommendations for Future Research 81
References 82

List of Figures

1. 1: Picture A was taken by Mary Schaffer, in 1906. Picture B was taken by Luckman in 1998. Both are taken from Sunwapta Pass. The arrows indicate the position of a LIA (early 1700s or mid-1800s) lateral moraine in both pictures. 3

1. 2: Location of Athabasca Glacier. Source: Google Maps..... 6

1. 3: A panoramic view showing the location of the Athabasca Glacier 7

1. 4: Location of Athabasca Glacier and Sunwapta Lake. 7

2. 1: Accumulation and ablation zones of a glacier, with the equilibrium-line 10

2. 2: Snow accumulation and ablation processes. 11

2. 3: An equilibrium line and equilibrium line altitude (ELA) on a glacier 12

2. 4: The energy budget of a typical glacier..... 13

2. 5: Diagram showing flow pattern of a typical glacier..... 14

2. 6: An aerial view of a glacier showing the pattern of ice movement. 14

2. 7: A cross-sectional view of a glacier, showing the pattern of glacier movement .. 14

2. 8: Shear experiment for a sample of polycrystalline ice. τ denotes the applied shear stress, γ the shear angle 16

2. 9: A flowchart showing the series of equation for flowband modelling..... 18

2. 10: Location of Canadian Rockies, from Heusser (1956)..... 27

3. 1: A Digital Elevation Model (DEM) showing the study area in clipped format.... 31

3. 2: A panchromatic SPOT 5 image showing the study area in clipped format. 32

3. 3: An aerial view showing the locations of Athabasca and Peyto Glacier 33

3. 4: Annual Mass Balance of Peyto Glacier, 1966-2010. 34

3. 5: The warm and cool phases of the Pacific Decadal Oscillation..... 35

3. 6 : A flow chart showing the steps involved in the model inputs. 38

3. 7: A flow chart showing steps involved in the watershed delineation..... 41

3. 8: An aerial view of glacier extent in 2009, along its centreline nodes. 42

3. 9: An aerial view of glacier extent in 1844, along its centreline nodes. 43

3. 10: A snapshot showing the output from the Fill Sinks tool in Arc Hydro. 44

3. 11: A snapshot showing the output from the Flow Direction tool in Arc Hydro. ...45

3. 12: A snapshot showing the output from the Flow Accumulation tool in Arc Hydro. 45

3. 13: A snapshot showing the output from the Stream Definition tool in Arc Hydro. 46

3. 14: A snapshot showing the output from the Stream to Feature tool in Arc Hydro.47

3. 15: A snapshot showing the output after performing Pour Point tool in Arc Hydro. 47

3. 16: A snapshot showing output from the Watershed Delineation tool in Arc Hydro. 48

3. 17: A snapshot of the output after editing and clipping the watershed boundary....49

3. 18: Creating skeleton of the watershed polygon. 50

3. 19: A snapshot showing the centreline (in pink) of the 2009 glacier boundary. 51

3. 20: A snapshot showing the centreline (in red) of the 1844 glacier boundary. 51

3. 21: A snapshot showing the nodes created along the Centreline. 52

3. 22: A snapshot showing the nodes and midpoints placed 25 m away within the boundary. Yellow dots are nodes, blue dots are midpoints between two nodes. 53

3. 23: A snapshot showing the contours lines at the nodes along the centreline. 53

3. 24: A snapshot showing the contours with elevation measurements in meters. 54

3. 25: A snapshot showing the contours lines, used for measuring the width. 54

4. 1: Net mass balance gradient on Peyto Glacier from 1966 to 2005.....56

4. 2: (a) Observed (black) and modelled (orange) mass balance at Peyto Glacier, using (b) Jasper summer (JJA) temperature and (c) the winter (DJFM) PDO index as predictor variables. 60

4. 3: Jasper summer (JJA) temperatures vs. tree-ring based temperature reconstructions from Luckman and Wilson (2006), for the period 1916-1998.....61

4. 4: Observed (orange) and tree-ring based (blue) summer temperatures in Jasper, 1916-1994. 62

4. 5: Luckman and Wilson (2006) summer temperature reconstruction in the Canadian Rocky Mountains. The anomalies in Luckman and Wilson (2006) are mapped onto mean observed summer (JJA) temperatures in Jasper from 1916-1998. 62

4. 6: Reconstructed mass balance at Athabasca Glacier for the period 1000-2017 AD, based on tree-ring based temperature estimates in the Canadian Rockies and PDO proxies prior to the 20th century. The period 1916-2017 is based on observed temperature and PDO indices. 63

4. 7: Reconstructed mass balance at Athabasca Glacier for the period 1844-2017 AD, based on tree-ring based temperature estimates in the Canadian Rockies and PDO proxies prior to the 20th century. The period 1916-2017 is based on observed temperature and PDO indices. 64

4. 8: Estimated Athabasca Glacier ice thickness along the centreline. The green line is from the classical theory of ice thickness, i.e. determined from the local surface slope, and the blue graph is from the Farinotti ice thickness model. 66

4. 9: Estimated bed topography of Athabasca Glacier. 66

4. 10: Modelled Athabasca Glacier 'spinup' simulation from the 2009 geometry (black) to an equilibrium state after 200 years (red line showing the maximum glacier extent). Ice thickness is plotted every 20 years. 68

4. 11: Modelled Athabasca Glacier bed (brown) and surface topography for 2009 (black) and the LIA equilibrium state (blue). 68

4. 12: Time series of modelled Athabasca Glacier evolution from 1650-2017. (a) Net annual mass balance (m w.e. yr^{-1}). (b) Annual glacier area (km^2) and volume ($10 \cdot km^3$). 73

4. 13: Modelled Athabasca Glacier Centerline transects at the end of the transient simulation (calendar year 2017). (a) Bed (brown) and surface (blue) topography. (b) Surface (blue) and basal (red) ice velocity. 73

4. 14: Ice thickness along the centreline of Athabasca Glacier based on the modelled present-day (2017) estimates (blue), the remote-sensing/Farinotti-based reconstructions (dark purple) and for the LIA equilibrium reconstruction (orange). 74

4. 15: Ice-thickness differences between the modelled present-day Athabasca Glacier (H_{2017}, red), the Little Ice Age equilibrium reconstruction (H_{LIA}, blue), and the remote-sensing/Farinotti-based reconstructions (H_0). 75

4. 16: Time series of modelled Athabasca Glacier evolution over the last millennium. Red lines show the glacier area (km^2) and dark purple lines plot glacier volume ($10 \cdot$

km^3), with the dashed lines from the 2009 initial model and solid lines from the Little Ice Age spinup. 75

List of Tables

2.1: The Shape factor for different cross-section of glacier valley. (γ is the aspect ratio, defined by the glacier half width / ice thickness at the centreline) 21

3.1: Impact of PDO-phases on climate elements. 36

4. 1: Correlation coefficients between net annual mass balance and different predictor variables at Peyto Glacier, 1966-2013. 58

4. 2: Multivariate regression statistics for the best model. 59

4. 3: Equilibrium reconstructions of Athabasca Glacier for different sliding speeds. The reference model is shown in bold, with v_s = 20 m/yr. 70

4. 4: Equilibrium reconstructions of Athabasca Glacier for different mass balance gradients. The reference model is shown in bold, with β = 5.73 mm w.e. m^{-1}. 70

4. 5: Equilibrium reconstructions of Athabasca Glacier for different equilibrium line altitudes. The reference model has an ELA of 2640 m. 71

Chapter 1: Introduction

1.1.Background

Glaciers are significant storage units for freshwater in mountain and polar regions. Mountain or alpine glaciers contain a very minute proportion of Earth's fresh water (about 1%) in comparison to the Antarctic and Greenland Ice Sheets (almost 99%), but their loss still proves to be significant for global sea level and regional water resources (Radic and Hock, 2011). The contribution of glacier melting to sea level rise is very much felt. The IPCC reports mention it and the Fifth Assessment Report did an elaborate study on deriving sea level equivalent rise due to the melting of glaciers (Vaughan, 2013). Along with this importance, glaciers affect day-to-day life for water supplies in the world's mountain regions. The balance between winter accumulation and summer melting, keeps the cycle continuing for the meltwater supply to downstream settlements.

Oerlemans (1989) mentioned that there are various ways in which glaciers respond to local and regional change of the climate, and this varies for changes in thickness, volume, shape and size, and hydrological factors. When a particular glacier is losing its size and volume and is probably retreating, it is necessary to estimate the volume loss over decades in order to understand how this change may be influencing water resources or sea level. This is the main motivation of my study: to track glacier volume change for a time period in the past, and to develop good modelling tools for making future projections. Looking into the moraine record (terminal and lateral), the outer boundary of a glacier can be drawn for a particular time period in the past. With the use of numerical glacier modelling, the year-to-year volume changes can be estimated.

Glacier melting, giving rise to rising sea levels, is one of the important aspects of the enhanced greenhouse effect that is driving present-day climate change (Oerlemans, 1989). At this time, when everybody is seriously talking about the problem of global warming and greenhouse gas emissions as its cause, sensitive indicators of such change play an important role. In particular, indicators that help to study past climatic variations are very much welcomed by researchers (Grove, 1988; Haeberli et al., 2000). This is one of the reasons why glacier fluctuations have been studied through the ages. It has

been more than one century that researchers are looking to understand the causes of glacier fluctuations. At the same time, they have found out that atmospheric warming from greenhouse gas emissions has aggravated glacial melting (Oerlemans et al., 1992; Marzeion et al., 2014; IPCC, 2014).

1.2.Scientific Rationale

Glaciers are a special source of freshwater for the downstream settlements for their daily household and commercial use. This source of freshwater is from summertime glacier melting, which includes both the seasonal snow and some of the underlying glacier ice. This local cycle of winter precipitation and summer melting need to be balanced, perpetually, for the glacier to remain healthy and sustainable. The problem is the degree to which this balanced cycle is affected and altered by recent changes in climate (Bitz and Battisti, 1999). These, in turn, are affecting rates of glacier retreat.

My particular study concentrates on Athabasca Glacier in the Canadian Rocky Mountains. The time period of retreat of Athabasca Glacier advance and retreat has been examined by Luckman (1988). Athabasca Glacier is very accessible via the Icefields Parkway that connects Lake Louise and Jasper, Alberta. It has been the site of extensive glaciological study, particularly during the 1960s (Paterson and Savage 1963; Savage and Paterson, 1963; Paterson, 1970, 1971, 1972; Raymond, 1971). More recent remote-sensing based studies of glacier change from Tennant and Menounos (2013) examine glacier area and volume change over several intervals from 1919-2009.

Going back in time, in 1896, Athabasca Glacier was first documented by W.B. Wilcox. This brought it into a quick limelight, in the way of climbing trips. Professor John Norman Collie, a British Scientist, mountaineer, and explorer accompanied by Hugh Stutfield climbed and explored the Canadian Rockies in 1897, 1898, 1900 and 1902 (Stutfield and Collie, 1903). They carried out several expeditions on Athabasca Glacier. The book published after their journeys gives us much light on the state of Athabasca Glacier at that time. Athabasca and Dome Glaciers were connected together somewhere near their terminus at that time. The authors also mentioned several unsuccessful attempts to take photographs, due to the poor weather conditions they confronted (Stutfield and Collie, 1903). Mary Schaffer, a nature-lover and a native of

Pennsylvania, was the first known person to photograph Athabasca Glacier from different aspects, in 1906, from Sunwapta Pass (Luckman et al., 1999). Luckman et al.

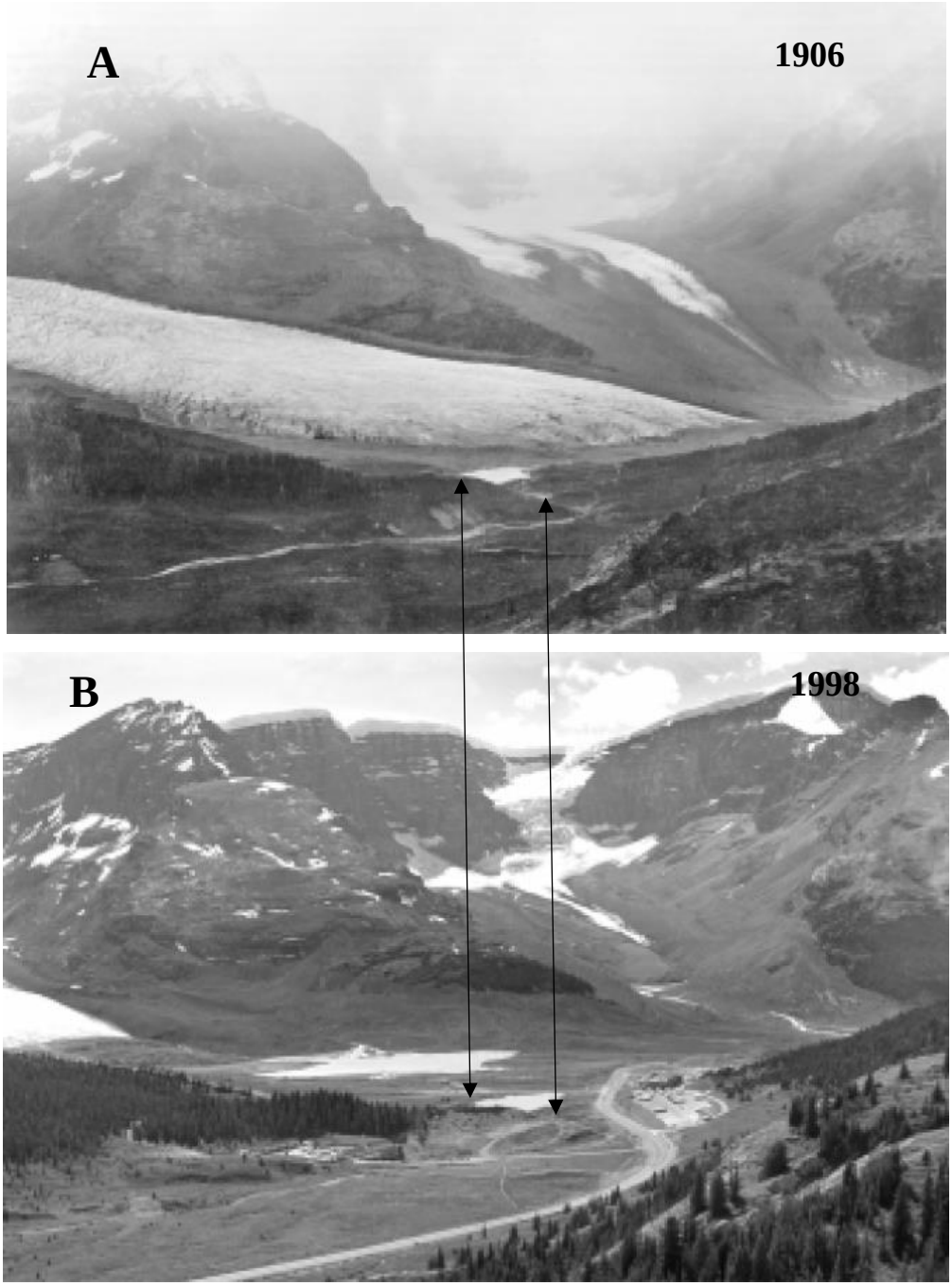

Figure 1. 1: Picture A was taken by Mary Schaffer, in 1906. Picture B was taken by Luckman in 1998. Both are taken from Sunwapta Pass. The arrows indicate the position of a LIA (early 1700s or mid-1800s) lateral moraine in both pictures.

(1999) figured out the locations from which Mary had taken the pictures in 1906. In 1998, Luckman shot similar pictures with similar exposures from the exact points, to document changes over the 92 years (figure 1.1).

In addition to the glacier's outstanding position and its accessibility, it offers remarkable glacial and glacial-geomorphological features. It is one of the best-studied glaciers in Canada, as concerns its glacial history. Heusser (1956) was the first to document the glacial history of the region, followed by Kucera (1972, 1981), Kite and Reid (1977), Luckman and Osborn (1988), and the notable work of Luckman (1986, 1988, 2000), Luckman et al. (1993, 1997) and Osborn et al. (2001).

The motivation for pursuing this study is to better understand glacier change, its relationship to climate change, and the three-dimensional view of glacier change that is not easily available from remote sensing images. My main contribution is to develop a glaciological flowband model which helps to simulate glacier flow and glacier response to climate change. As specific objectives, I wish to know the LIA volume of Athabasca Glacier and to understand area and volume changes of the glacier over the last millennium.

One of the applications of such a study is to attain the approximate volume of meltwater runoff into the Athabasca River, which will help further to determine the effects of continuous glacier recession (Marshall, 2014). Studies have been done to estimate the meteorological parameters which govern glacier runoff and contribute to streamflow (Hirose and Marshall, 2013), but such studies need a dynamic glacier model if they are to extend into the past or the future, to track changes in glacier geometry.

I hope to fill this gap with the help of numerical glacier modelling, with remote-sensing imagery used to generate the essential model datasets. The contribution to glacier and climate science is the development of a model for glacier response to climate variability and change that can capture the essential glacier physics but is simple enough to be applied to large ensemble of glaciers.

1.3.Research Objective

The primary research objective of my study is to develop and test a flowband model of glacier dynamics for Athabasca Glacier. This model can be used to reconstruct the glacier volume in the Little Ice Age or in the future, as a function of different climate scenarios.

1.4. Study Area

Athabasca Glacier (figure 1.2) is located at 52°12´N and 117°14´W, just east of the Alberta-British Columbia border, Canada, as it drains out from the Columbia Icefield. Athabasca Glacier is located within Jasper National Park of Canada, and is the only glacier of the icefield which is readily accessible by road – the Icefields Parkway. It is viewed each year by thousands of visitors from everywhere in the world (National Post, 2016). Athabasca Glacier flows between two mountain peaks, named Mt. Andromeda (3450 m) on the left and Snow Dome (3456 m) on the right in figure 1.3. The photograph also shows the outlet of Dome Glacier.

The papers of Paterson and Savage (1963a, 1963b, 1970) give excellent overviews of the morphology and dynamics of Athabasca Glacier. It is a typical 'isothermal' glacier like other glaciers of the Canadian Rockies, which means this glacier is at the melting point at all depths, save a thin near-surface layer that cools seasonally (Marshall and White, 2010). In winter the glacier develops a surficial crust a few metres thick which is temporarily chilled below freezing by conduction and outgoing radiation. In summer, this chilled layer is brought back to the melting point, largely by the refreezing of downward-percolating meltwater (Sharp, 1960). The outlet glacier has a smooth shape with a length of about 6 km, which covers an approximate area of 6.34 km^2 (Kucera and Henock, 1978).

Tennant et al. (2013) gives 3630 m to be the highest point of the icefield. In my study, the topmost elevation of the Athabasca drainage starts at 3483 m and flows more southwards and then bends to eastwards to 2068 m. The elevation of the ice surface at the glacier toe is 1920 m. Columbia Icefield holds the zone of accumulation of the glacier, whereas the outlet glacier holds its ablation zone below the third icefall. In between, roughly around the midpoint of the outlet glacier at an elevation of 2600 to

2700 m, above the highest ice fall, is the equilibrium line of altitude (ELA) (Paterson, 1964).

In the 1960s, the thickness of the outlet glacier ranged from 250 to 320 m along the centreline (Paterson, 1964). The average surface slope on the lower glacier is 3-4°. Savage and Paterson (1963) report a maximum velocity of 75 m yr^{-1}, beneath the icefall, and near the margin it was 15 m yr^{-1}. Meltwater runoff from the glacier feeds the immediate Sunwapta Lake, which is at the toe of the glacier. The river that originates from this lake flows northward, meeting Athabasca River which eventually joins the Mackenzie River and drains into the Arctic Ocean (Marshall, et al., 2011).

Figure 1. 2: Location of Athabasca Glacier. Source: Google Maps.

Figure 1. 3: A panoramic view showing the location of the Athabasca Glacier. Source: Self.

Most of the surface of the glacier is debris-free (figure 1.4), whereas the margins have exceptionally large amounts of debris. In Luckman et al. (1999), various photos taken around the glacier give a good representation of the glacier advance and retreat in the past. Luckman (1988) gives the date of the last advance of this particular glacier. In the era of Little Ice Age, AD 1840-44, this glacier reached about 1.5 km beyond its 2009 margin.

Figure 1. 4: Location of Athabasca Glacier and Sunwapta Lake. Source: Self.

Summary and Significance of Study area:

Athabasca Glacier is easily accessible and has attracted many climbers and explorers. Well- known explorers and avid climbers, Stutfield and Norman, traversed this glacier from around 1897 till 1902. In 1903, they presented to the world their experience of

climbing expeditions in Canadian Rockies in the form of a book. This book presents the early scenarios of the glacier through their story-telling. Athabasca Glacier at that time was stretched out to the present-day location of the Icefields Parkway.

The Athabasca Glacier, being one of the important and accessible outlets of Columbia Icefield, has also fascinated varied researchers and glaciologists (figure 1.4). Studies from glacier dynamics pattern by Paterson and Savage (1963a, 1963b) to glacier fluctuations by Luckman (1988), have helped to understand this glacier very well. At the same time, it lacks any proper GPR (ground-penetrating radar) survey to know its ice thickness, which could give a more accurate understanding of its volume and support more accurate glaciological modelling.

1.5. Thesis Organization

Chapter One of the thesis introduces the research.

Chapter Two presents the background of the study, including essential literature on glacier response to climate change, glacier dynamics, and the Little Ice Age (LIA) in the Rockies.

Chapter Three is comprised of the methodology of the research: data collection, data preparation, data processing, and data analysis.

Chapter Four contains the main results of the dataset and model development, and their application to simulations of Athabasca Glacier.

In Chapter 5 I discuss the results and make recommendations for further research.

Chapter 2: Background and Literature Review

2. Introduction

Alpine glaciers are one of the important indicators of climate change (Haeberli, 2003). Glaciers are retreating globally and this on-going process is working as an evident sign of global warming (Oerlemans, 1986, 1994, 2005). He further mentions that the retreat of glaciers over the last 100 years is consistent throughout the globe. Reports and observations of glacial retreat over the last few decades can be used to learn and understand more about past and present climate conditions (WGMS, 2012). Understanding of recent trends will help to visualize the future. Therefore, this thesis considers and connects the past, present, and future with a goal of better understanding of climate and glacier conditions in the Columbia Icefields area of Jasper National Park, Alberta.

In the Fifth Assessment Report (AR5) of the IPCC, Vaughan et al. (2013) estimates an approximate total number of 170,000 glaciers that are known worldwide, covering about 730,000 km^2 total area. Pfeffer et al. (2014) give an update to this, with a more complete glacier inventory estimating there to be about 200,000 glaciers. Glacier cover in Arctic and Western Canada comprises about 144,590 km^2 and 14,503 km^2 of area, respectively (Vaughan et al., 2013), with Canada having more glacier cover than any other country in the world after Greenland (Denmark).

2.1. Glaciers and Climate

Sharp (1960) notes that ‘glaciers are a progeny of climate’. They are solely dependent on different constituents of climate which control their health, size, degree of activity, and life span. The relationship between climate and glacier is not a simple one; rather it is complicated and varied, and should be handled properly with in-depth knowledge (Ahlmann, 1953). As glaciers grow in the climate, they keep indirect records of that climate (Ahlmann, 1953). This gives us insight into past climate based on the present observation. This motivates my research, and also relates to an important application of my study, the development of better models to predict how glaciers are likely to respond to changing climate in the future.

2.1.1. Glacier Mass Balance

Every glacier is formed of two main components – zones of accumulation and ablation. Accumulation is considered as an essential process of mass gain, through snowfall, whereas ablation is the process of removal of its mass (figure 2.1). Typically, the zone of accumulation lies on the upper portion of a glacier, which is a region of mass surplus ($b_n > 0$), and the zone of ablation is located at the bottom of the glacier, with mass deficit ($b_n < 0$), for net annual mass balance b_n (Cuffey and Paterson, 2010).

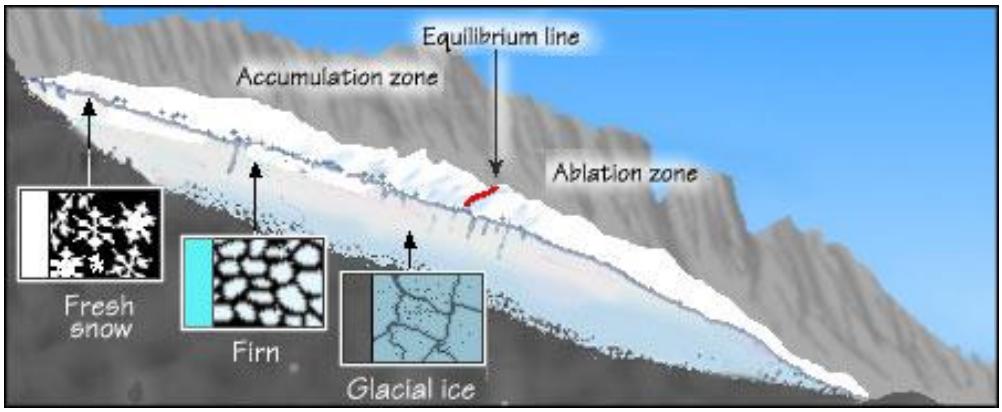

Figure 2. 1: Accumulation and ablation zones of a glacier, with the equilibrium-line. Source: www.glaciers.pdx.edu

Glacier mass balance is the rate of change of mass through time. It is calculated as the sum of accumulation (c) and ablation (a) (Hock, 2010).

$$b_n = c + a$$

This is sometimes written as the sum of the winter and summer mass balances, $b_n = b_w + b_s$ (Cogley et al., 2011), where ablation and summer mass balance are taken to be negative numbers (mass loss or glacier thinning). Mass balance for a point on a glacier is denoted as b_n, measured in metres water equivalent (m.w.e) per year, whereas overall glacier mass balance is often denoted B_n, and can be expressed through the rate of change of mass (kg yr^{-1}) or the glacier-averaged specific mass balance (m w.e. yr^{-1}). Net mass balance changes with elevation and location.

Mass balance decides a glacier's advance or retreat processes (Vaughan et al., 2013). A glacier that has a positive mass balance becomes more active, and it advances with increased mass and area. In contrast, when mass balance is negative a glacier loses ice

mass, becomes passive, and retreats (Cogley et al., 2011). This happens when summer ablation exceeds winter accumulation.

In the zone of accumulation, collection of snow occurs mainly by means of snowfall, wind drift, deposition of avalanches, and sometimes by means of rime, frost, or freezing of rain or meltwater in the snowpack (Paterson, 1981; Hock, 2010). At the same time, in the zone of ablation, removal of mass happens due to melting, sublimation, or wind, loss of ice by avalanches or ice falls, or by the calving of icebergs (Paterson, 1981; Cuffey and Paterson 2010) (figure 2.2). Oerlemans (2001) mentions that the preservation of accumulated snow is more important than the amount of snow the accumulation zone collects.

Dyurgerov and Meier (1997) investigated the mass balance of numerous small glaciers, in order to estimate the annual variation and determine their contribution to the sea level rise. They mention that the surface mass balance of a mountain glacier is usually calculated as a function of altitude:

$$b_n = [\sum b_n(z_i) \cdot s(z_i)] / S,$$

where, the sum is taken over the entire glacier, where b_n is the measured mass balance along the centreline at altitude z_i, i refers to the altitude range, S is the total area of the glacier, and $s(z_i)$ is the area-altitude distribution.

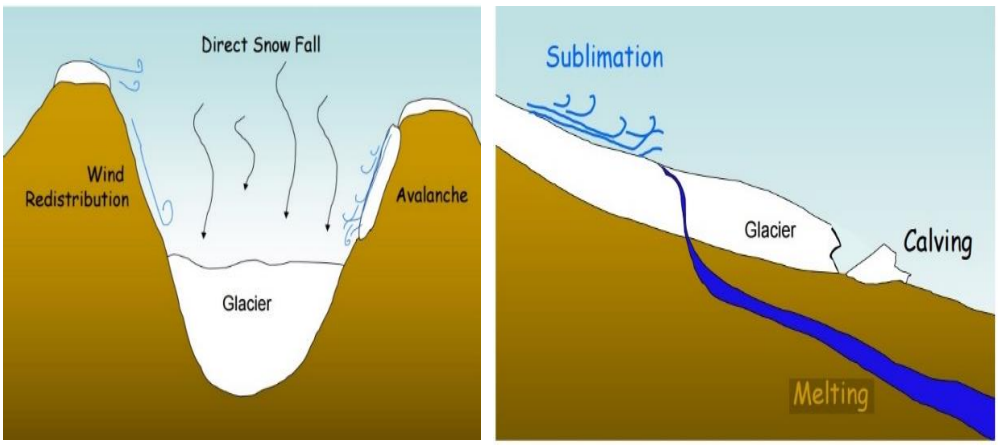

Figure 2. 2: Snow accumulation and ablation processes. Source: www.physicalgeography.net

The region where ablation equals accumulation, is termed the equilibrium line (EL), with the altitude here known as the Equilibrium Line Altitude (ELA), measured in metres (figure 2.3).

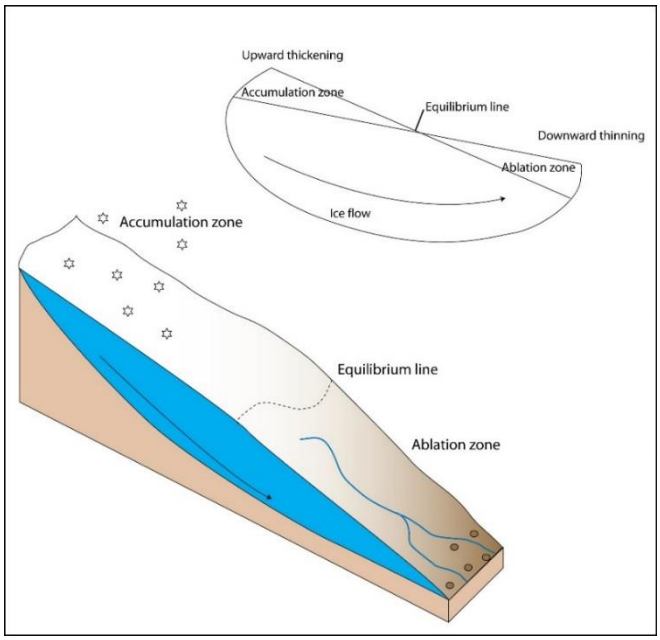

Figure 2. 3: An equilibrium line and equilibrium line altitude (ELA) on a glacier. Source: www.antarcticglaciers.org

The equilibrium line is controlled by temperature and precipitation as well as radiation fluxes (Cuffey and Paterson, 2010). Its location on every glacier differs and varies with the latitudinal and altitudinal location of the glacier itself. Generally, assuming the atmospheric temperature decreases with latitude, the equilibrium line rises for more equatorial latitudes.

2.1.2. Surface Energy Balance and Feedback Mechanisms

Surface energy balance is the balance between different energy fluxes, i.e., radiation, conduction, and turbulent heat exchange, at the glacier surface and the different layers of snow and ice below the surface. Glacier ice starts to melt when it reaches 0°C, if there is excess heat within the atmosphere and the surface energy balance is positive (Molg and Hardy, 2004; Cuffey and Paterson, 2010).

The main source of energy transfer to a glacier is the solar radiation, of which a certain fraction is absorbed into the glacier and the rest is reflected back (figure 2.4). This is known as albedo. Glacier albedo depends on the glacier surface cover. The range of

albedo values for different types of snow and ice surfaces is 0.2 to 0.8 (Shea et al., 2005). Old snow reflects less than the fresh snow; this means wherever the old snow is exposed, more energy is absorbed. This gives rise to an increase of snow grain size and lower albedo (Wiscombe and Warren, 1980; Oerlemans et al., 2009), such that there is a strong feedback of decreasing albedo through the summer melt season.

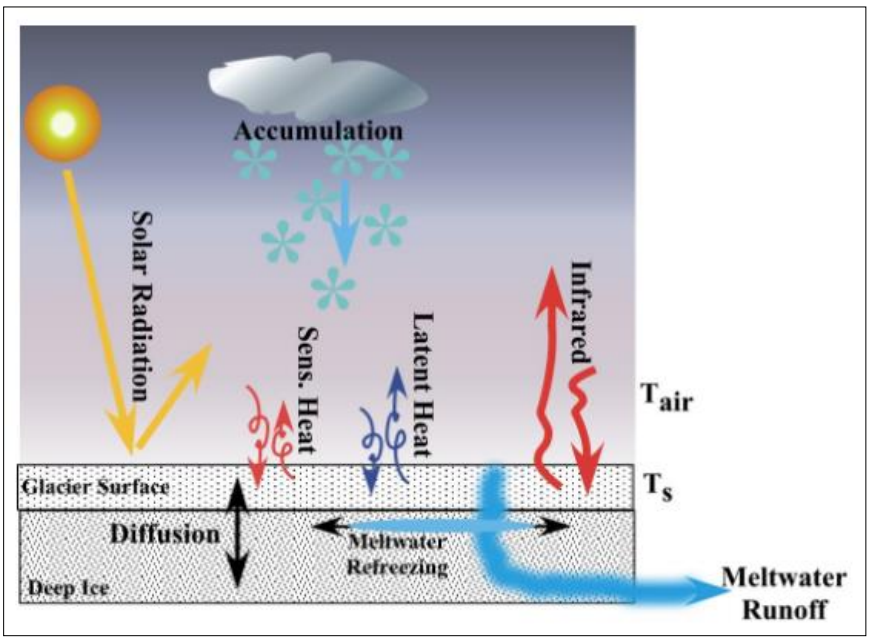

Figure 2. 4: The energy budget of a typical glacier.

Source: http://geosci.uchicago.edu/~rtp1/glaciers/EnergyBudget.html.

Glacier mass balance can be modelled through a full consideration of distributed snow accumulation and ablation processes, but in the absence of local meteorological data, more simple techniques are often used, such as assumption of a local mass balance gradients and ELA positions (Marshall et al., 2011).

2.2. Flow of a Glacier

Glaciers flow when the growing ice mass becomes too heavy to hold its rigid shape, and then it begins to flow by visco-plastic deformation (Duval et al., 2010), due to the gravitational force acting on it. Figure 2.5 shows a typical flow pattern of a glacier. By flowing downwards, glaciers transfer mass from the accumulation zone to the ablation zone.

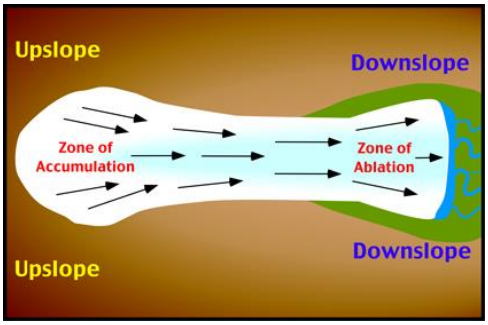

Figure 2. 5: Diagram showing flow pattern of a typical glacier.

Source: www.physicalgeography.net

2.2.1. Idealized Flow Patterns of a Valley Glacier

A glacier flows because of three basic mechanisms; deformation, sliding of ice over the bedrock, and deformation of the bed (Cuffey and Paterson, 2010). When seen from above, the middle part of the glacier moves with greater speed than the margins, due to the effect of friction from the valley walls (Figure 2.6).

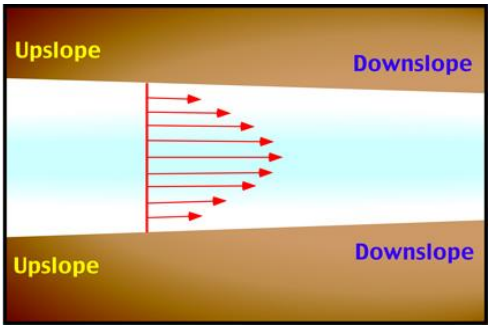

Figure 2. 6: An aerial view of a glacier showing the pattern of ice movement.

Source: www.physicalgeography.net

The cross-sectional motion of the glacier shows that the highest flow rates are in the upper glacier. This is again due to the frictional force, but at the bed (Figure 2.7).

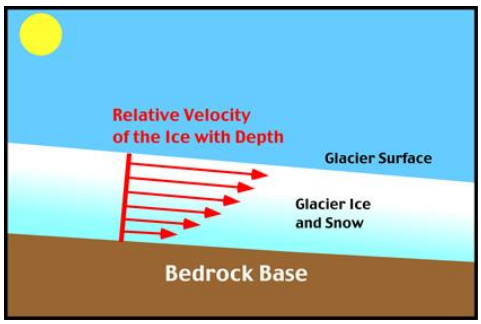

Figure 2. 7: A cross-sectional view of a glacier, showing the pattern of glacier movement. Source: www.physicalgeography.net

2.2.2. Stress and Strain

Stress in a glacier is a function of the mass of glacier ice and gravitational force acting on it (Paterson, 1981). It is the measurement of force over an area, with units Pascal (1 Pa = 1 N m^{-2}) (Benn and Evans, 1998). Strain is the 'deformation of a solid due to stress'. It measures the amount of deformation that happens as a result of the stress. Stress can be divided into 'normal and 'shear' stress.

The dominant *normal stress* (σ) in glaciers, due to gravity, is the component which is perpendicular to basal plane. It is expressed as,

$$\sigma_{zz} = \rho_i g H,$$

where, σ_{zz} = normal stress (N/m^2), ρ_i= density of ice (~900 kg/m^2), g = acceleration due to gravity (9.81 m/s^2), and H = ice thickness. There is also a normal stress in the downglacier direction, σ_{xx}, which can be either tensile or compressive (Cuffey and Paterson, 2010). *Shear stress* (τ) is the stress parallel to the basal plane. The vertical shear stress can be expressed as the following:

$$\tau_{xz} = \rho_i g h(\sin\alpha)$$

where, τ_{xz} = shear stress, (N/m^2), ρ_i= density of ice(~900 kg/m^2), g = acceleration due to gravity (9.81 m/s^2), h = ice thickness and α = slope of the surface of ice (Cuffey and Paterson, 2010).

Strain rate ($\dot{\varepsilon}$) is defined as strain per unit time (Cuffey and Paterson, 2010). It is a measure of the deformation of a solid due the applied stress on it. For the study of glacier flow, we are concerned with the velocity field *v (x,y,z),* which describes the velocity of every particle in the glacier. At every point *(x,y,z),* the velocity field is expressed by the components (from now on *u,v,* and *w* are used to denote the components of the velocity vector) (Cuffey and Paterson, 2010) *: u (x, y, z), v (x, y, z), w (x, y, z),* or by v_i (x_1, x_2, x_3). Strain rate can be expressed as

$$\dot{\varepsilon} = \frac{L_{deformed} - L_{original}}{L_{original} . Time} = \frac{\Delta L}{L.t}$$

i.e., the change in length of the ice crystals over its original length in a given time. This naturally leads to ice velocity gradients as a representation of strain rates, e.g. $\dot{\varepsilon}_x = \frac{\partial u}{\partial x}$.

2.2.3. Internal Deformation

Internal deformation occurs as a result of strain in response to stress. This leads to deformation of the ice, leading to the displacement of mass. Resistance to strain depends on ice temperature, crystal structure, bed smoothness, impurities, water content, and other factors. Due to certain stresses acting on the glacier ice block, ice responds by viscous deformation or 'creep' (Figure 2.8). Applying stress on an ice block leads to permanent deformation – termed - 'creep' or 'viscous flow'. Creep or viscous flow is well-known for its dissipative nature. At about 1-3% of strain, an ice crystal becomes completely recrystallized (Cuffey and Paterson, 2010). Glen's flow law relates strain rates and stress, which forms the basis for glacier flow models.

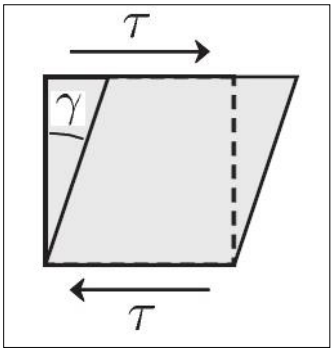

Figure 2. 8: Shear experiment for a sample of polycrystalline ice. τ denotes the applied shear stress, γ the shear angle. Source: Greve, 2009.

Glen (1952, 1955) introduced the expression relating stress to strain rate in glacier ice, and Nye (1957) modified Glen's results as a part of generalized flow law. Nye introduced normal stresses as σ_x, σ_y, σ_z; shear-stress components as τ_{xy}, τ_{yz}, τ_{zx}; and strain–rate components as $\dot{\varepsilon}_x$, $\dot{\varepsilon}_y$, $\dot{\varepsilon}_z$, $\dot{\varepsilon}_{xy}$, $\dot{\varepsilon}_{yz}$, $\dot{\varepsilon}_{zx}$ (Nye, 1957; Paterson, 1981).

Deviatoric Stress

The form of stress that is used for the flow law is the deviatoric stress. According to Glen (1958), the hydrostatic pressure does not drive the flow law; therefore, a new form of stress is involved here, the deviatoric stress. The stress tensor is divided into two components – mean stress and deviatoric stress. Deviatoric stress is calculated by substracting the mean or hydrostatic stress/pressure (σ_M) from each principal stress.

The mean stress is $\sigma_m = \frac{\sigma_{xx}+\sigma_{yy}+\sigma_{zz}}{3}$, whereas

deviatoric stress is $\tau = \begin{pmatrix} \sigma_{xx} - \sigma_M & \sigma_{xy} & \sigma_{xz} \\ \sigma_{xy} & \sigma_{yy} - \sigma_M & \sigma_{yz} \\ \sigma_{xz} & \sigma_{yz} & \sigma_{zz} - \sigma_M \end{pmatrix}$.

By definition, the normal component of the deviatoric stress($\tau_{xx} + \tau_{yy} + \tau_{zz}$) add to zero.

Glen's Flow Law

Glen's flow law describes how individual ice crystals deform in response to stress (Glen, 1955; Cuffey and Paterson, 2010). It is the way to describe ice deformation as a function of the stress field. This law considers ice as a nonlinear visco-plastic fluid (non-Newtonian fluid), where ice is an incompressible material. The flow law is expressed as:

$$\dot{\varepsilon} = A\tau^n$$

where, $\dot{\varepsilon}$ is the strain rate, τ is the stress, A is an ice stiffness coefficient related to ice temperature, and n = exponent with an average value of 3 (Nye, 1952). Therefore, strain rate in Glen's flow law is proportional to the stress cubed (Paterson, 1981).

2.3. Numerical Glacier Modelling

In glaciology, numerical modelling refers to the representation of real-world physical processes by a series of equations. These equations are solved to understand how the system will respond under different scenarios. Models are used to predict and to investigate the behaviour of ice under past and future environmental conditions. These numerical models differ from laboratory models, which are difficult to create for glaciers. Hence they are one of the best ways to describe the interrelationships between mass balance, ice dynamics and climate. Numerical glacier models help to quantify the sensitivity of valley/alpine glaciers to climate change (Oerlemans, 1998).

Numerical glacier modelling incorporates a combination of two fundamental processes. Firstly, models require an estimate of the mass balance of the glacier, which requires climate information. Glacier melt is commonly calculated through degree-day or energy balance models. Secondly, models compute flow of ice downslope under its own weight. Adhikari and Marshall (2011) stress the relevance of glaciological studies and

modelling. Glaciological studies are important from various perspectives, but my main application and interest is to better understand the relation between glaciers and climate.

There are different approaches to attaining climate information for glaciological models. Meteorological data can be measured at the site (Zhang, 2013), or different atmospheric models can be used to derive input data for glaciers (Tennant, 2012; Frey, 2014), local tree-ring or ice-core records can provide proxies for past evolution of climate (paleoclimate application) (Radic et al., 2007), or measurements can be collected from a distant glacier.

A simple flowchart is easy to follow the series of equations necessary to complete the flow band modelling (figure 2.9).

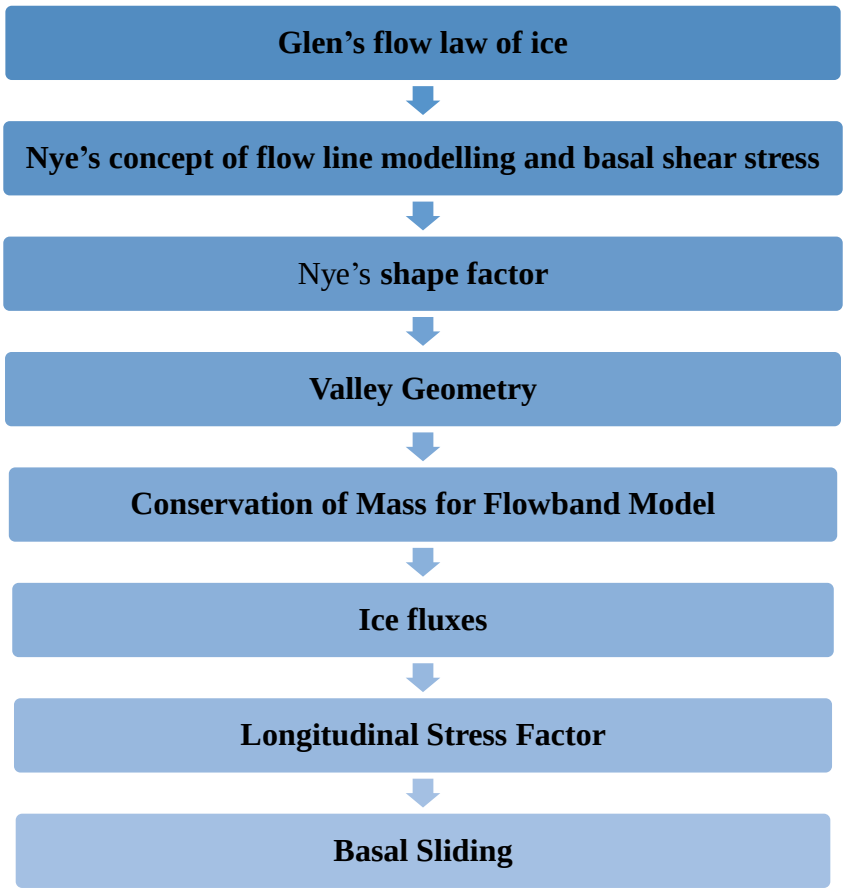

Figure 2. 9: A flowchart showing the series of equation for flowband modelling.

2.4. Flowband Modelling and its Constitutive Equations

Flowline and flowband models are important and well-known numerical techniques to represent the evolution of glaciers (Oerlemans, 1997b; Li, et al. 2011; Zhang, 2013). By the term 'flowline', glaciologists mean the virtual line or the path of the glacier along which the maximum amount of glacier flow occurs. The flowline generally closely coincides with the glacier centreline, although this depends on the local topography and ice thickness. Where bedrock information (subglacial valley morphology) is generally unknown, it is commonly assumed that the flowline is the same as the centreline. Flowband models are an extension of flowline models that account for spatially-varying glacier width; these can be thought of as 1.5D: lateral variations are included, but lateral flow is not modelled. The glacier is essentially divided into different elevation bands with specific elevations and widths, as is common in mass balance monitoring.

In general, there are three basic types of glacier models, which differ technically from each other along with their functionality and performance. One dimensional (1D) flowline or (1.5D) flowband model are 'depth integrated' because they average the processes of ice flow vertically in the ice column. Spatially distributed models discretize the whole glacier domain and include both downslope and lateral flow. There are widely used when the influence of regional topography is complex, as needed for icefields or ice caps. These require detailed knowledge of the subglacial topography, however. There are two types of spatially distributed model: 2-dimensional and 3-dimensional. Two-dimensional (2D) models are also termed 'isothermal', because they are depth-integrated models and they vertically average the processes of ice flow and temperature through the ice column (Plummer, 2003). Three-dimensional (3D) models- are depth-dependent, and they are used for ice dynamics studies where vertical structure is important (Pattyn, 2003). In this, the ice temperature is allowed to vary in the ice column, which affects the ease with which the ice deforms; this is important in polythermal glaciers and ice sheets.

Flowline models are well-known glacier dynamics models to simulate the evolution of alpine glaciers (Sujiyama, 2007). Radic et al (2007) acknowledge the works of Greuell (1992) and Oerlemans (1997a) for their respective work with flowline models in reconstructing glacier fluctuations. The classical flowline model of Oerlemans (1986)

considers simple shearing flow and basal sliding. The vertical mean ice velocity U is entirely determined by the local 'driving stress'τ, which is proportional to the ice thickness H and surface slope $\frac{dh}{dx}$ (h = surface elevation) (Oerlemans, 1997b).

2.5. Flowline Modelling

2.5.1. Evolution of Flowline Modelling

Paterson (1970) elaborated on Nye's (1952) work, and mentioned that Nye promoted the possibility of modelling glacier dynamics via numerical models. For a constant gravitational driving stress working on an infinitely wide glacier and for no-slip conditions (no basal flow), the basal shear stress is:

$$\tau_b = -\rho g H dh/dx \ .$$

This means that the basal shear stress equals the gravitational driving stress at the bed. Based on Glen's flow law, this stress can be related to strain rates in the ice. From this, Nye estimated the flow of ice along the glacier flowline, including the influence of different shapes of the valley cross-sections. He formulated equations for the steady rectilinear flow of ice along uniform channels including rectangular, semi-elliptical and parabolic cross-sections. To simplify modelling, he determined shape factors f_N for each idealized valley form (Nye 1952, 1965).

Nye's Shape Factor

Due to some support applied by the valley walls on the weight of the glacier, the amount of basal shear stress on the centreline is less than its value for a very wide channel. Nye introduced the equation $\tau_b = -f_N \rho g H \ dh/dx$ to describe lateral drag from the ice margins, where f_N is a shape factor varying from zero for an infinitely deep channel to unity for an infinitely wide channel (Waddington, 1981). The purpose of choosing a shape factor is the integration of the best approximation equation in Glen's flow law to give the correct downslope velocity at the glacier centreline (Paterson, 1981; Waddington, 1981). Nye presents values of the shape factor for a series of rectangular, elliptical and parabolic channels (Table 2.1). Here γ is the half-width divided by the ice thickness at the centreline: $\gamma = w/H$.

Table 2.1: The Shape factor for different cross-section of glacier valley. (γ is the aspect ratio, defined by the glacier half width / ice thickness at the centreline) Source: Nye, 1965.

γ	f_N		
	Rectangle	Ellipse	Parabola
	0	0	0
1	0.558	0.5	0.45
2	0.789	0.709	0.65
3	0.884	0.799	0.75
4	0.849	0.849	0.8
∞	1	1	1

Nye's model has been used by many glaciologists like Budd (1971), Waddington (1981); Paterson (1981); Oerlemans (1986), Huss (2012), and Zhang (2013). Oerlemans (1997b) Sujiyama (2007), Leclercq (2012) and Nuth (2013) have all studied the length change of a glacier over time using flowline models. Heid and Kaab (2012) and Melkonian (2013) studied velocity fields of a glacier in flowline models, and Kienholz et al. (2014) worked out on a new method to derive a glacier centreline.

2.5.2. Valley Geometry and Flowline Modelling

Glacier geometry means the area and width of the glacier, along with the shape and cross section of the glacier valley. Some studies have considered glacier valley shapes (Davis, 1900). Glaciologists and glacio-geomorphologists introduced the notion of an 'approximately parabolic' shape to glacier cross-sections (Svensson, 1959; Nye, 1965). Very first comment about the cross-section of a glacier valley, noting their U shape, was made by McGee (1883). Svensson (1959) was the first to employ the mathematical analysis on the cross-section of glacier, considering it to be a parabola.

The parabolic profile of the valley topography can be represented by the equation $b(y) = b_0 + ay^2$, where b_0 is the elevation at the centreline, $y = 0$, and $a = H/w^2$ is a parameter

that describes the valley shape. As the ice thins or thickens, the glacier width will also change, and the rates of change are linked:

$$\frac{\partial H}{\partial t} = 2aw\frac{\partial w}{\partial t},$$

or rearranging for purposes below,

$$\frac{\partial w}{\partial t} = \frac{1}{2aw}\frac{\partial H}{\partial t} = \frac{w}{2H}\frac{\partial H}{\partial t}.$$

The Nye (1965) shape factor for a parabola is a function of the ratio w/H. From Nye's tables, $w/H = 3$ gives $f_N = 0.75$, which is broadly representative of the main trunk of Athabasca Glacier; up on the plateau, the system is much wider and $f_N \sim 1$. It is also possible to let f_N vary for each node in the flowband model.

2.5.3. Conservation of Mass for Flowband Models

Conservation of mass is a fundamental concept in physics referring to 'the amount of mass remains constant as mass is neither created nor destroyed by any means' (Merriam-Webster, 2018). The evolution of glacier thickness with time is modelled through consideration of the conservation of mass: the final mass = original mass + mass added – mass removed. I divide the glacier length into a network of bands with a spacing of 50 m. Ice thickness and velocity are resolved along the glacier centreline with a 'node' in the centre of each flowband. Locally, i.e., at each node, conservation of mass is expressed:

$$\frac{dS}{dt} = -\frac{dQ}{dx} + 2wb,$$

where S is the cross-sectional ice area, t is the time in years, Q is the cross sectional ice flux at a certain node ($m^3\ yr^{-1}$), x is the distance along the flowline, with $x = 0$ at the top of the glacier, w is the glacier half-width, and b is the net annual specific mass balance at x. The first term is the change in cross-sectional ice area with time, the second term is the divergence of the ice flux, and the third term is the surface mass balance. Ice flux $Q = \bar{u}S$, where $\bar{u}$ is the average glacier velocity in the flowband cross-section. For a parabola, $S = 4Hw/3$ and the mass balance equation can be expanded as follows:

$$\frac{dS}{dt} = -\frac{d}{dx}(S\bar{u}) + 2wb$$

$$\frac{d}{dt}\left(\frac{4}{3}Hw\right) = -\frac{d}{dx}\left(\frac{4}{3}Hw\bar{u}\right) + 2wb$$

$$w\frac{dH}{dt} + H\frac{dw}{dt} = -\left(Hw\frac{du}{dx} + H\bar{u}\frac{dw}{dx} + w\bar{u}\frac{dH}{dx}\right) + \frac{3}{2}wb.$$

Dividing through by *w* and substituting the expression for *dw*/*dt* = ½ *w*/*H dH*/*dt*,

$$\frac{dH}{dt} = -\frac{2}{3}\left(H\frac{du}{dx} + \bar{u}\frac{dH}{dx} + \frac{H\bar{u}}{w}\frac{dw}{dx}\right) + b.$$

2.5.4. Ice Fluxes

It is possible to model glacier velocity as a function of the local geometry. Using Glen's flow law, the surface ice velocity can be estimated from

$$u_s = u_b + \frac{2A}{n+1}\,[\rho g dh/dx]^n\, H^{n+1},$$

where *A* is the ice effective viscosity, a function of ice temperature, u_b is basal sliding velocity, and *n* = 3 is Glen's flow law exponent. I use the flow law factor *A* is from Adhikari and Marshall (2012), based on an ice flow modelling at Athabasca Glacier.

The average velocity over the full valley cross section, $\bar{u}$, is less than u_s, as the bed of the glacier and the valley walls introduce friction and slow the flow. Ice flow or flux is simply calculated by multiplying the average velocity of glacier ice by area of the cross-section. It is then necessary to relate the surface velocity at the centreline, u_s, to the average cross-sectional velocity $\bar{u}$. The effects of lateral drag and longitudinal stress can be directly included in 3D models, or they can be estimated through geometric/form factors as a function of valley shape and slope (Nye, 1965; Adhikari and Marshall, 2011, 2012).

2.5.5. Parameterization of Lateral Drag and Longitudinal Stress

I adopt the concept of longitudinal stress (L) developed by Adhikari and Marshall (2011). They define L as a correction factor, in the spirit of Nye, which modifies the basal shear stress following:

$$\tau_b = L\rho g H dh/dx$$

The L-factor will help us the estimate the effects of longitudinal stress on glacier velocity. Both the shape factor (f_N) and longitudinal stress factor (L) act to modify the shear stress and scale the ice velocity accordingly:

$$\bar{u} = \left[u_b + \frac{2A}{n+1}\,[f_N L\rho g dh/dx]^n\, H^{n+1}\right].$$

I implicitly include the high-order stress effects on the basal velocity, as this is prescribed based on observations rather than as a function of gravitational driving stress; hence, u_b is not modified in this equation. The basal velocity u_b refers to the average rate of basal sliding across the glacier cross-section. L consists of two components – a deformational factor (L_d) and a sliding factor (L_s). Usually, L_d is calculated to understand the relationship between basal drag and driving stress. L_d is based on 'the correction factor required to produce the correct surface velocity'. Adhikari and Marshall gave some different values for different domains, among which they note that that L_d is less sensitive to aspect ratio than bedrock slope. They parameterize L_d from the average bed slope, $\alpha_b = db/dx$:

$$L_d = 1 - 0.18\alpha_b - 0.7\alpha_b^2.$$

The sliding contribution, L_s depends on the slip ratio, c, which has been defined as a ratio between sliding and deformational velocities, $c = u_b/u_d$. For a glacier with length L, with a sliding length l_s, having a uniform ice thickness, H, the horizontal extent of sliding, expressed through the ratio l_s/H, refers to length scale of regional influence of longitudinal stresses. In the case of Athabasca Glacier, I follow Adhikari and Marshall (2011) and assume that ls = 4 km and H = 200 m, so l_s/H = 20. Paterson (1970) inferred basal velocities of up to 32 m yr^{-1} and surface velocities reaching 70 m yr^{-1} for the lower reaches (4 km) of the valley glacier, from the base of the icefall to the terminus.

Sliding velocities decrease with ice thickness and distance down-glacier. On average for 14 points reported by Paterson (1970), the slip ratio $c = 1.9 \pm 1.7$, with a range from 0 to 5.2. An appropriate average value of L_s, according to Table 5 in Adhikari and Marshall (2011), would be ~1.4, decreasing to ~1.2 near in the lower part of the glacier.

2.5.6. Basal Sliding

Weertman (1957) was the first person to formulate a mathematical theory of glacial sliding and he mentioned the process of regelation as a mechanism for glacier sliding. Under its own weight and pressure of ice, the melting point temperature is reduced, which causes melting around bedrock obstacles. This same meltwater acts as a lubricant for the movement of glacier.

Basal sliding and bed deformation both takes place in a thin layer under the glacier ice, so glaciologists sometimes liked to refer to both together as 'basal motion'. The term 'slip' has been used by Cuffey and Paterson (2010) as a synonym to basal motion. Basal sliding is more effective under some special conditions. It depends on basal friction, which is a function of bed roughness and the distribution of water at the bed. A certain amount of basal shear stress (τ_b) is generated as a glacier slides over its bed at a rate u_b, which is expressed as follows:

$$\tau_b = \psi\, u_b,$$

where, ψ a drag factor. The slip relation [u_b (τ_b)] or sliding law is one of the most important problems in glacier motion. This sliding law is a relation between basal velocity (u_b), shear stress (τ_b), bed relief, and the presence of water and sediments. Cuffey and Paterson (2010) mention two vital aspects of sliding relations. The basal shear stress should be interpreted as the residual gravitational force, after the bed provides a counter-force to the glacier's flow. The slip relation $u_b(\tau_b)$ is related to basal friction and the basal drag is a result of the basal flow, not something which drives it. There are no reliable equations for this.

Savage and Paterson (1970) studied sliding velocity (u_b) of Athabasca glacier with the help of borehole measurements at two points, and they extrapolated that number with 12 more boreholes where they measured ice thickness and other parameters. Paterson measured the surface velocity from conventional survey methods, with sliding

velocities equal to 21 ± 11 m/yr and ranging from 0 to 32 m yr^{-1}. Hence we could prescribe a constant value of about 20 m yr^{-1}. Paterson (1970) observed no prominent relation between sliding velocity and the gravitational shear stress, but he did find a strong relation between sliding velocity and ice thickness. I also experiment with this dependence, allowing sliding rates to increase with ice thickness.

2.6. Glacial Fluctuations

Mountain glaciers have continued to fascinate readers and scientists to carry on scientific researches with their magnificent beauty and glory. Glaciers have a capacity of eroding material and leaving beautiful and spectacular landform features. The eroded material is partly deposited along the sides of the glacier, and also at the terminus in the form of moraines. These deposited moraines become visible and provide an idea about the particular glacier's historical width and length. Scientists have studied these records of past fluctuations, which ultimately prove to be helpful in the study of glacier dynamics as well as understanding past climate scenarios.

2.6.1. The Global Neoglacial Fluctuation

Fluctuation is the word commonly used with glacial activities of advancing or retreating (Cogley, 2009). Paterson (1981) mentions that individual glaciers do not respond the same way to climatic fluctuations, so it can be difficult to interpret glacier fluctuations. Oerlemans (1994, 2005) notes that for a mountain glacier, the response time to the climate forcing ranges from years to decades, as a function of the glacier geometry.

Manifestations of global glacial retreat in recent decades are found everywhere (Leclercq and Oerlemans, 2012). Though there is strong dissimilarity among the periods of glacier advance and retreat during the epoch of Holocene, general patterns in these records are found. Millennial trends of glacier fluctuations in the high and mid-latitudes of the northern hemisphere are similar (Leclercq and Oerlemans, 2012). The Holocene is the time period roughly between 10,000-12,000 years ago and the present day (Osborn and Luckman, 1988). It is an interglacial period which also includes the neoglacial period (Porter and Denton, 1967), with occasional periods of glacier advance. Matthes (1939) introduced the term "Little Ice Age" as an equivalent to the Neoglaciation time period. Records indicate that temperatures 4500 years ago were

lower than the Holocene thermal maximum, which marked the beginning of the LIA time period.

2.6.2. The Canadian Rockies Neoglacial Fluctuation

The Canadian Rockies, as shown in figure 2.10, are located in the southwestern Alberta and eastern British Columbia. They cover an area of 170,000 km^2 and are about 150 km wide, on an average. According to Bolch et al. (2010), from his inventory of glaciers in western Canada, there were a total of 17,595 glaciers in British Columbia and Alberta in 2005, covering an area of 26,728 km^2. About 5% of this ice is in the Canadian Rockies.

Luckman and Osborn (1979) studied the Holocene glacier fluctuations in the Canadian Rockies. Luckman (2000) mentioned that early 17th century to early 18th century experienced the largest glacier advances in the Neoglacial time period, followed by significant advances in the early to mid-19th century and then late 19th century to early 20th century.

Figure 2. 10: Location of Canadian Rockies, from Heusser (1956).

2.6.3. Neoglacial Fluctuation of Athabasca Glacier

Athabasca Glacier studies include notes taken by photographers like Mary Schaffer, reports in popular booklets (Kucera, 1978), and examination of terminal moraines (Heusser, 1956; Luckman, 1988). Schaffer's photographs taken in 1906 (Luckman, 1999) were the first to provide an idea about the glacier extent. Heusser (1956) was the

first person performing tree-ring dating of the moraines for Athabasca Glacier. He identified two time periods of glacier advance, which were the 1710s and the 1840s. Luckman has confirmed these periods and argued for the greatest advance to date to 1844, based on a tilted tree near the present-day visitor information centre.

Chapter 3: Methodology

3. Flowband Modelling for Glacier Volume Reconstruction

This chapter focus on the methods and techniques used to reconstruct the volume of the glacier. The purpose of this chapter is to discuss the details of the data sets and document the techniques used to develop the flowband model and historical climate forcing for Athabasca Glacier. The flowband model is a generalization of flowline modelling that allows for variable glacier width. It calculates the ice thickness and flow velocity of a glacier along the central flowline. The methods are physically based and simple to use. The chapter is divided into three sections: datasets, glacier model inputs, and the study area.

3.1. Datasets

The main datasets used for the extraction of model inputs are:

i) Digital Elevation Model (DEM), 18.5m by 18.5 m. Natural Resources Canada. Downloaded from GeoGratis extractor: (http://maps.canada.ca/czs/index-en.html)

ii) SPOT 5 imagery, Natural Resources Canada. Downloaded from GeoGratis, (http://ftp.geogratis.gc.ca/pub/nrcan_rncan/image/spot/geobase_orthoimages/s5_11707_5215_20090916/)

iii) Environment Canada Temperature and Precipitation Data for Jasper Weather Station (1916-2017) (http://climate.weather.gc.ca/historical_data/search_historic_data_e.html),

iv) Pacific Decadal Oscillation Index (PDO) (1900-2017),

v) Mass balance measurements of Peyto Glacier (1966-2017).

vi) Tree-ring based temperature reconstruction data (Luckman and Wilson, 2006), ftp://ftp.ncdc.noaa.gov/pub/data/paleo/treering/reconstructions/canada/icefields-summer-maxt.txt

vii) PDO proxy data (MacDonald and Case, 2005) ftp://ftp.ncdc.noaa.gov/pub/data/paleo/treering/reconstructions/pdo-macdonald2005.txt

3.1.1. Digital Elevation Model (DEM)

Input variables for the glacier geometry are needed to run the model. The main variables are glacier area, length, elevation, slope, and thickness (Nye, 1965). Digital elevation models (DEMs) offer a data source for most of these, without ice thickness. A digital elevation model (DEM) is a form of the digital model, also known as a three-dimensional representation of Earth's surface. It is a raster data-type, having X, Y dimensions as spatial coordinates, and Z dimension as elevation values (Lilisand et al., 2004; Longley, et al., 2005). I use Arc Map v.10.3.1 to derive glacier geometry based on a DEM (figure 3.1). The dimensions of the DEM are 18.25 m by 18.25 m., which was collected from the GeoGratis extractor (http://maps.canada.ca/czs/index-en.html) of open data.

Using Arc Hydro tool, a watershed was delineated using DEM, which gives the glacier boundary for the year 2009. The reason behind the use of this watershed delineation tool is because the upper portion of the glacier is embedded into the icefield which makes it hard to identify the upper boundary. The watershed delineation tool makes it easy to find and draw the actual watershed based.

3.1.2. SPOT 5 Imagery

Landsat and ASTER images (Kaab, et al., 2002) have been used extensively to map glacier cover. Pellikka and Rees (2010) studied various techniques of mapping and examining glaciers and their characteristics with the use of satellite images. The SPOT 5 image used here is a panchromatic one with the dimension of 10 m spatial resolution. The image was collected from the digital resources' database of the library of University of Calgary, also referred as SANDS (Spatial and Numeric Data Service). Figure 3.2 provides a screenshot of the image with an overlying boundary of the study area.

3.1.3. Surface Air Temperature and Precipitation

There is no continuous dataset of surface air temperature and precipitation from the Athabasca weather station, but the Jasper weather station has good records for 20th century climate conditions. Jasper is the closest station with long-term data. For surface air temperature, monthly mean temperatures are used for the study and for the precipitation, total precipitation is utilized. These datasets were extracted from the

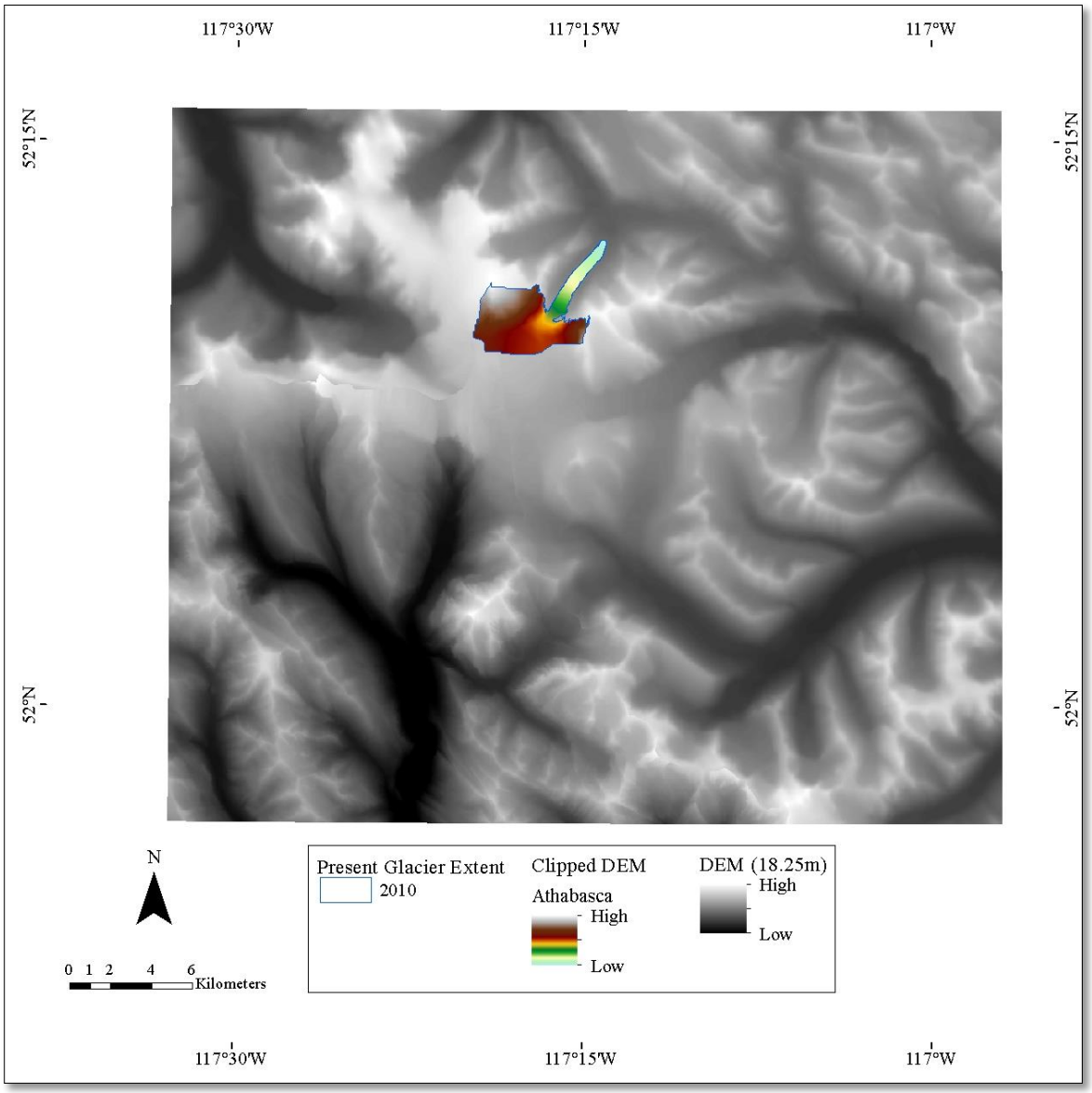

Figure 3. 1: A Digital Elevation Model (DEM) showing the study area in clipped format.

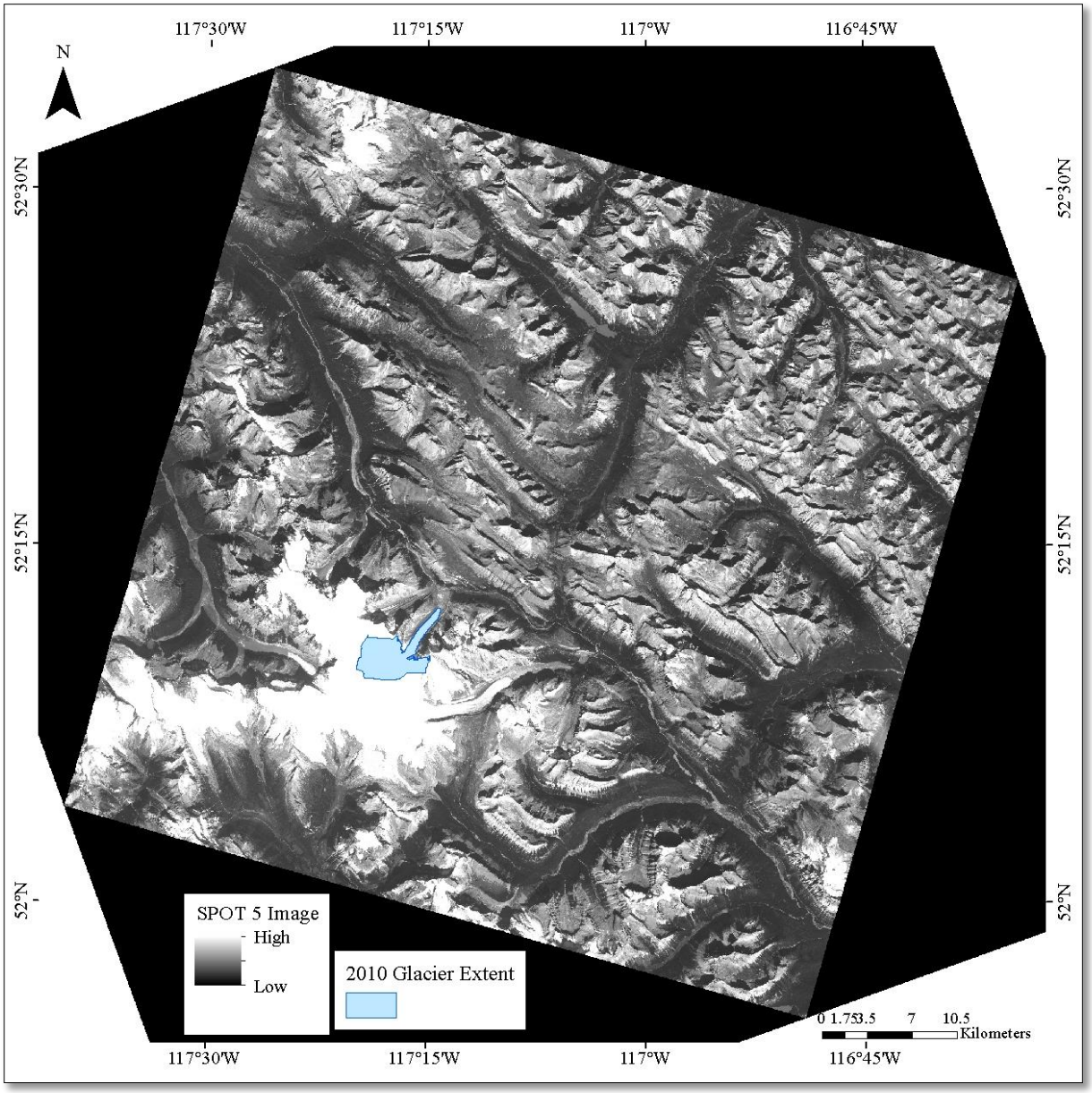

Figure 3. 2: A panchromatic SPOT 5 image showing the study area in clipped format.

Environment Canada website (http://climate.weather.gc.ca/historical_data/search_historic_data_e.html) for the period 1916–2017 for the Jasper weather station.

3.1.4. Peyto Glacier Mass Balance

Athabasca Glacier lacks mass balance measurements; thus, we have to rely on its nearest glacier which has similar weather conditions. Peyto Glacier is located ~88 km south-east of Athabasca Glacier (figure 3.3) and covers a similar elevation range, so is expected to have similar climatic conditions and influences.

Figure 3. 3: An aerial view showing the locations of Athabasca and Peyto Glacier. Source: Google.

Letreguilly (1988) notes that the Jasper climate records have a strong correlation with the Peyto Glacier mass balance series, confirmed with an additional two decades of data by Shea and Marshall (2007). This supports my assumption that both Jasper and Peyto are relevant to conditions at Athabasca, as it lies between these two sites.

Peyto Glacier mass balance measurements were obtained from the world glacier monitoring surface website (WGMS) (www.wgms.ch). The annual mass balance data of the glacier during 1966-2010 (Figure 3.4), was investigated by Demuth and compiled in the reports by Dyurgerov (2002) and WGMS bulletin (2013).

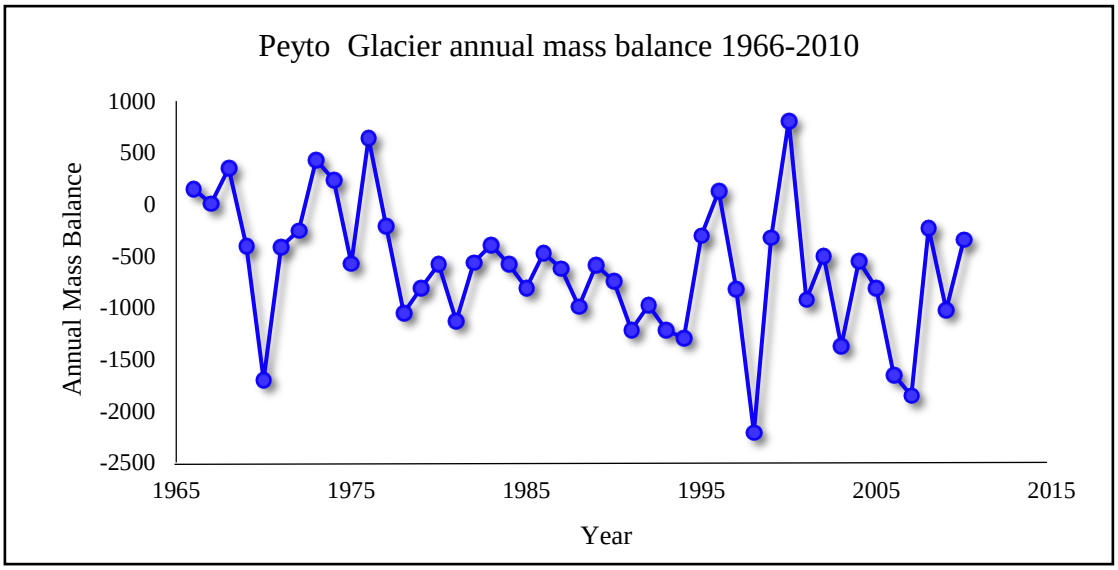

Figure 3. 4: Annual Mass Balance of Peyto Glacier, 1966-2010.

3.1.5. Pacific Decadal Oscillation (PDO)

A significant body of researchs examines the relationship between ocean-atmosphere circulation patterns and annual cycles of temperature, precipitation, glacier mass balance in the Canadian Rockies (Mantua et al., 1997; Shabbar, 1996, 1997; Zhang et al, 2000). El Nino Southern Oscillation (ENSO) and the Pacific Decadal Oscillation (PDO) are two such circulations which affect the atmospheric circulation, precipitation, and glacier mass balance in western North America. ENSO is a circulation pattern in the tropical Pacific which influences the position of the jet stream and storm tracks in southwestern Canada (Zhang et al, 1996). PDO is an ENSO-like mode of climate variability, with the PDO index developed by Hare (1996), Zhang et al. (1996), Mantua et al. (1997) and Mantua and Hare (2002). PDO also has warm and cool phases (Figure 3.5), but is longer-term variability and it more directly speaks to conditions in the North Pacific.

Gershunov and Barnett (1998) and Biondi et al. (2001) studied the relation between PDO and air temperature, precipitation, snowpack dynamics, glacier mass balance, and streamflow in the western U.S. The impact of PDO on western Canada is also well-studied and well-documented (Bitz and Battisti, 1998; Bonsal et al., 2001).

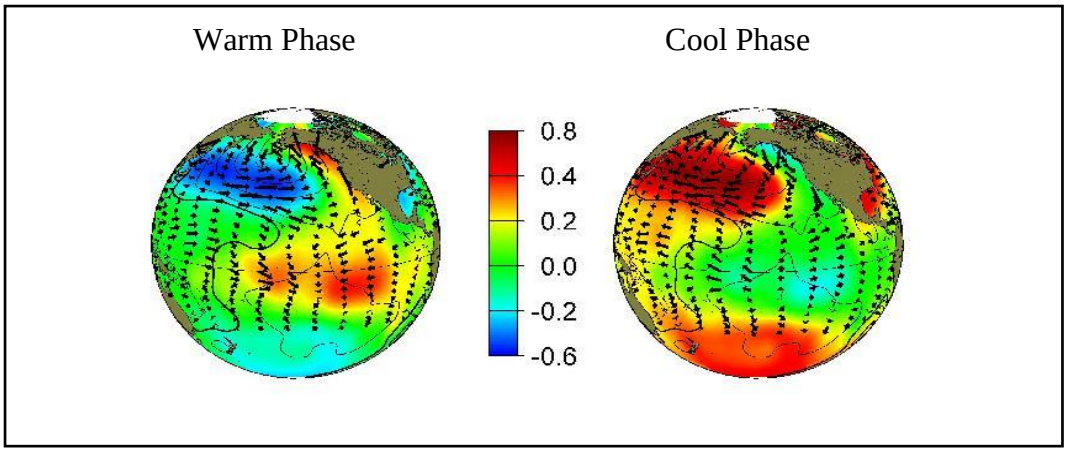

Figure 3. 5: The warm and cool phases of the Pacific Decadal Oscillation. Source: http://research.jisao.washington.edu/pdo/

Temperature: Bonsal et al (2001) studied the impacts of ENSO, PDO, and NAO on interannual winter temperature over Canada. They note that it is hard to separate the impacts of PDO from ENSO. It is known that PDO has more influence on western Canada, whereas combined PDO and ENSO influences extend further into central areas of Canada. In their study, it is mentioned that a strong winter response can be observed over western Canada whenever the ENSO phases (positive/negative) works in association with the PDO phase (positive/negative). Warm winters are associated with positive phases of PDO and ENSO (Bonsal et al., 2001). The summer impact is much weaker.

Winter Precipitation: Different studies have examined the link between winter precipitation and PDO in western Canada. Fleming et al. (2010) worked to understand the signals of ENSO and PDO and their impact on the glaciers of British Columbia, Yukon, and southern Alaska. Those regions receive less precipitation in the warm phases of PDO and ENSO.

Snow Accumulation and Melting: With the PDO phases, winter air temperature and precipitation fluctuate, which in turn affects snow accumulation and melting processes. Most of the studies undertaken in western North America (Rodenhuis et al., 2007; Mote, 2003; Hamlet et al., 2005) gives similar opinions about the effect of PDO on snowpack accumulation and melting. The warm phase of PDO brings lower snow

accumulation and in turn early snowmelt, giving an early disappearance of snow. This probably does not apply at the high elevations of the glaciers, but this is unknown.

Glacier Mass Balance: PDO-related changes in annual precipitation due appear to be correlated with glacier mass balance. Bitz and Battisti (1999) studied the relationship between the PDO index and glacier mass balance for southern British Columbia, finding a negative correlation between these two. At the same time, the low phase of the PDO is associated with abundant winter precipitation.

Streamflow: Streamflow and runoff systems in western Canada are also influenced by winter air temperature and precipitation. In the positive (warm) phase of PDO, there is less summertime runoff, associated with reduced snowpacks. The negative (cool) phase of PDO is associated with high levels of late spring and summer runoff. Table 3.1 sums up the impacts of PDO-phases on different elements of climate.

Table 3.1: Impact of PDO-phases on climate elements.

	PDO positive phase (warm)	PDO negative phase (cool)
Air Temperature	High	low
Winter Precipitation	Low	high
Snow Accumulation/Melting	low/early melt	high/late melt
Glacier Mass Balance	Low	high
Streamflow (summer)	Low	high
Streamflow (winter)	High	low

Tennant and Menounos (2013) studied the change in glaciers of Columbia Icefield from 1919-2009, and also note the correlation with PDO phase and regional climate. They agreed with other studies (Dyurgerov and Meier, 2000; Demuth et al., 2008), that air temperature and precipitation in the Canadian Rockies vary with the PDO phase, ultimately affecting glacier mass balance (Bitz and Battisti, 1999; McCabe and Fountain, 1995). This, in turn, affects streamflow and runoff patterns (Rood et al, 2005).

In order to find out which is the most predominant factor controlling the climate and mass balance in the Canadian Rockies, I analyze several possible climate variables, including Jasper station records of average summer (JJA) temperature (AST), average melt-season (MJJAS) temperature (AMST), and winter precipitation (WP), along with annual PDO (PDOA), and winter PDO (PDOW) indices. These are regressed against the observed mass balance record at Peyto Glacier for the period 1966-2017. Correlations and multivariate regressions were run. PDO data are taken from the website of the Joint Institute for the Study of the Atmosphere and Ocean (JISAO) at the University of Washington in Seattle (http://research.jisao.washington.edu/pdo/PDO.latest.txt).

Peyto Glacier mass balance data are from Dyurgerov (2002), with updates available at the World Glacier Monitoring Service (http:www.wgms.ch). The period of data collected was from 1966-2017. The average summer temperature (AST) for each year from 1966-2017 was calculated with mean monthly temperature (°C) for the months of June, July, and August, from the Environment Canada station data in Jasper. The average melt season temperature (AMST) was calculated for each year from 1966-2017 for May through September. Winter precipitation (WP) is calculated from the total precipitation for the span of nine months for every year in Jasper: September of the previous year through to May. Annual average and winter PDO indices were explored, with PDOW calculated using the average of the index from November to March.

After performing correlations, it was seen that the average summer temperature (AST) and PDO winter (PDOW) both significantly correlate with the annual net balance (b_n). This combination of functions touches on both winter and summer mass balance influences, and are logical predictor variables for the annual mass balance in the Rockies.

3.2. Glacier Model Inputs

The essential model inputs derived and used are (Figure 3.6):

- Glacier geometry;
- A central flow line (CFL);
    - Elevation,
    - Shape factor and glacier width
    - Surface slope,
- Initial ice thickness;
- Mass balance profile;

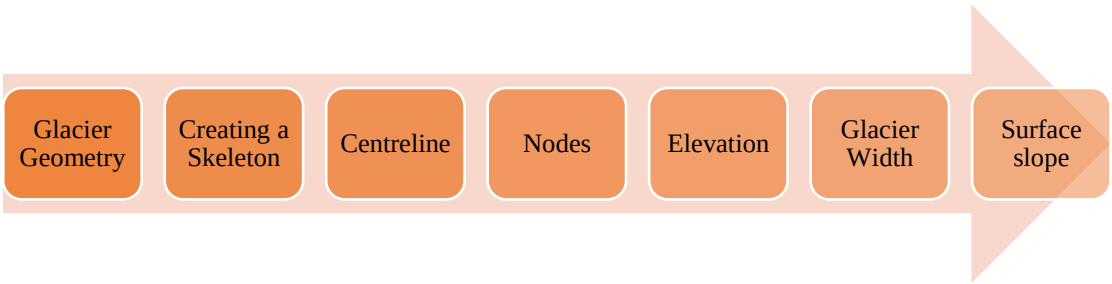

Figure 3. 6 : A flow chart showing the steps involved in the model inputs.

3.2.1. Glacier Geometry

Nye (1965) derived a numerical solution for the steady rectilinear flow of the ice, based on Glen's nonlinear flow law. His experiment was with three primary shape of the cross section: rectangular, semielliptical and parabolic. He defined and introduced a shape factor- *f* (section 2.6.1., table 2.1) which is a correction factor to include the effects of lateral stress, varying with the shape of the cross-section.

The flowband modelling performed in this research follows Nye's concept of cross-section and shape of a glacier valley. In this research, the location of the studied glacier is such that, it is connected with an icefield at the top end. The upper glacier is considered to have a rectangular cross section and the outlet valley is assumed to have a parabolic shape.

3.2.2. Central Flowline

A central flowline is a hypothetical line traversing the glacier from top to bottom. The central flowline is considered to have the maximum ice flow through that zone. It is not

necessary, in principle, for the central flow line to coincide with the central position of the glacier. It is the line which connects the nodes of maximum curvature on its surface contours, i.e. denoting the highest surface elevation in a lateral transect. The present-day Athabasca Glacier is about 9 km in length. I divided the central flow line into 181 equidistant segments, with Δx = 50 m.

Elevation of the glacier surface

As the model input elevation is another important parameter for flow line modelling. In this research, the elevation was derived from the DEM after deriving the contours at an interval of 50 m, based on the central node in each 50-m flow band.

Surface Slope

Along with the elevation of the glacier, I calculated and used the surface slope $\alpha = dh/dx$ for every node along the flow line.

3.2.3. Initial Ice Thickness

Glacial ice thickness is one of the important parameters for the study of glacier dynamics. Huss et al. (2008) stressed on the importance of studying ice thickness as it determines ice volume and flow, via Glen's flow law, while the underlying bedrock topography needs to be known to assess the hydrological characteristics of a glacierized basin. Estimation of ice thickness distribution is one of the foremost challenges for glaciological models (Hubbard et al., 1998; Bjornsson et al., 2006).

Well-known ice thickness measurement techniques include radio-echo sounding and borehole measurements (Zhang et al, 2013). The problem with these technique is their cost and logistical requirements. Radar surveys are very laborious and tedious, and at the same time are not viable for some rugged terrains. Volume-area scaling is the most simple and widely used method for the estimation of glacier volume (Chen and Ohmura, 1990; Bahr et al., 1997; Radic and Hock, 2010), although its validity to individual glaciers is arguable (Arendt et al., 2002). It also gives just a single value for glacier volume, not the distributed ice thickness.

Theoretical approaches to estimate ice thickness are also possible, based on local surface slope and an estimate of the basal shear stress (Mayer and Siegert, 2000; Cuffey and Paterson, 2010),

$$H = \tau_b/(\rho g dh/dx)$$

This equation has been used to estimate local ice thickness on valley glaciers as well as ice sheets, but the influences of lateral drag from valley side-walls, longitudinal stresses, and basal sliding are not taken into consideration (Huybrechts et al., 1989; Oerlemans, 1997b). One also needs to assume a value for the basal shear stress, which is typically taken to be 100 kPa, a rough result of the assumption of Glen's flow law in a no-slip condition (Nye, 1952; Cuffey and Paterson, 2010). An alternative to this approach was introduced by Farinotti et al. (2009), and is discussed further below.

3.3. Data Preparation and Extraction

Delineating the 2009 glacier extent

Digitization of the satellite image is the first step to delineate the 2009 glacier extent. This function was performed using ArcMap v10.3 software in addition to a SPOT 5 image (10-m resolution). The digitized area covers an approximate area of 15.33 km^2 (Figure 3.8). From the top, the glacier starts with an elevation of 3400 m, and it flows downslope in a southward direction. The average width of the glacier in the accumulation area of the icefield (above 2620 m) is about 3 km. It starts to narrow down at 2620 m, with a mean width of about 0.7 km. From such measurements it can be said that the upper portion of the glacier is not confined in a valley, so we approximate it to be rectangular in shape. The narrower part of the outlet glacier is channelized in a valley with steep side walls, more appropriately approximated as a parabola.

Delineating the 1844 glacier extent

Similar techniques were applied to derive the 1844 glacier extent, but based on the glacier moraines. The approximate area in the mid-1800s was 19.1 km^2 (Figure 3.9). A crucial problem was encountered while digitizing the 1844 glacier boundary, which gives some uncertainty. The problem was finding a proper boundary at the toe of the glacier. While digitizing with the help of SPOT 5 imagery this problem became

prominent. The lateral moraines were taken as the side boundary, while the vegetation trim lines at the toe were taken as the frontal boundary. Portions of the lateral moraines at the toe were either washed away or did not leave a clear lateral/terminal moraine, possibly due to the confluence with its neighbouring glacier (Dome) or due to construction of the icefield parkway (Luckman, 1988). Thereby, the continuation of the lateral moraine was disrupted. The extent of the lower outlet lobe was estimated in order to complete the boundary of the LIA glacier extent.

The width of the topmost boundary of the LIA glacier is the same as in 2009, 3 km. The average width of the main trunk of the LIA outlet glacier is measured to be 1.5 km, which is roughly twice the 2009 width.

3.3.1. Deriving Glacier Boundaries

The boundary of the glacier was determined by applying a Geographic Information System (GIS), using Arc Hydro tool for drainage extraction based on the DEM. Following are the steps and techniques followed to derive the glacier boundaries. A snapshot for each step is provided here for the reader's ease.

Watershed Delineation

All the functions explained in the later section, are parts of single tool, named 'watershed delineation'. In that tool, under the sub-tool terrain procession, all the functions are stacked. It follows the following format (figure 3.7):

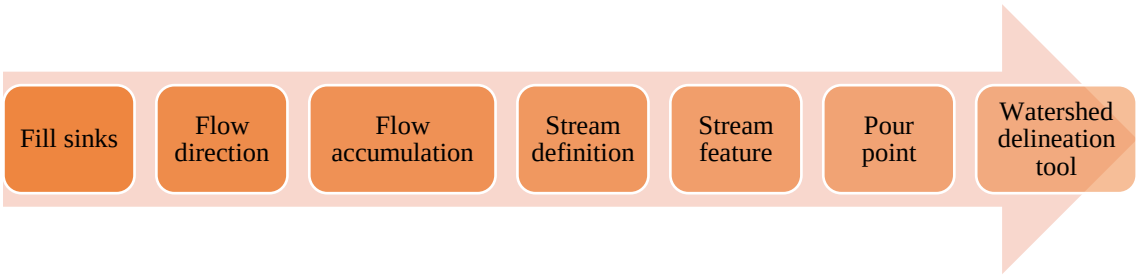

Figure 3. 7: A flow chart showing steps involved in the watershed delineation.

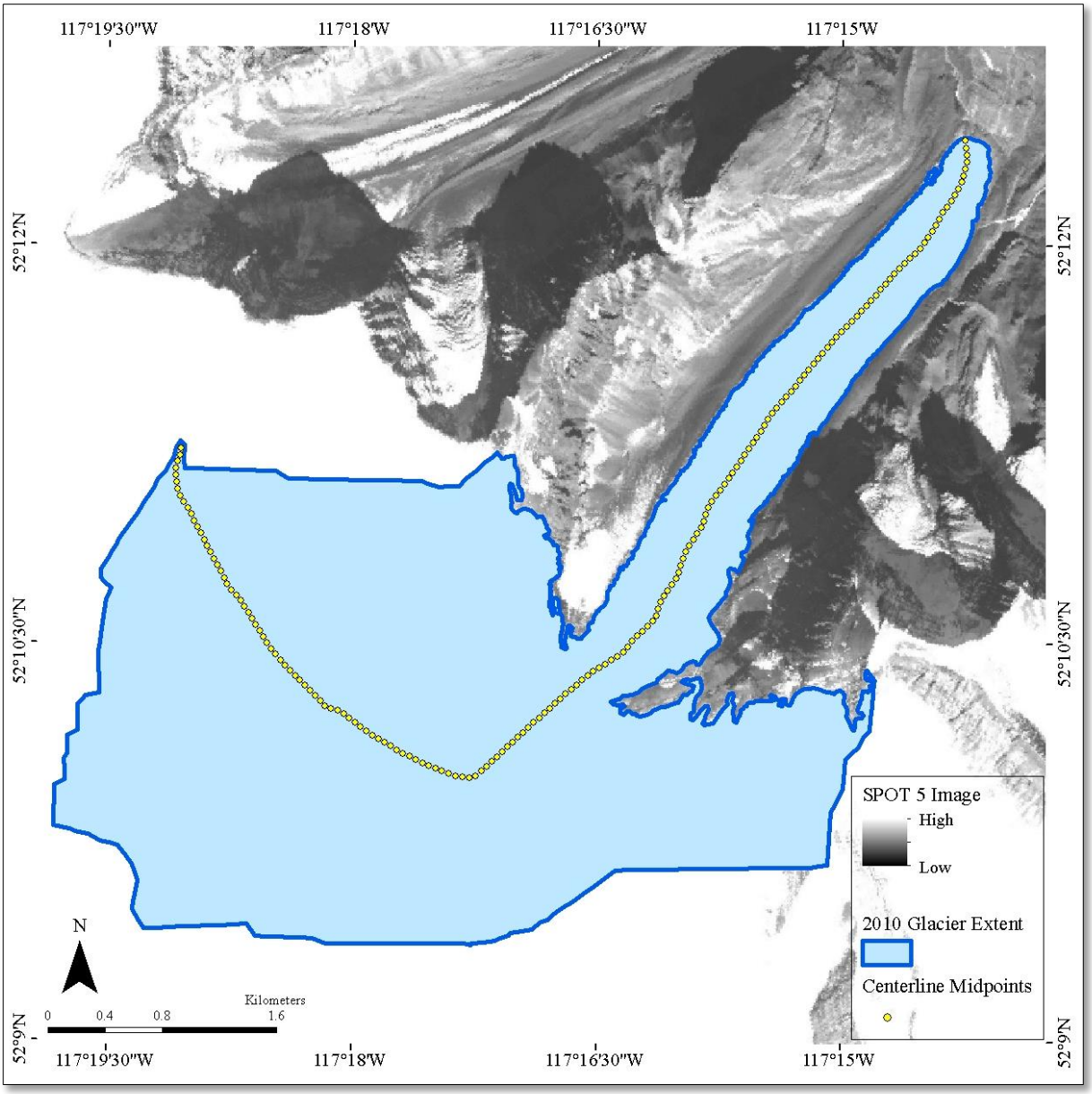

Figure 3. 8: An aerial view of glacier extent in 2009, along its centreline nodes.

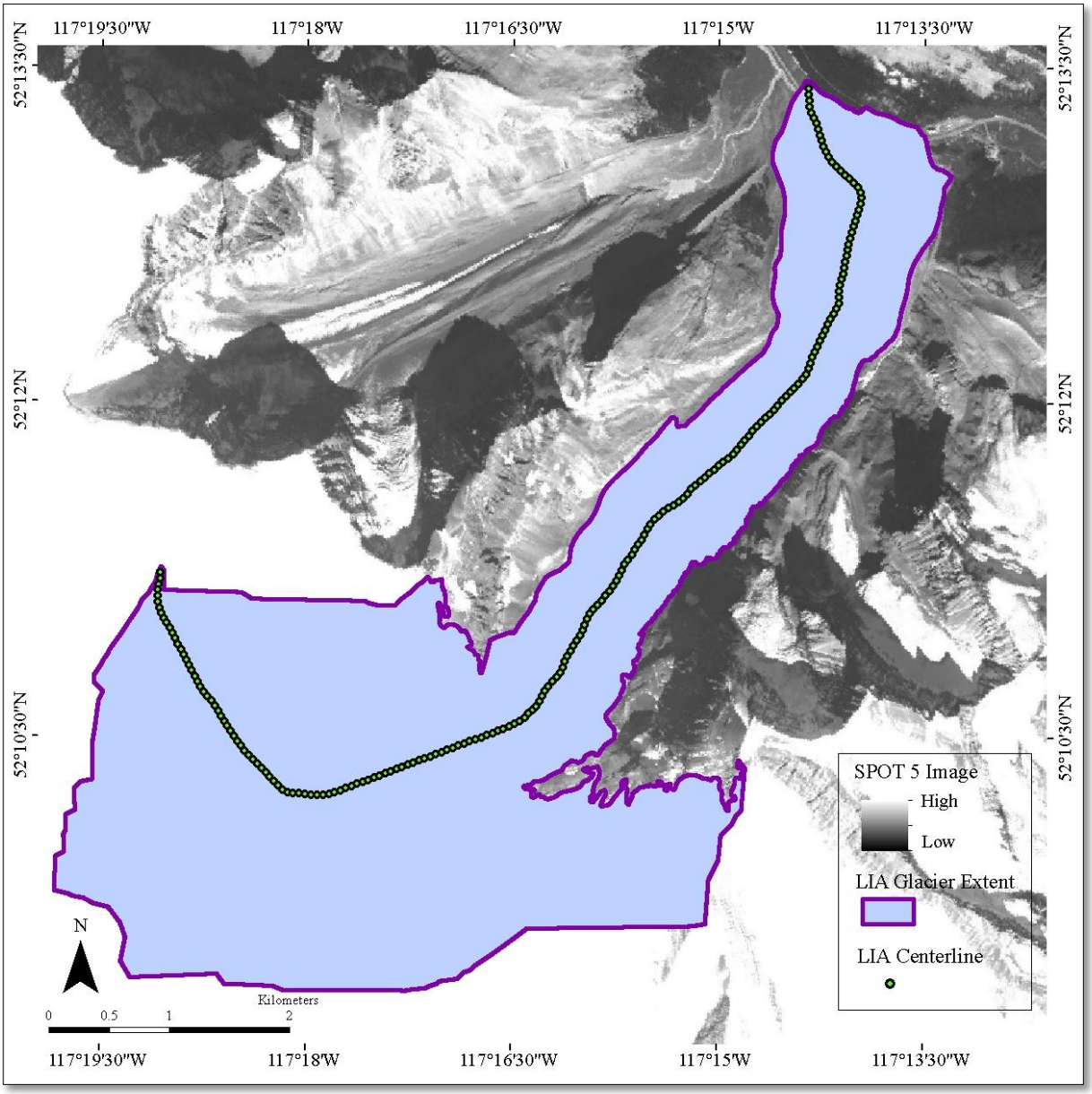

Figure 3. 9: An aerial view of glacier extent in 1844, along its centreline nodes.

Fill Sinks

The fill sink function helps to fill up the DEM. Artificial sinks which are not actually part of the image will get filled and gives a better quality digital elevation image, with very minor differences. Figure 3.10 gives a clear idea about the operation.

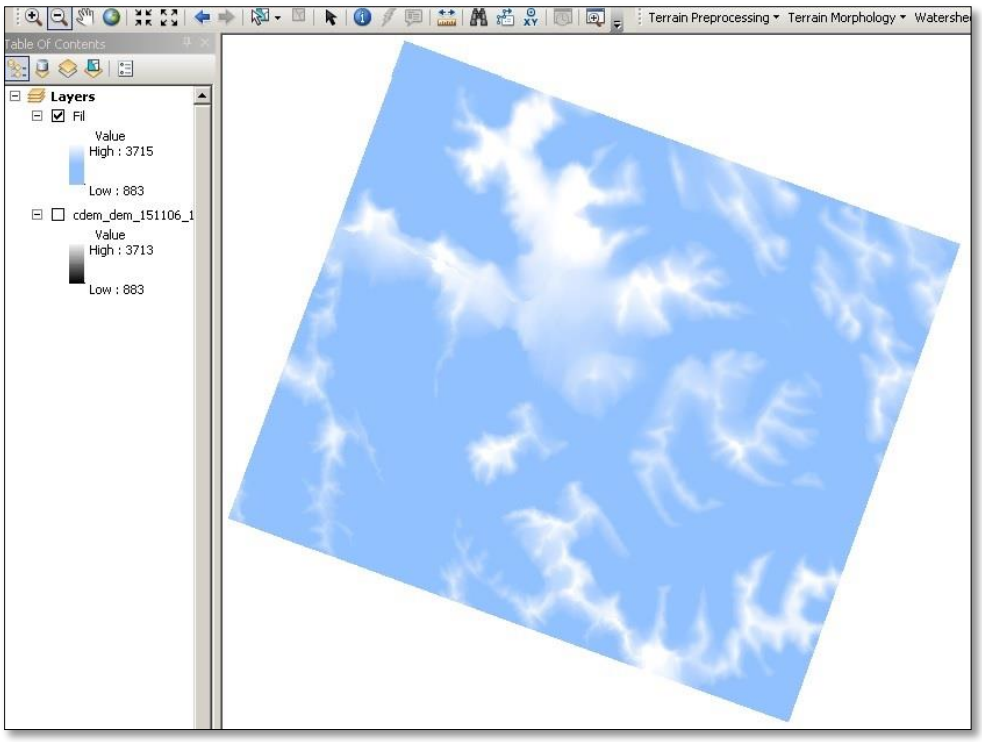

Figure 3. 10: A snapshot showing the output from the Fill Sinks tool in Arc Hydro.

Flow Direction

In Figure 3.11 it is shown how the flow direction tool works, which determines the 8 directions of flow within the map. Water falling (or river runoff, or glacier flow) in every pixel has a chance of moving in 8 different directions, and the downstream direction/cell with the steepest slope will capture this water. The image is shown in 8 different colors, because every pixel has 8 neighbors.

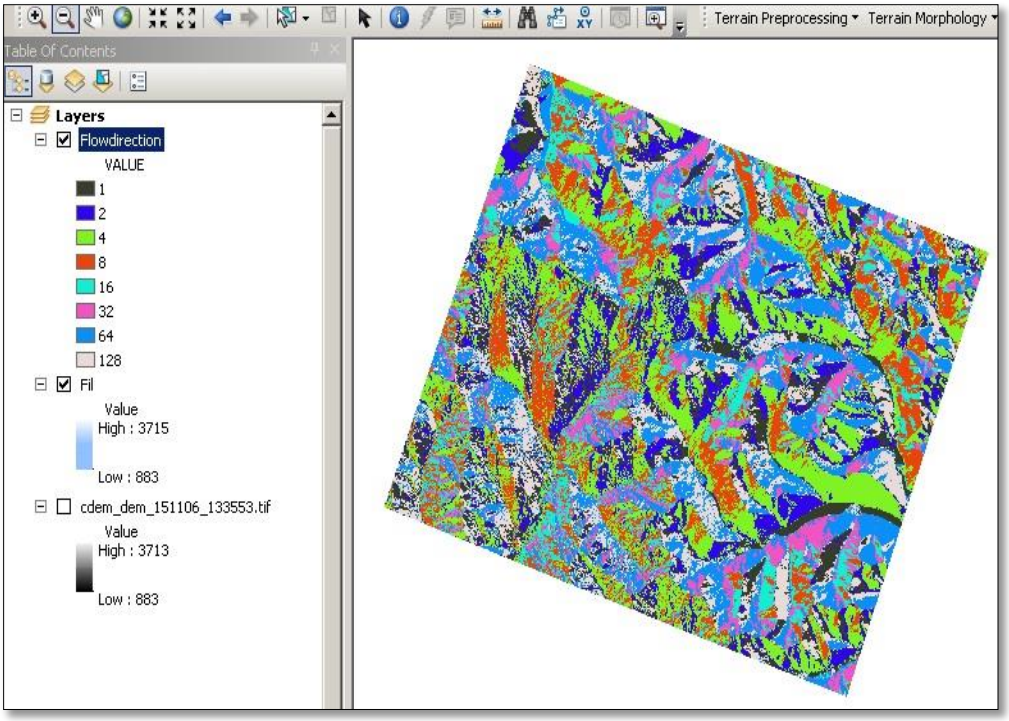

Figure 3. 11: A snapshot showing the output from the Flow Direction tool in Arc Hydro.

Flow Accumulation

Flow accumulation is calculated based on the flow direction grid. Figure 3.12 gives a view of the resulting drainage network.

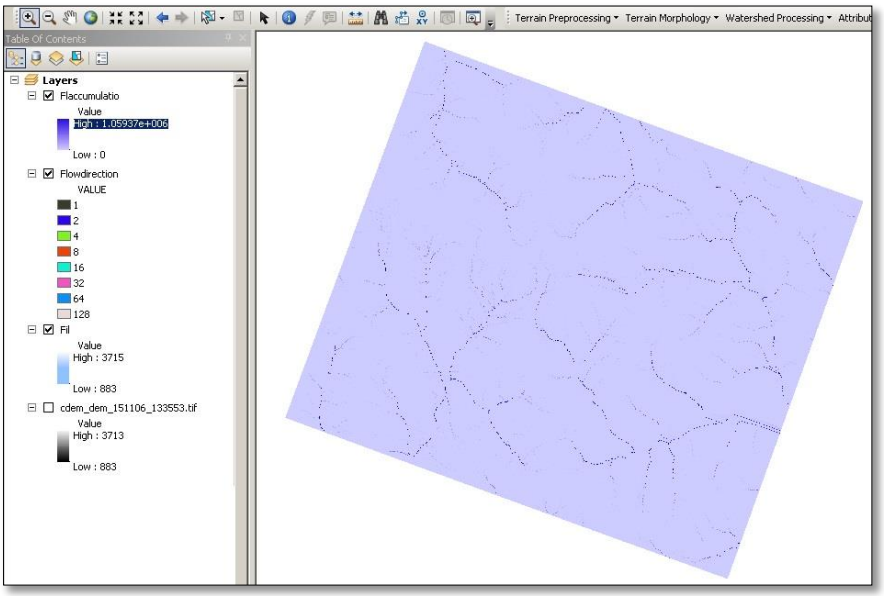

Figure 3. 12: A snapshot showing the output from the Flow Accumulation tool in Arc Hydro.

Stream Definition

One needs to select the number of cells that define a river for that one need to specify a value for which a stream should be constructed. I had to set the minimum river size of 1,000 pixels, in order to look for the major drainage system (Figure 3.13).

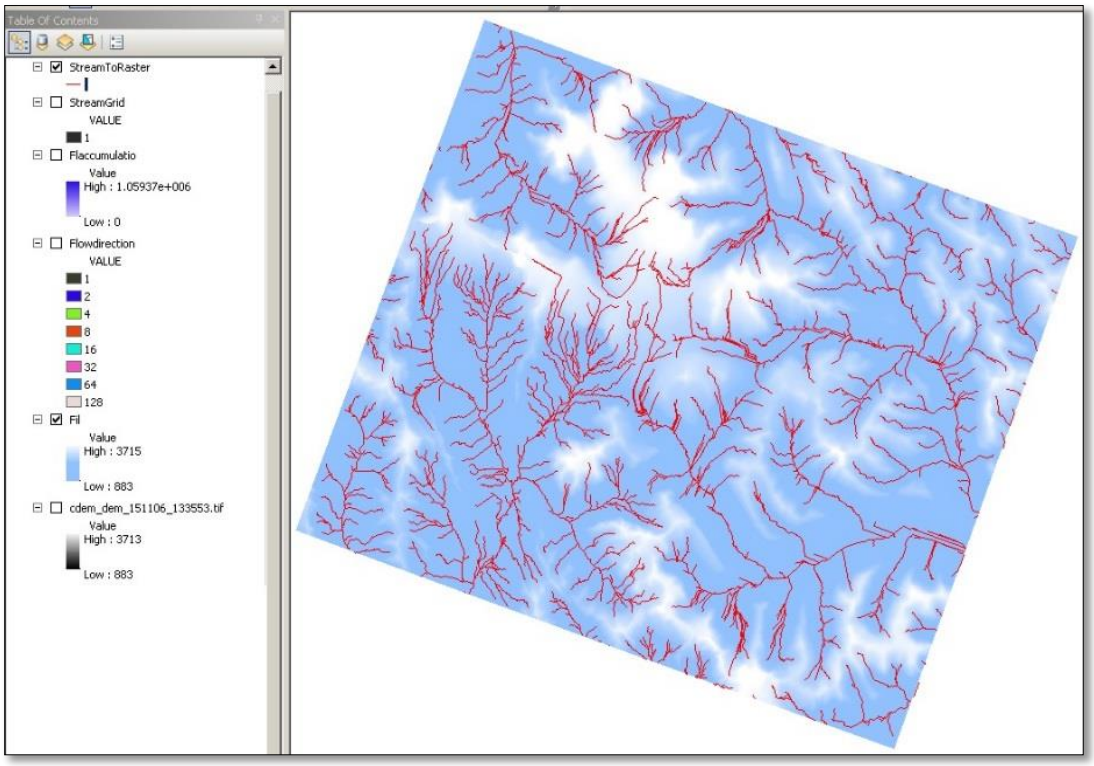

Figure 3. 13: A snapshot showing the output from the Stream Definition tool in Arc Hydro.

Stream to Feature

The output of the stream definition function is in a grid format. For that, the current function is needed, which will convert the grid into a feature (vector) format. In Figure 3.14, it can be seen that there are some streams which are not delineated; it is because I have defined 10000 in my stream definition. These minor drainages will be delineated by putting a lesser number for the stream threshold.

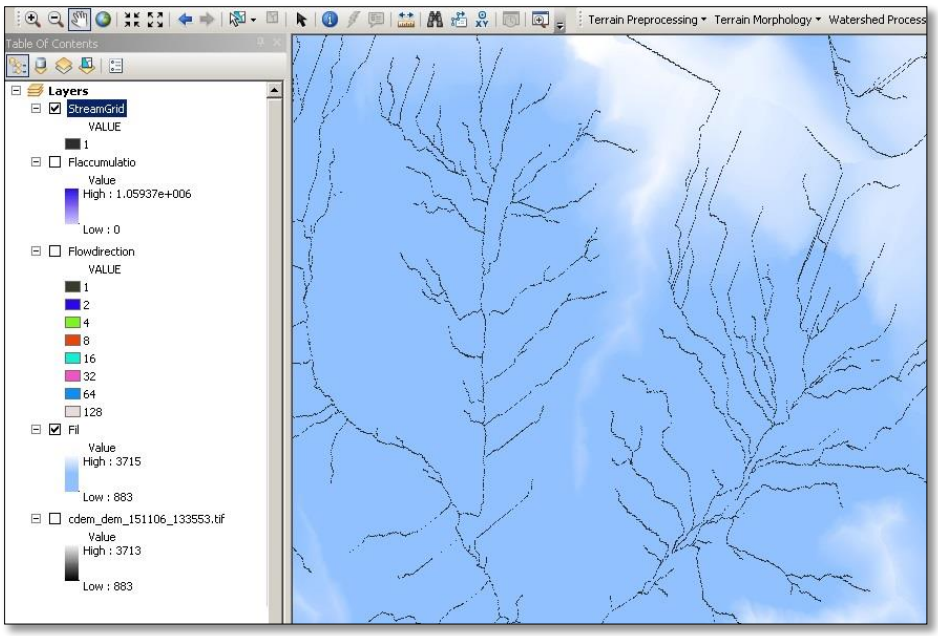

Figure 3. 14: A snapshot showing the output from the Stream to Feature tool in Arc Hydro.

Pour Point

Pour points define the stream outlet. Anything upstream of the pour point will be defined as a single watershed. Then using the snap pour point tool, where the main inputs are pour-point features, and giving a snap distance, it will execute to present a new output added onto the layer (Figure 3.15).

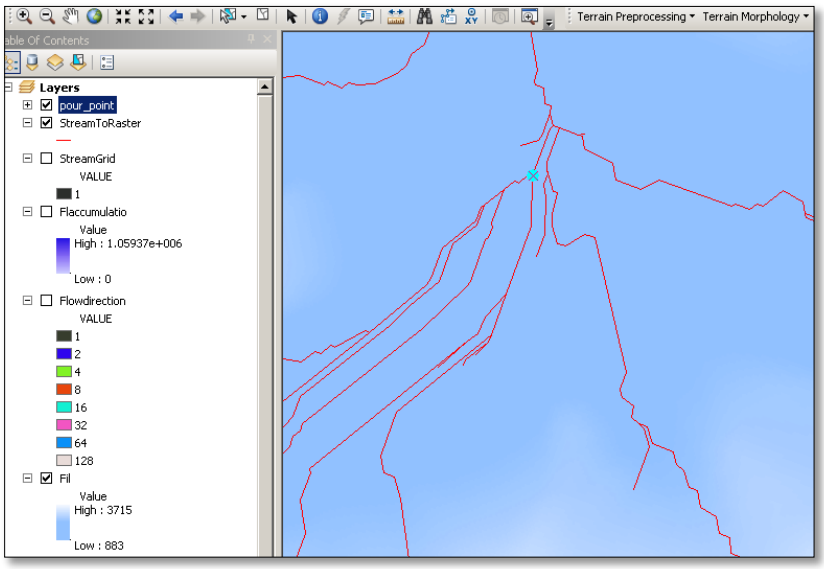

Figure 3. 15: A snapshot showing the output after performing Pour Point tool in Arc Hydro.

Watershed Delineation Tool

Next is to delineate the final watershed, which needs the flow direction and pour points to help generate the watershed. The placement of the pour point (Figure 3.16) determines the shape and size of the watershed. If it is too small, it means the pour point is very close to the stream, and vice versa. The raster map is changed into a polygon (vector) to give the 'watershed' (iceshed) boundary for Athabasca Glacier.

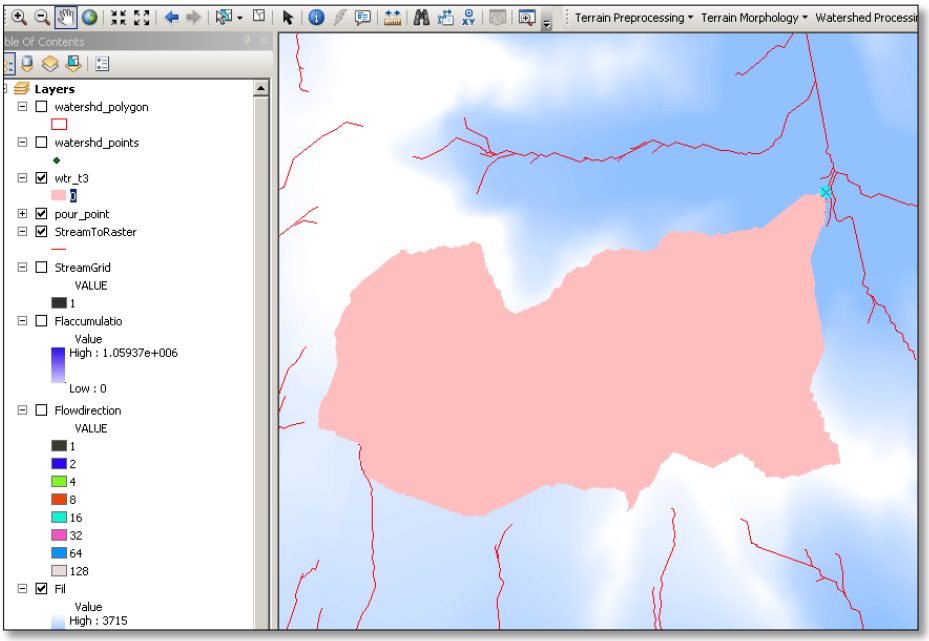

Figure 3. 16: A snapshot showing output from the Watershed Delineation tool in Arc Hydro.

The upper boundary is totally inside the icefield, so it is the true glacier catchment. For the outlet glacier, I used the clipped SPOT 5 imagery boundary for a clear idea and edited the watershed polygon according to that. Figure 3.17 demonstrates the function.

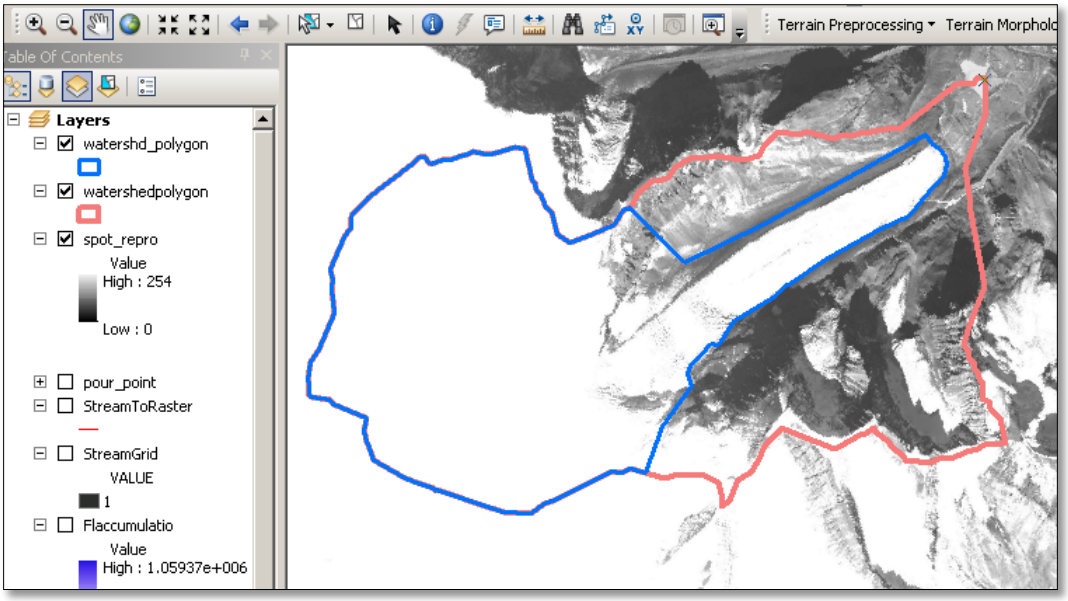

Figure 3. 17: A snapshot of the output after editing and clipping the watershed boundary.

3.3.2. Central Flow Line (CFL)

Similar to the glacier boundary, the central flow line of the glacier is delineated by using simple techniques after deriving the glacier boundary. For this one, the DEM is the main dataset that has been used. A detailed list of steps follows for the derivation of central flow line.

Creating a Skeleton

'Skeleton' tool is the first step of creating a centreline from a polygon. The tool is one of the subtools of 'Polygon to Centreline Tool set' which was added separately to Arc Map. The only input for this tool is the glacier boundary i.e., the polygon. After selecting the proper boundary, the skeleton tool generates an outline of the boundary (figure 3.18).

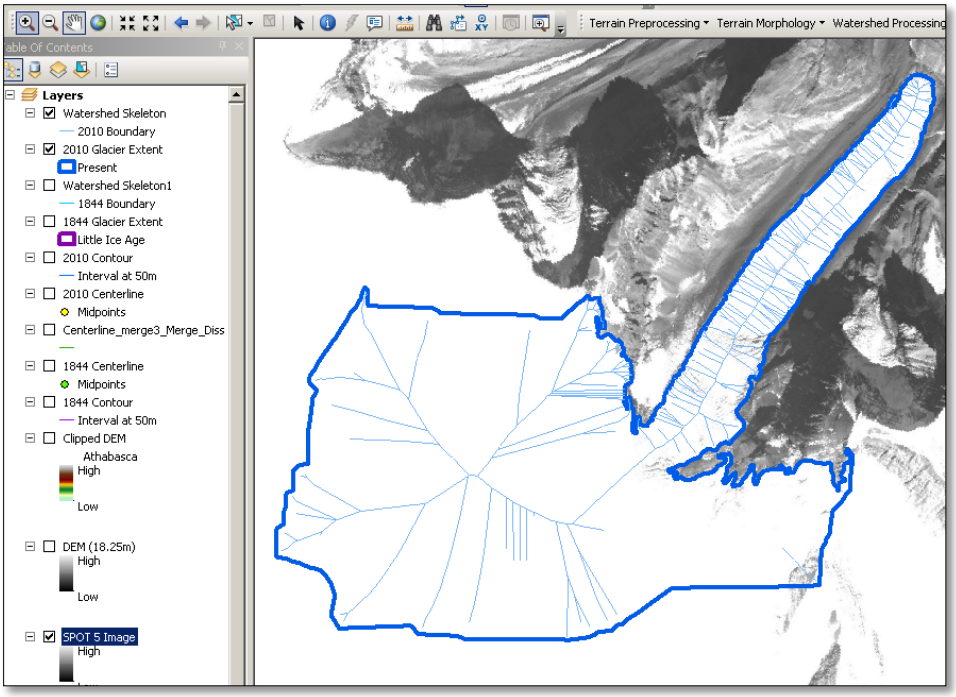

Figure 3. 18: Creating skeleton of the watershed polygon.

Centreline

The creation of the skeleton provides the main centreline and diverging lines into the centreline. All of these lines are made up of tiny segments which can be merged to derive a single one. Using the 'merge' tool, the centreline was achieved. After merging, the next function, 'dissolve', was performed, which gives a new line after dissolving the tiny segments. The 'dissolve' function allows merging of the adjacent and overlapping lines into a single and continuous one. This whole process was performed twice, to derive centrelines for the two time periods: 2009 and 1844 (figures 3.19 and 3.20). The length of the centreline for the 1844 limit is about 10.7 km, and 8.8 km in 2009.

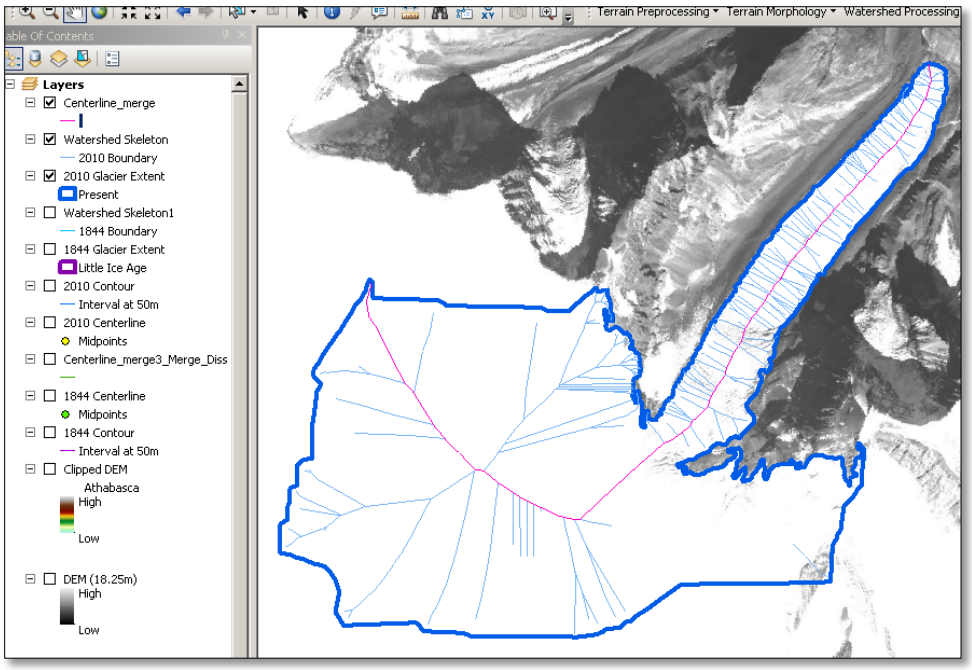

Figure 3. 19: A snapshot showing the centreline (in pink) of the 2009 glacier boundary.

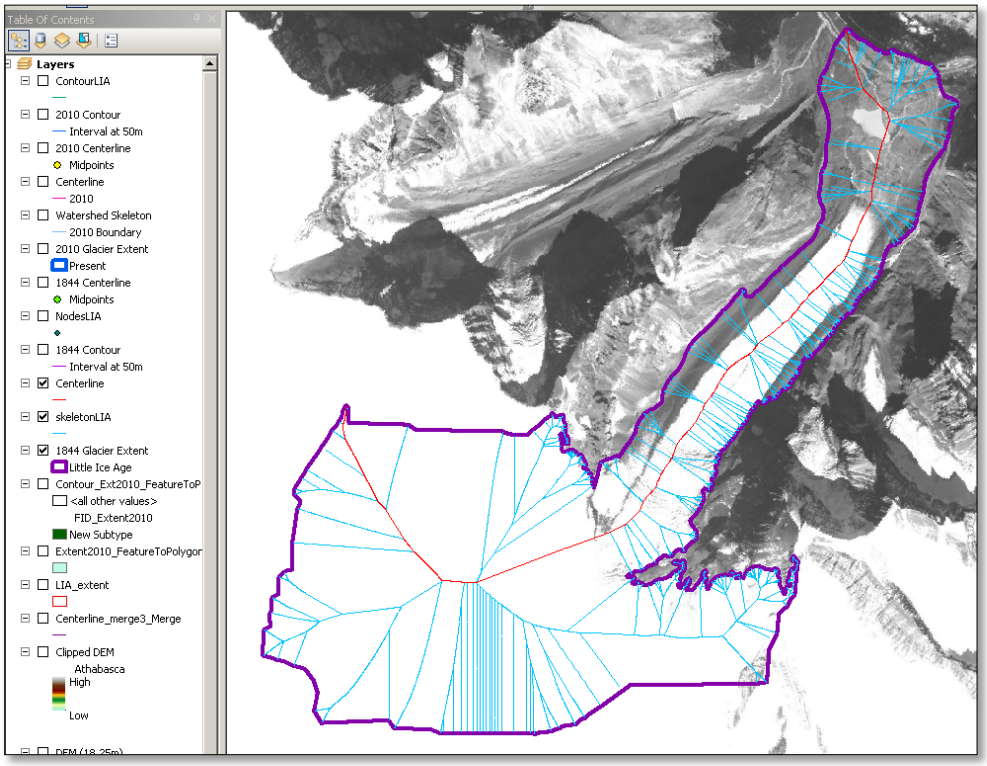

Figure 3. 20: A snapshot showing the centreline (in red) of the 1844 glacier boundary.

Nodes

Glacier width, elevation, and surface slope are based on flowbands with central nodes. Nodes are the equidistant points created along the centreline, at 50-m intervals (Figure 3.21).

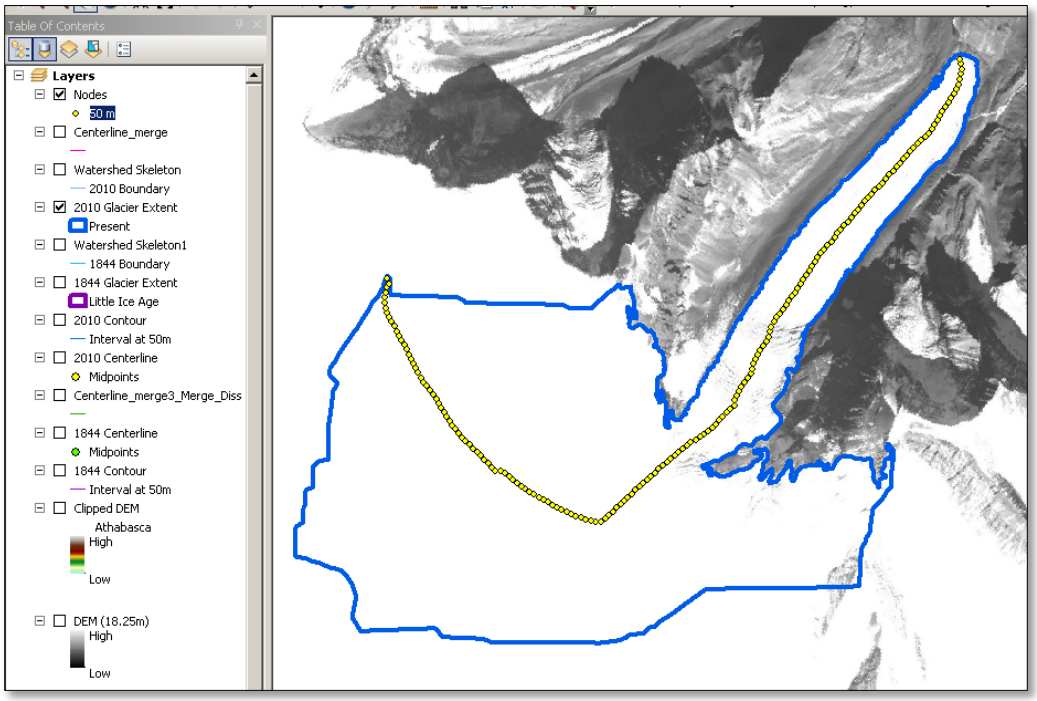

Figure 3. 21: A snapshot showing the nodes created along the Centreline.

The distance of 50 m was chosen to give appropriate detail about the elevation and surface slope. A number more than 50 m gives poorer resolution about the position of the glacier terminus. Higher resolution is not justified because the surface elevation changes very gently over 50 m in the interior of the icefield and sections of the outlet glacier; two adjacent nodes with the same elevation would result in no slope and no flow. Discretization of 50- to 100-m is in better accord with changes in elevation and ice dynamics, as well as the (lack of) knowledge of the bed topography.

After getting 181 points along the centreline, midpoint nodes were placed at 25-m distance to delineate the flowbands. In that case, the central node is assigned to the middle of the box (figure 3.22). Along each midpoint, a perpendicular line is drawn to the glacier edge, to determine the width of the cross section. From this, I considered the half width (*w*) (Nye, 1965) for my calculations.

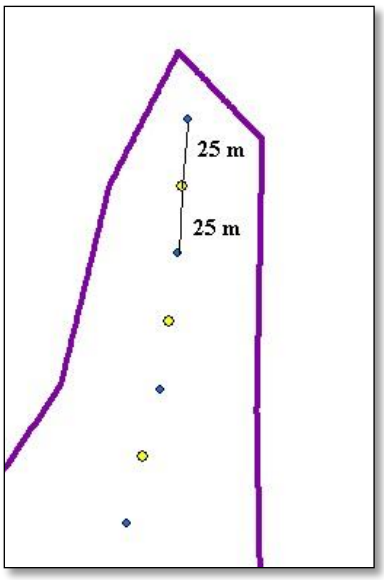

Figure 3. 22: A snapshot showing the nodes and midpoints placed 25 m away within the boundary. Yellow dots are nodes, blue dots are midpoints between two nodes.

Elevation: The primary way to measure the elevation of the nodes is to perform a 'contour' function with a 50-m spacing. This extracts the elevation measurements from the digital elevation model, with an example given in figure 3.23.

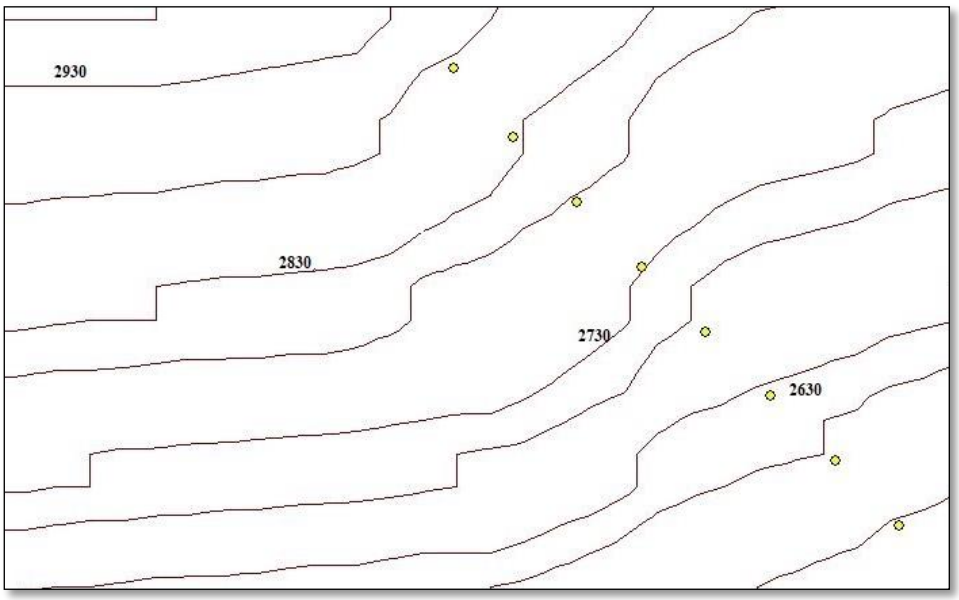

Figure 3. 23: A snapshot showing the contours lines at the nodes along the centreline.

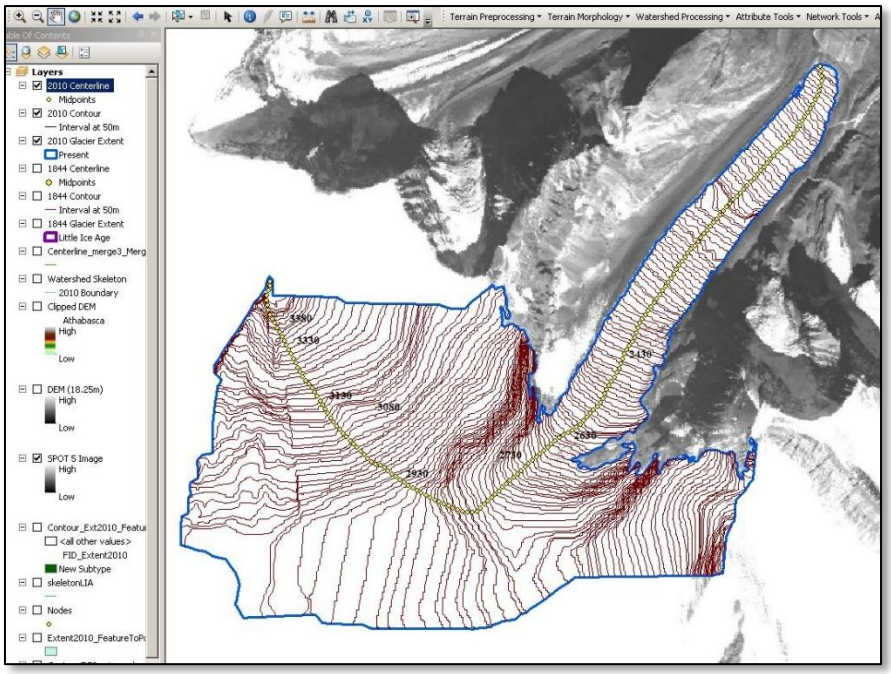

Figure 3. 24: A snapshot showing the contours with elevation measurements in meters.

Glacier Width: Glacier width is determined by measuring the length of the contour line between the flowline and the glacier outline. Some error exists here as the lines were not straight. A snapshot is attached here for the reference (figure 3.24 and 3.25).

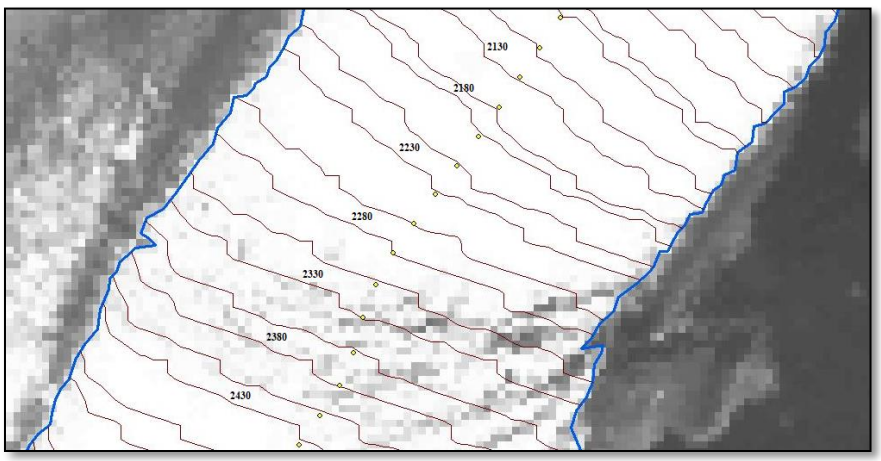

Figure 3. 25: A snapshot showing the contours lines, used for measuring the width.

Surface slope: Surface slope (α), expressed as $\left(\frac{dh}{dx}\right)$, was calculated with the elevation and the contour interval for each node. After that, to stabilize the model calculations, an 11-point moving average function was performed.

3.4.Ice Thickness

It has been possible to measure the amount of ice thickness with the equation formulated with the shear stress exerted onto ice as τ_b = 100 kPa and the density of ice (ρ), amount of gravitation (g) applied on to it and the surface slope (α). Marshall (2011) considered it to be the classical model which could be utilized for the estimation of ice thickness, as follows:

$$H = \frac{\tau_b}{\rho\, g\, \alpha}$$

I use this simple model to estimate local ice thickness from the surface slope. I also explore a newer approach that has been introduced by Farinotti et al. (2009). Farinotti considers the ice-flow equations under an "apparent" (steady-state) mass balance and Glen's flow law, deriving an equation for the ice thickness as follows:

$$H_i = \sqrt[n+2]{\frac{\bar{q}_i}{2A} \cdot \frac{n+2}{(C\rho g sin\bar{a})^n}}$$

where, H_i is the ice thickness of the ith node, $\bar{q}_i$ is the ice volume flux at the centre of the cross profile, A and n are parameters in Glen's flow law, C is a correction factor, ρ is the ice density, g is the acceleration of gravity and $\bar{a}$ is the mean surface slope along the considered ice flow line. To use Farinotti's equation, we need estimates of ice flux, which are calculated based on 'balance fluxes', using an assumed net mass balance profile and the assumption of glacier equilibrium.

Chapter 4: Results

4.1. Mass Balance Model

Mass balance measurements at Peyto Glacier are used to inform the mass balance model applied to Athabasca Glacier. I assume that the gradient in net mass balance with elevation at Peyto, $\beta = db_n/dz$, applies regionally and is valid at Athabasca. Net mass balance data as a function of elevation are available from Peyto for the period 1966-2005. Assuming a linear balance gradient, a linear regression of this data gives the slope db_n/dz as plotted in figure 4.1. The mean value for the observational period is 5.73 mm w.e. m^{-1}.

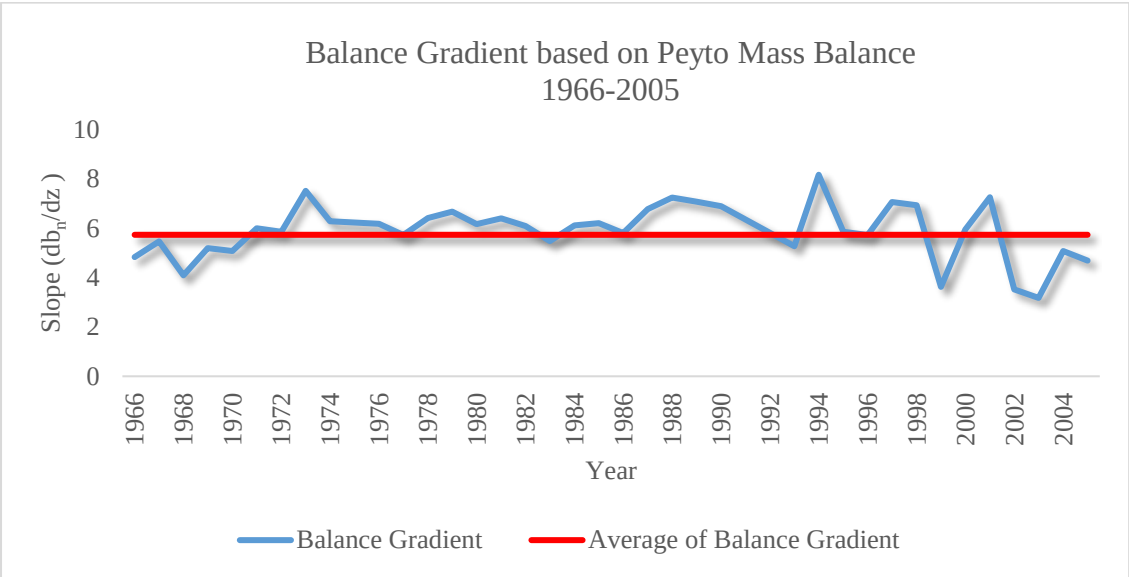

Figure 4. 1: Net mass balance gradient on Peyto Glacier from 1966 to 2005.

Bilinear or quadratic fits to net mass balance data have been used elsewhere (e.g., Farinotti et al., 2009; Bahr et al., 2015), but a simple linear model has the best fit with data from Peyto, with a single mass balance gradient applying to both the ablation and accumulation areas. Peyto has an elevation range of almost 1000 m, from 2200 to 3150 m, which corresponds well with Athabasca Glacier. The upper accumulation area of Athabasca reaches higher than this, with the Columbia Icefield plateau at elevations above 2900 m and Snow Dome extending higher than 3400 m. Hence, there is some extrapolation in extending the Peyto mass balance gradient to the upper reaches of Athabasca. In reality, net mass balance may level off on the upper plateau rather than increasing continually with elevation, due to the relatively smooth topography and

reduced orographic forcing on the plateau. In the absence of local mass balance data, however, it is difficult to assess this.

The Athabasca Glacier mass balance model is then set up following:

$$b_n(t) = b_0(t) + \beta z \ ,$$

for time t and intercept b_0. The intercept captures interannual variability in mass balance, and I allow this value to differ from Peyto Glacier, specific to the Athabasca Glacier reconstructions. The Athabasca simulations extend to times prior to observations on Peyto, so a more general treatment is needed for the long-term mass balance forcing at Athabasca. I return to how the intercept $b_0(t)$ is determined in section 4.3.

4.2. Multivariate Model of Regional Mass Balance

As discussed in section 3.1, a multivariate regression is explored to identify the best possible climate indices to account for the glacier mass balance variability in the Canadian Rockies. I again assume that mass balance at Peyto Glacier is regionally representative and that larger-scale (regional to synoptic) features of the climate explain much of the variance in the mass balance record. To determine if multiple (two or more) independent variables account for a significant portion of the total variation in the dependent variable (annual net mass balance), I include Jasper temperature and precipitation records as well as PDO indices, which are known to affect snow accumulation and glacier mass balance in western Canada (e.g., Bitz and Battisti, 1999; Whitfield et al., 2010). I consider the multivariate regression for net annual mass balance at Peyto, b_n, for the years 1966-2017. Two years of data are missing, giving $n = 50$. Table 4.1 gives the correlation table between b_n and several different predictor variables.

Table 4. 1: Correlation coefficients between net annual mass balance and different predictor variables at Peyto Glacier, 1966-2013.

Correlations							
		AB	AST	AMST	WP	PDOA	PDOW
Annual Balance (AB)	Pearson Correlation	1					
	Sig. (2-tailed)						
	N	50					
Average Jasper Summer Temperature (AST) (JJA)	Pearson Correlation	-.68**	1				
	Sig. (2-tailed)	0					
	N	50	50				
Average Jasper Melt Season Temperature (AMST) (MJJAS)	Pearson Correlation	-0.59**	.51**	1			
	Sig. (2-tailed)	0	0				
	N	50	50	50			
Winter Precipitation in Jasper	Pearson Correlation	-0.02	0.04	-0.04	1		
	Sig. (2-tailed)	0.88	0.80	0.79			
	N	50	50	50	50		
PDO Annual (PDOA)	Pearson Correlation	-0.51	0.32	0.13	-0.13	1	
	Sig. (2-tailed)	0.09	0.24	0.83	0.42		
	N	50	50	50	50	50	
PDO Winter (PDOW)	Pearson Correlation	-0.56*	0.39	0.33	-0.19	.90**	1
	Sig. (2-tailed)	0.04	1.0	0.84	0.22	0	
	N	50	50	50	50	50	50

**. Correlation is significant at the 0.01 level (2-tailed).

*. Correlation is significant at the 0.05 level (2-tailed).

Summer (JJA) temperature in Jasper is the strongest predictor, consistent with expectations that summer melt is the main determinant of net annual mass balance (e.g., Shea et al., 2007). The winter PDO index is also significant, with a strong PDO index correlated with lower net annual mass balance, in association with lower winter snowfall. These two components – JJA temperature in Jasper and the winter PDO index – form the basis for the best-performing multivariate model.

The multivariate regression model provides several outputs (Table 4.2). Multiple *r*, the correlation coefficient is calculated as the square root of the multivariate coefficient of

determination (R^2). In the best model, r = 0.71, a relatively strong linear relationship between the variables. The net mass balance is negatively correlated with both Jasper temperatures and the PDO index, with both variables contributing to the explained variance.

Table 4. 2: Multivariate regression statistics for the best model.

Multiple r	0.76[a]
R^2	0.58
Adjusted R^2	0.56
Standard error of estimate	444 mm w.e.
Observations	50

a. Predictors: (Constant), AST, PDOW

The next component is R^2, the coefficient of determination. In this output, R^2 = 0.58 and the adjusted R^2 = 0.56. This indicates that 56% of the total variation in annual balance is explained by the two predictor variables, accounting for the variable interaction. The standard error of the estimate is 440 mm. This can be viewed as the accuracy of the regression in estimating net annual mass balance.

Figure 4.2a plots the observed and modelled mass balance for the period 1966-2017, while Figures 4.2b and 4.2c show Jasper summer temperatures and the wintertime PDO index over this period. The multivariate equation for the mass balance is:

$$B_n = 6845 - 504\ T_{JJA} - 248\ PDO_w$$

The multivariate mass balance model has muted variability compared to the observed mass balance, especially in the positive mass balance years, but the general year-to-year variability is well-captured, as well as the temporal trend.

Summer temperature in Jasper

Summer (JJA) temperature in Jasper averaged 14.2°C from 1966-2017, slightly warmer than the long-term (1916-2017) average of 14.0°C. The standard deviation in JJA temperatures is 0.8°C, providing a measure of interannual variability. There is a weak warming trend in the JJA temperature data from 1916 to 2017, +0.6°C per century. The warmest summers (e.g., 1970, 1998, and 2015) correspond to very negative mass balance years (figure 4.2).

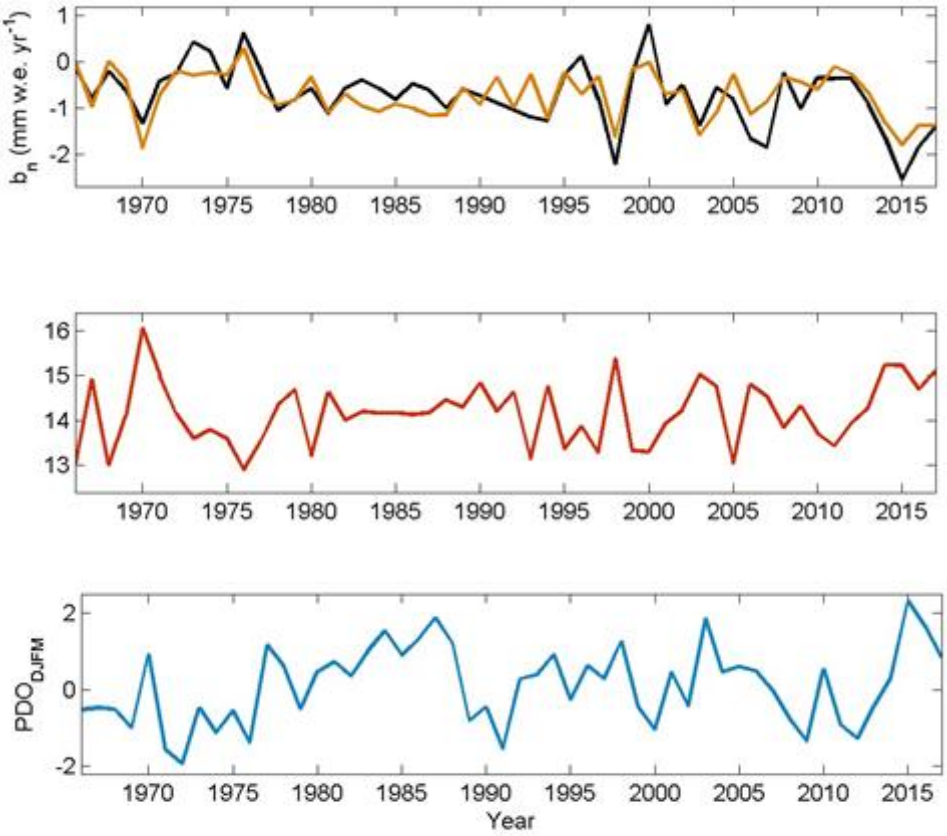

Figure 4. 2: (a) Observed (black) and modelled (orange) mass balance at Peyto Glacier, using (b) Jasper summer (JJA) temperature and (c) the winter (DJFM) PDO index as predictor variables.

The Jasper weather station was moved in 1931 and again in 1996. Mean summer temperatures do not appear to have a discontinuity (figure 4.2b), and overlapping data show minimal difference, so the Environment Canada data are not adjusted. However, minimum summer temperatures at the current site (1996 to present), Jasper warden station, are roughly 1.6°C cooler than the original Jasper station. The new site may be prone to some cool air ponding overnight, so mean daily temperatures could be affected by this and the Jasper temperatures from 1996 to present may be biased cool relative to the data from 1916 to 1995.

The Pacific Decadal Oscillation

The winter PDO index is a standardized (dimensionless) measure of pressure and temperature patterns in the North Pacific Ocean. It is known to correlate with precipitation totals in western Canada, through its association with circulation and

storm tracks. In its positive phase, the eastern North Pacific has a warm anomaly and this is associated with northern displacement of the polar jet stream, with warmer and drier conditions in southwestern Canada. The negative phase features more zonal flow and cool, wet conditions, hence greater snow accumulation on the glaciers in the Rockies. Positive PDO years are also weakly correlated with warm summers in Jasper, and the most negative mass balance years at Peyto coincide with both warm temperatures in Jasper and a positive phase of the PDO.

4.3 Climate Proxies for the Last Millennium

Luckman and Wilson (2005) published millennial summer temperature reconstructions for the Canadian Rockies, based on tree rings, with an extended reconstruction published subsequent to this at the U.S. National Climate Data Center (Luckman and Wilson, 2006). The proxy data run from 950 A.D. through to 1998. For the current research, this reconstruction data was examined to see if it can help extend the Jasper temperature record back in time, for simulation of LIA glacier conditions. The tree-ring data are presented as anomalies, which I convert to actual temperature by adding the anomalies to the mean Jasper summer temperature. The resulting summer temperature time series is positively correlated with the Jasper station data for the period of overlap, 1916-1998: $r = 0.68$. Figure 4.3 plots the tree-ring based summer temperature vs. Jasper station data for the period 1916-1998. The annual time series are plotted in figure 4.4.

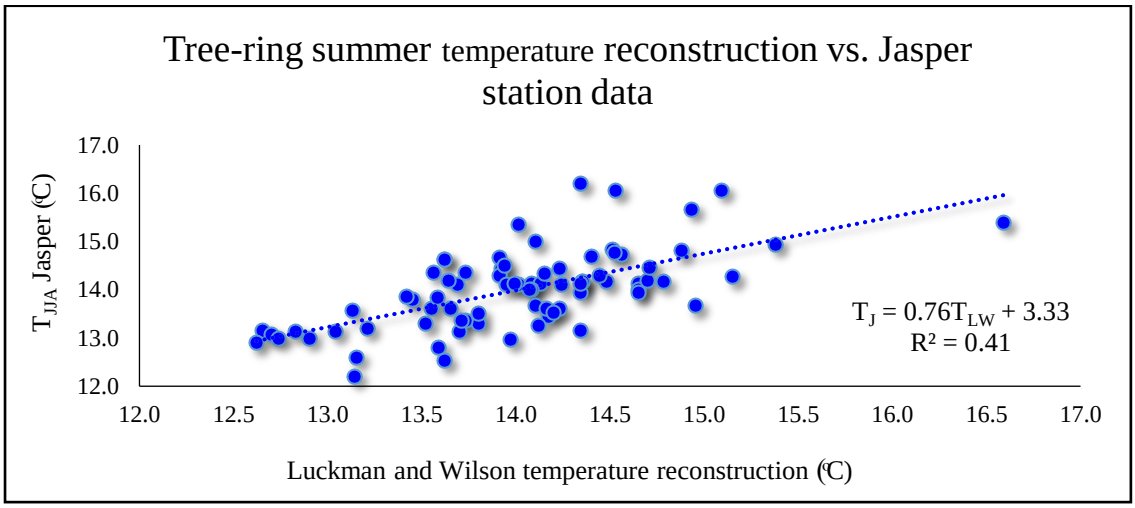

Figure 4. 3: Jasper summer (JJA) temperatures vs. tree-ring based temperature reconstructions from Luckman and Wilson (2006), for the period 1916-1998.

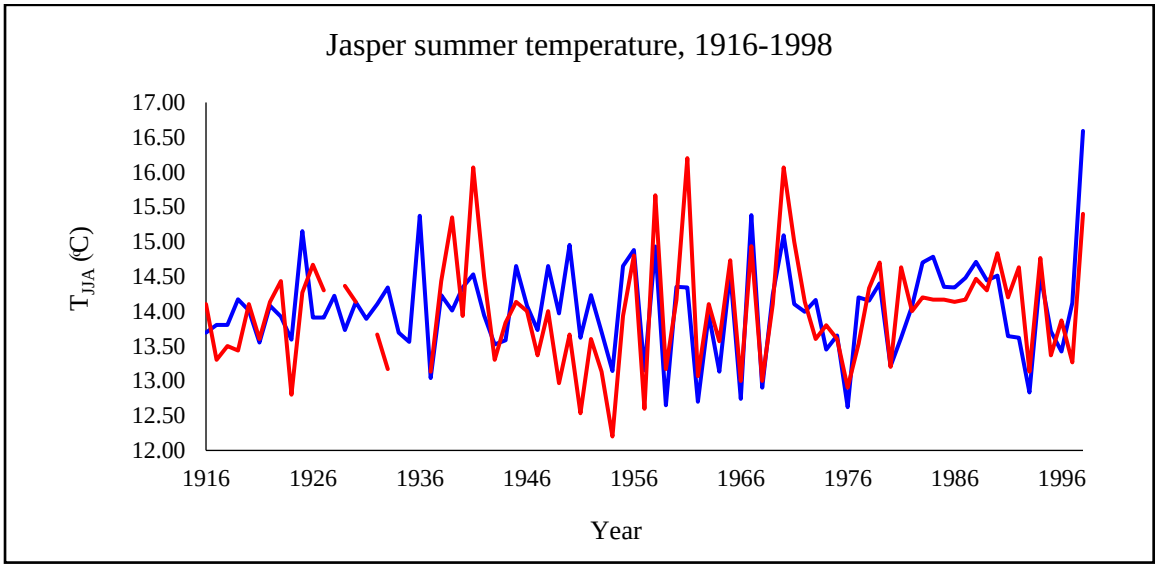

Figure 4. 4: Observed (orange) and tree-ring based (blue) summer temperatures in Jasper, 1916-1994.

The tree rings explain only 41% of the variance in the actual data, but the correlation is significant, so the resulting regression (Figure 4.3) offers an expression that can be used to estimate Jasper summer temperature over the last millennium, via the tree-ring proxies: $T_J = 0.76\,T_{LW} + 3.3$. The result is plotted in figure 4.5.

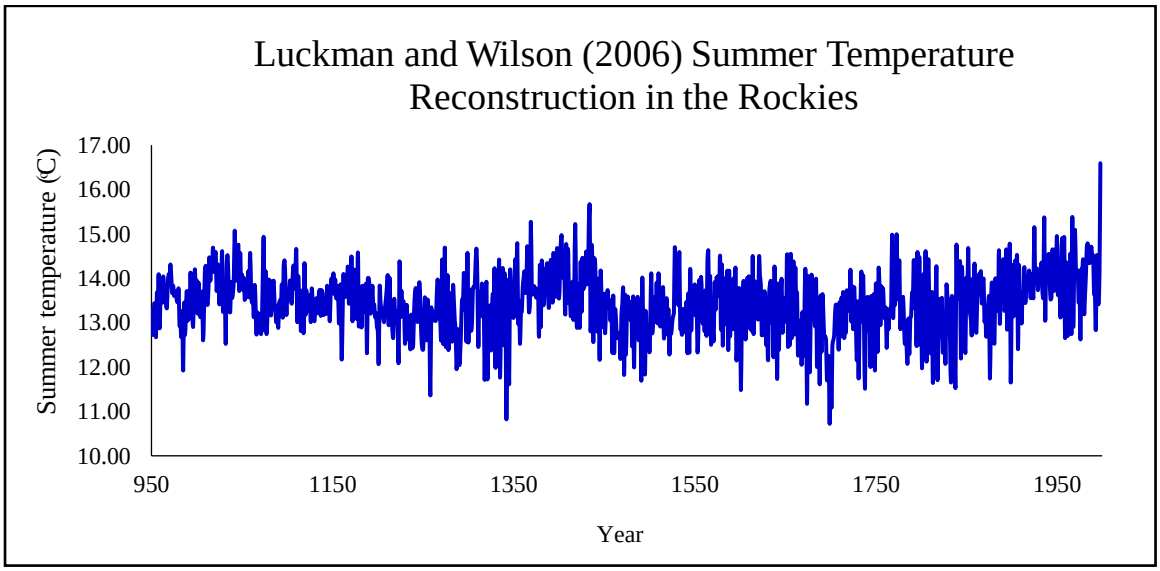

Figure 4. 5: Luckman and Wilson (2006) summer temperature reconstruction in the Canadian Rocky Mountains. The anomalies in Luckman and Wilson (2006) are mapped onto mean observed summer (JJA) temperatures in Jasper from 1916-1998.

Some tree species are more sensitive to moisture than temperature, and have been used to reconstruct PDO over the last millennium in western North America (MacDonald and Case, 2005). The PDO proxy data of MacDonald and Case are based on limber (white) pine trees from California and the Canadian Rockies (near Nordegg, AB) and data from 993 to 1996 AD are available at MacDonald and Case (2006). These data are used to extend the PDO time series back beyond the historical period (1900-2017).

Using the tree-ring based temperature and PDO proxies, stitched together with the observed conditions from the last century, Athabasca Glacier mass balance estimates can be extended to the last millennium, including Little Ice Age conditions that I need in order to simulate the LIA extent of Athabasca Glacier. Figures 4.6 and 4.7 plot modelled Athabasca Glacier mass balance through the last millennium and for the period 1844-2017, which is the focus of my model simulation.

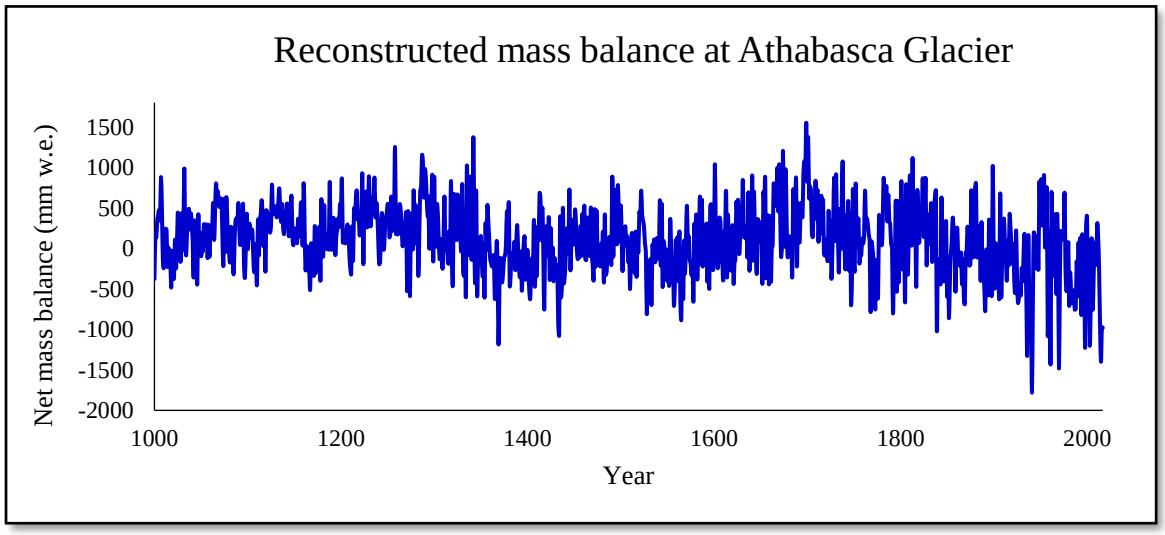

Figure 4. 6: Reconstructed mass balance at Athabasca Glacier for the period 1000-2017 AD, based on tree-ring based temperature estimates in the Canadian Rockies and PDO proxies prior to the 20th century. The period 1916-2017 is based on observed temperature and PDO indices.

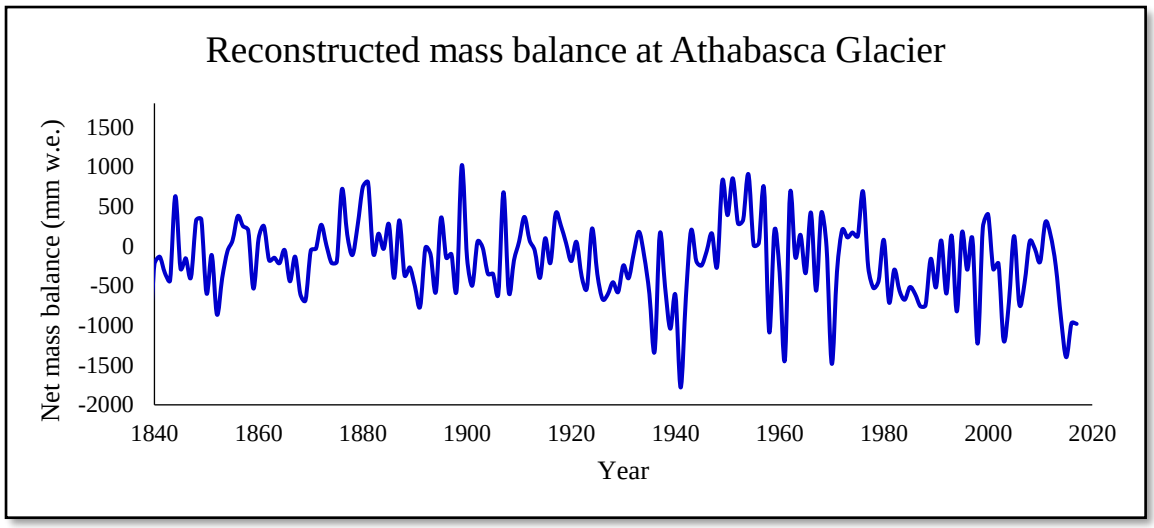

Figure 4. 7: Reconstructed mass balance at Athabasca Glacier for the period 1844-2017 AD, based on tree-ring based temperature estimates in the Canadian Rockies and PDO proxies prior to the 20th century. The period 1916-2017 is based on observed temperature and PDO indices.

Athabasca Glacier mass balance model

Temporal variations in mean specific mass balance, b_n, are introduced through the multivariate model and climate proxies described here (figure 4.7), but the modelling requires a mass balance profile with elevation, $b_n(z, t)$. I calculate this from the multivariate regression output along with the linear mass balance model $b_n(z,t) = b_{n0}(t) + \beta z$, with the mass balance gradient, β, taken from Peyto Glacier and assumed to be regionally applicable. The net mass balance is calculated for the hypsometry of Athabasca Glacier and $b_n(t)$ is prescribed to be equal to the output of the multivariate model. This yields a unique annual value for the intercept $b_0(t)$. In mathematical terms, this is calculated from:

$$b_n(t) = \frac{1}{A}\sum_k a_k b_{nk} = \frac{1}{A}\sum_k a_k [b_0(t) + \beta s_k],$$

where k refers to the vertical level in the model, A is the total glacier area, and a_k is the area of the glacier at elevation s_k. This can be rearranged to give the equation for the intercept,

$$b_0(t) = b_n(t) - \frac{1}{A}\sum_k a_k \beta s_k .$$

This is calculated as a function of the 2009 reference surface, $s(z)$.

In combination, the results in sections (4.1)-(4.3) provide a means to model the net annual mass balance of Athabasca Glacier as a function of elevation and time, for the last millennium or, in my application, from the Little Ice Age to present.

4.4. Ice Thickness

In section 3.2.3., it was mentioned that ice thickness estimates are needed for glacier flow modelling. Figure 4.8 (green line) shows the output of the classical theory of estimating the ice thickness distribution from the surface slope (see section 3.4.). In the same figure, the blue graph represents the output deduced from Farinotti's method.

A similarity is found between these two graphs, with more or less similar crests and troughs. Estimated ice thickness is greater at lower elevations and is maximum from the elevations 2100 to 2300 m, whereas the middle portion of the glacier (from 2600 m to 2750 m) have some sections with thicker ice. According to classical theory, the average ice thickness along the centerline is 94 m, whereas following Farinotti's theory it is 86 m. I use the latter as the reference geometry. Taking into account the 3D glacier geometry, with an assumption that the outlet glacier valley is parabolic and the upper icefield is a flat plateau, the average ice thickness from the Farinotti model is 69 m.

These thicknesses are glaciologically realistic, but the classical equation and the Farinotti method are both approximate, and do not easily allow for deep over-deepening of the bed (i.e., eroded basins where there will be reverse bed slope, allowing for unusually thick ice). This is a valid point because there is limited radar data of actual ice thickness available at Athabasca Glacier, but measurements by Paterson in the 1960s suggest an ice thickness of more than 300 m along some of the outlet glacier, about 2 km up from the current margin. The glacier has thinned since then, by perhaps 50 m (assuming a thinning rate of 1 m/yr for the outlet glacier, in line with the observations at Peyto Glacier since 1966). However, the remaining ice should still be up to 250 m thick, so the glacier thicknesses in Figure 4.6 may underestimate the true thickness, at least in the outlet valley. Ice depth on the upper plateau is unknown.

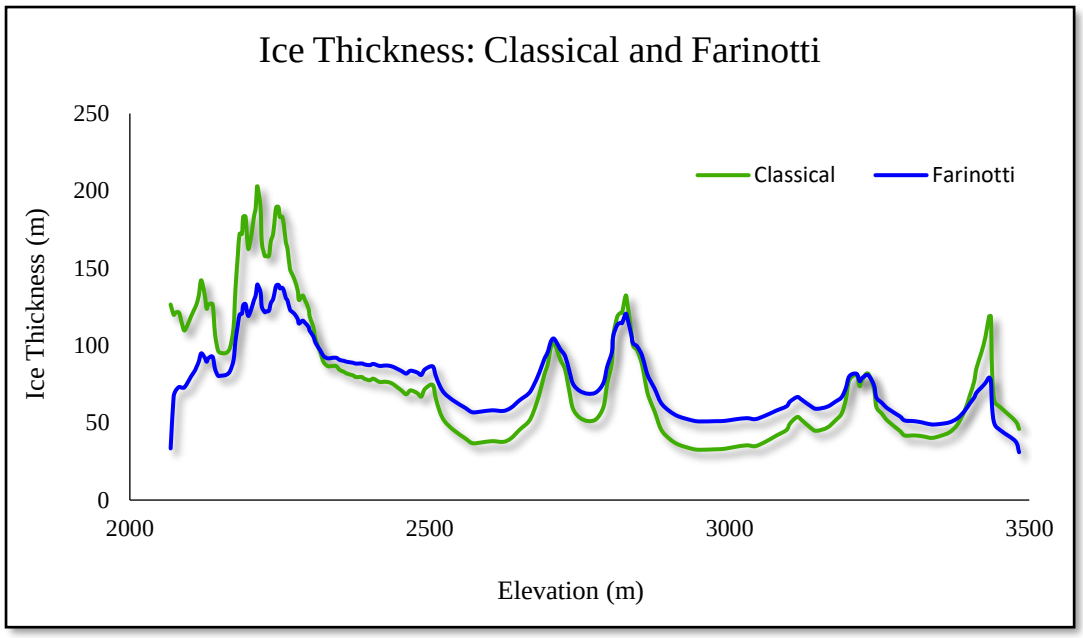

Figure 4. 8: Estimated Athabasca Glacier ice thickness along the centreline. The green line is from the classical theory of ice thickness, i.e. determined from the local surface slope, and the blue graph is from the Farinotti ice thickness model.

Bed Topography

After calculating the ice thickness, one can estimate the bed topography. In my case, the bed topography follows a gentle gradient (Figure 4.9) starting from 2068 m up to 3483 m.

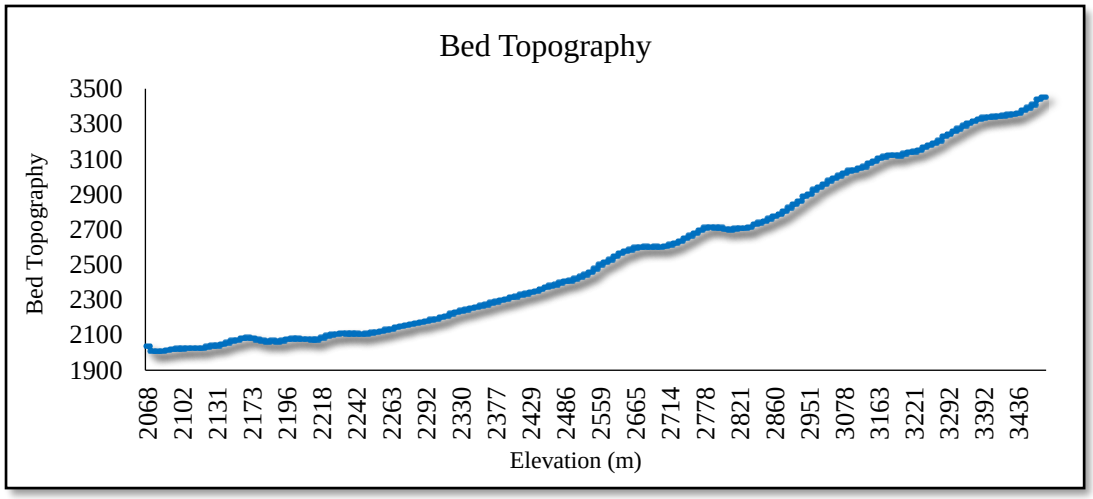

Figure 4. 9: Estimated bed topography of Athabasca Glacier.

4.5. Creating an Initial Model

The ice thickness and glacier geometry (width, length, area, and elevations) are calculated based on the data available for the period 2009, in order to create an initial condition for the glacier model. Given a climate (mass balance) scenario, the glacier will advance or retreat from this initial state. In the end, I am interested in the evolution of the glacier from the Little Ice Age to present: 1844 to 2017. Hence, I need to create an initial condition for 1844, the LIA glacier maximum. The area and length of the glacier are well-constrained by moraines from that time, so it should be possible to develop an LIA initial model that is glaciologically sensible.

To grow a LIA glacier, I start with the present-day (2009) ice geometry and the equilibrium mass balance and I make it colder, leaving the temperature fixed at this colder temperature. The ice thickens and advances until it reaches an equilibrium, with its geometry evolving to be consistent with the glacier physics. This takes between 100 and 200 years. I start by adopting the mean climate and mass balance conditions of the period 1600-1850, which is equivalent to setting the equilibrium line altitude (ELA) to 2640 m. Figure 4.10 plots the evolution of the glacier in this scenario. There is no visible change in the glacier geometry after 150 years of simulation.

Interesting transients in the modelled evolution of the glacier are evident in Figure 4.10. The initial 2009 geometry (estimated ice thickness) is not in good accord with the glaciological flow and mass balance profile, at least as prescribed with the parameters in my simulations. Despite the positive net mass balance, averaged over the glacier, the glacier terminus thins and retreats for about 60 years, due to modelled ablation exceeding the flux of ice to lower elevations. After this point, however, the excess accumulation on the upper glacier results in thickening and an increase in the flux of ice. The glacier responds by advancing down-valley to my approximation of the LIA geometry.

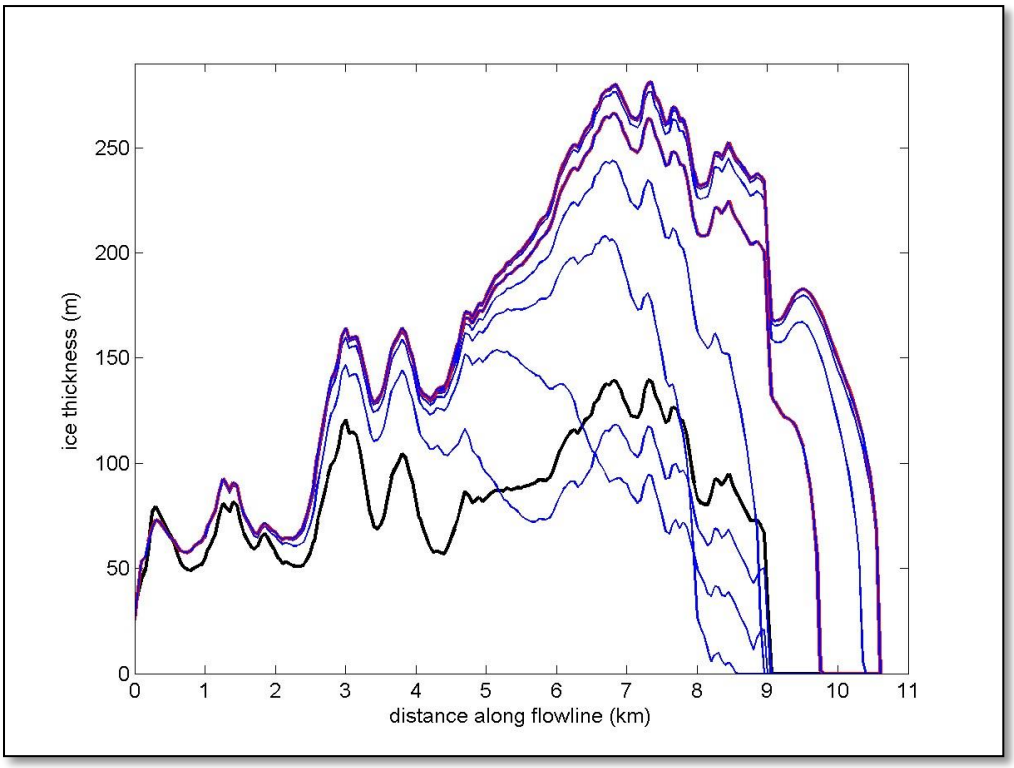

Figure 4. 10: Modelled Athabasca Glacier 'spinup' simulation from the 2009 geometry (black) to an equilibrium state after 200 years (red line showing the maximum glacier extent in every 100 years). Ice thickness is plotted every 20 years.

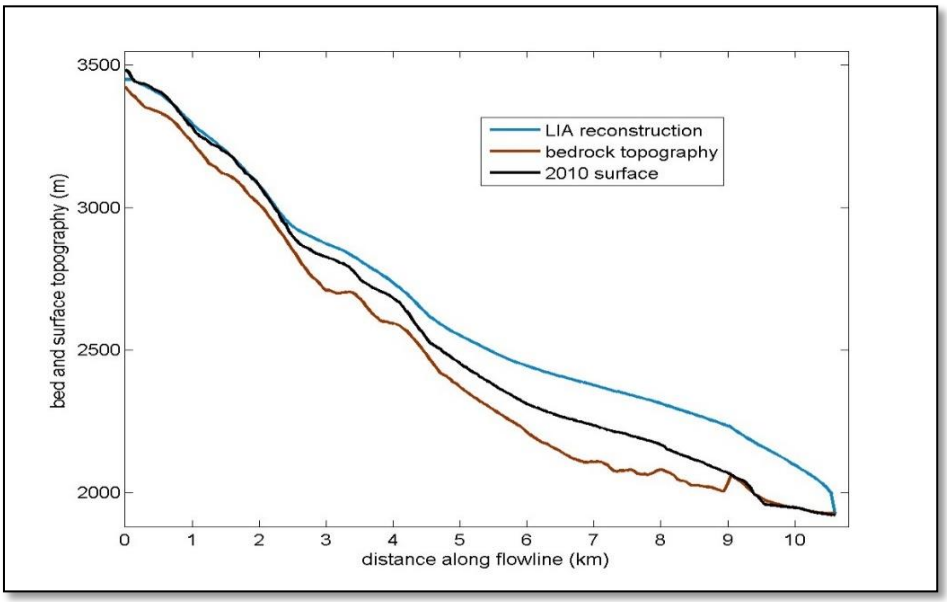

Figure 4. 11: Modelled Athabasca Glacier bed (brown) and surface topography for 2009 (black) and the LIA equilibrium state (blue).

The equilibrium extent, which I will use for the LIA initial condition, has a length of 10.6 km: 1.6 km further down-valley than the modern glacier. The glacier is also much thicker than the initial estimate from the Farinotti method (black line in Figure 4.10). The average ice thickness is 106 m, compared with 69 m in the initial (Farinotti) model for 2009, with most of the outlet glacier thicker than 200 m. Figure 4.11 shows the bed and surface topography for the initial model and the 2009 and LIA reconstructions.

Sensitivity Tests for the LIA Spinup

There are a number of choices to make in the spin-up simulation, as to the optimal glaciological and climatic (mass balance) parameters. This includes the amount of glacier sliding, the ice rheology (ice stiffness parameter in Glen's flow law), the amount of cooling or the elevation of the ELA during the 19th century, and the mass balance gradient. I test these through a range of possible values, to determine how sensitive my LIA reconstruction is to some of these poorly-constrained parameters. The results are summarized in Tables 4.2 to 4.4.

Most scenarios that are presented are restricted to those that might be considered plausible, i.e. a LIA glacier reconstruction in reasonable accord with the outer moraine record, dating to about 1844. LIA glacier extent is largely constrained by the geometry of the valley. Mountain sidewalls and adjacent glaciers constrain the width, while the slope starts to rise on the opposite side of the Icefields Parkway valley, at the site of the present-day visitor centre. The glacier terminus thickens and widens in the valley, but glacier length is limited to about 10.6 km. Hence, the LIA equilibrium area and length are less sensitive to different glaciological parameters than the modelled ice thickness and volume.

The LIA ice thickness and volume are not strongly sensitive to the amount of sliding, within the bounds of what is expected at Athabasca given the observations of Paterson and Raymond. A 50% decrease or increase in sliding from the reference model is associated with a 3% change in the glacier volume. Higher sliding rates give a thinner glacier.

Table 4. 3: Equilibrium reconstructions of Athabasca Glacier for different sliding speeds. The reference model is shown in bold, with v_s = 20 m/yr.

v_s (m/yr)	*L* (km)	*A* (km2)	*V* (km3)	*H* (m)
5	10.6	17.69	1.97	111.3
10	10.6	17.64	1.93	109.7
20	**10.6**	**17.6**	**1.87**	**106.4**
30	10.6	17.54	1.82	104
40	10.6	17.49	1.76	100.6
50	10.6	17.44	1.7	97.4
60	10.6	17.38	1.64	94.3
80	10.6	17.31	1.51	87.3
100	10.6	17.22	1.39	80.8

Table 4. 4: Equilibrium reconstructions of Athabasca Glacier for different mass balance gradients. The reference model is shown in bold, with β = 5.73 mm w.e. m^{-1}.

β (μμ/μ)	*L* (km)	*A* (km2)	*V* (km3)	*H* (m)
4.02	10.6	17.38	1.69	97.2
4.59	10.6	17.46	1.76	100.8
5.17	10.6	17.53	1.82	103.8
5.73	**10.6**	**17.6**	**1.87**	**106.4**
6.31	10.6	17.65	1.93	109.3
6.89	10.6	17.71	1.98	111.8
7.46	10.6	17.75	2.02	113.8
8.03	10.6	17.79	2.07	116.3

Results are also insensitive to the choice of mass balance gradient, with a 6% difference in ice volume for a 20% change in the balance gradient, between 4.59 and 6.89 mm w.e. m^{-1}. Average glacier thicknesses in this range vary from 101 to 112 m. Steeper balance gradients give greater accumulation on the upper plateau of the icefield, leading to a thicker glacier. The weak sensitivity is likely because the overall glacier mass balance is not strongly affected, as the ELA is fixed in these tests. However, the distribution of mass and the steepness of the equilibrium glacier are affected as a consequence of higher rates of ablation and accumulation in the cases with larger balance gradients.

Table 4. 5: Equilibrium reconstructions of Athabasca Glacier for different equilibrium line altitudes. The reference model has an ELA of 2640 m.

ELA (m)	***L* (km)**	***A* (km^2)**	***V* (km^3)**	**H (m)**
2500	10.6	17.86	2.07	115.9
2550	10.6	17.78	2.01	113
2600	10.6	17.69	1.94	109.7
2650	10.6	17.55	1.85	105.4
2700	10.6	17.39	1.76	101.2
2750	10.5	16.79	1.6	95.3
2800	9.6	15.59	1.38	88.5
2900	6.3	13.22	0.94	71.1
3000	3.3	10.81	0.47	43.5

The results are highly *sensitive to the equilibrium line altitude*, with values above 2750 m giving a glacier that is retracted relative to its known LIA terminus position. Below 2750 m, it is difficult to discriminate between different ELA scenarios, based on modelled ice area and length. Athabasca Glacier volume is relatively sensitive to this, with average ice thicknesses between 95 and 116 m for the range of plausible reconstructions (glacier volume differences of ±10%), for ELA values from 2750 to 2500 m.

Sensitivity to the effective viscosity of the ice is not significant compared to these parameters, as this value (i.e. Glen's flow law) is relatively well-constrained by past work at Athabasca Glacier. Overall, an estimate of uncertainty of ±10% seems reasonable for the LIA glacier reconstruction: V = 1.87 ± 0.2 km^3. This estimate is subject to structural uncertainty in the model, such as the assumption of a linear mass balance gradient, glacier model physics relative to a full stress solution, limitations of flowband vs. 3D ice dynamics, and uncertainties about the bed topography and the assumption of a parabolic valley cross-section.

For comparison, the present-day (2009) ice volume estimate is 1.01 km^3, a 46% reduction from the LIA volume. Ice area declined from 17.6 km^2 at the LIA to its present-day value of 14.6 km^2, a 17% reduction, and the glacier has thinned by about 35% since the LIA glacial maximum, from 106 to 69 m.

4.6. Transient Simulations of the Historical Athabasca Glacier Evolution

The numbers in Section 4.5., give an estimate of how ice volume has changed at Athabasca Glacier over the historical period, and the associated contributions to the Athabasca River. However, the model can also be run in transient mode to simulate the annual changes from the LIA to present. The glacier has retreated about 1.6 km from 1844 to present, an average terminus retreat rate of about 9 m yr^{-1}. At a horizontal model resolution of 50 m, I cannot simulate annual changes in the glacier terminus, but the general historical evolution of the glacier can be modelled.

Given the millennial proxy climate record that is available in the Rockies, it is possible to do a spinup simulation of the LIA glacier extent that does not assume equilibrium. That is, the model can be run from 1000 AD to present to track glacier advance and retreat through this period (subject to uncertainties in the climate and mass balance reconstruction, and limitations of the model). Figure 4.12 shows the result of this simulation with the default model parameters for the period 1650-2017, concentrating on the Little Ice Age. The mass balance forcing is plotted in 4.12a and the glacier area and volume are plotted in 4.12b. The final (2017) ice geometry is plotted in Figure 4.13. At least two things are of immediate interest in Figure 4.12. Most obvious is that the modelled LIA maximum extent of the Athabasca Glacier occurs through the period 1710-1740, followed by a moderate retreat and then a secondary maximum in the 1840s. The secondary maximum is in excellent accord with the geological record of the LIA limit for Athabasca Glacier, dated to 1844. Secondly, modelled changes in ice area lag glacier volume changes by one to two decades. This is consistent with climate (mass balance) inducing an immediate thinning or thickening, which takes time to propagate down-glacier into changes in glacier length or area.

A third, more subtle point is that the modelled present-day ice geometry differs from the remote-sensing and Farinotti-based estimates in some important ways. The mass balance forcing can be adjusted up or down to give a present-day reconstruction that is close to the observed ice area (14.5 km^2) and length (9 km). Even with such tuning, however, there are several differences in the ice thickness distribution compared with the Farinotti reconstruction.

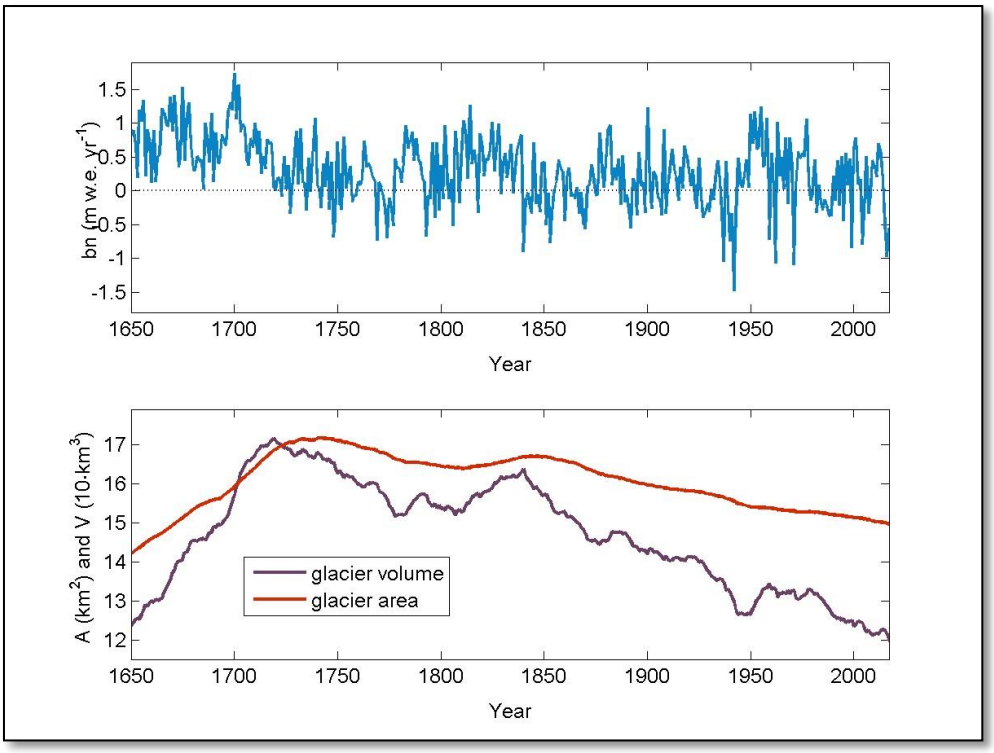

Figure 4. 12: Time series of modelled Athabasca Glacier evolution from 1650-2017. (a) Net annual mass balance (m w.e. yr^{-1}). (b) Annual glacier area (km^2) and volume ($10 \cdot km^3$).

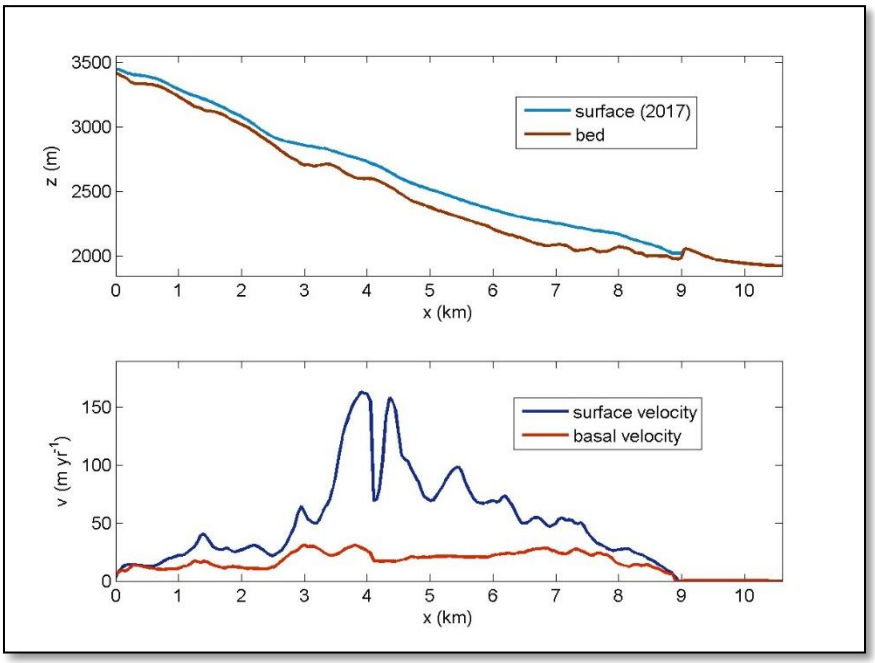

Figure 4. 13: Modelled Athabasca Glacier Centerline transects at the end of the transient simulation (calendar year 2017). (a) Bed (brown) and surface (blue) topography. (b) Surface (blue) and basal (red) ice velocity.

Figure 4.14 plots ice thickness profiles along the centreline of the modelled present-day (2017) glacier, along with thickness estimates for the equilibrium Little Ice Age reconstruction and from the Farinotti method. The associated ice thickness differences are shown in Figure 4.15. Upper portions of the glacier are similar in the Farinotti and modelled reconstructions, but from about 3 to 8 km along the flowline, the modelled reconstruction is 40 to 50 m thicker than the 2009 reference model. Below this, the modelled glacier terminus is thinner than the 2009 estimates, perhaps in association with the steady glacier thinning and retreat over the last three decades. It is difficult to assess whether these differences are an artefact of the structure of the model, or an indication that the Farinotti ice thickness estimates may be inappropriate.

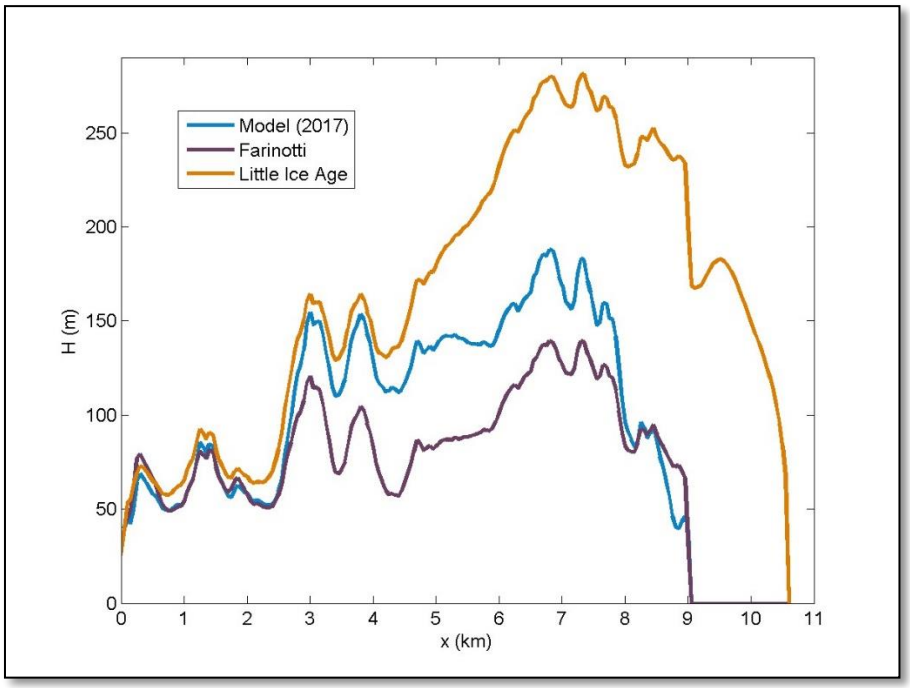

Figure 4. 14: Ice thickness along the centreline of Athabasca Glacier based on the modelled present-day (2017) estimates (blue), the remote-sensing/Farinotti-based reconstructions (dark purple) and for the LIA equilibrium reconstruction (orange).

The LIA equilibrium glacier is more than 150 m thicker than the two present-day reconstructions in the deglaciated terminus region, from 9-10.6 km. Most of the additional ice volume in the LIA is in the ablation zone of the glacier, for $x > 4$ km along the centreline. The strong transition at $x = 4$ km is associated with the shift from the upper icefield to the channelized outlet glacier.

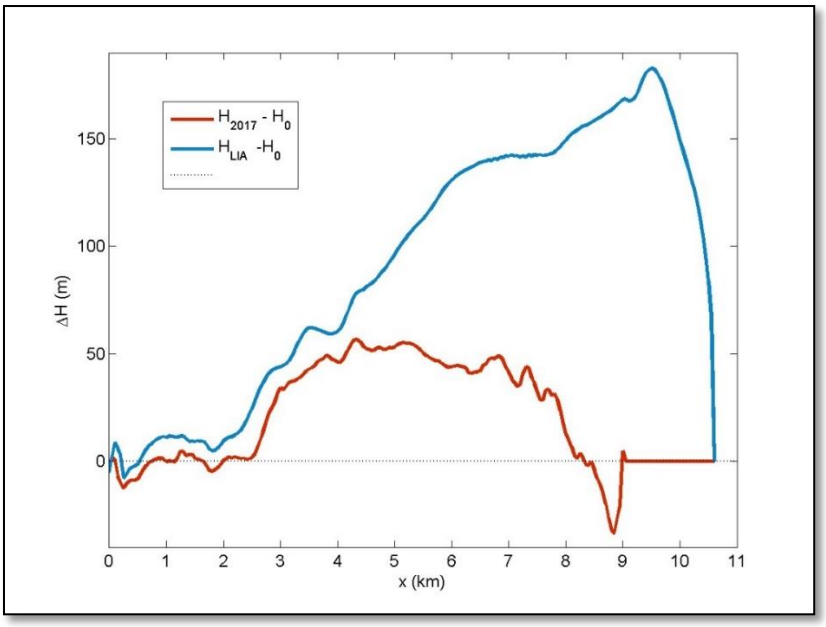

Figure 4. 15: Ice-thickness differences between the modelled present-day Athabasca Glacier (H_{2017}, red), the Little Ice Age equilibrium reconstruction (H_{LIA}, blue), and the remote-sensing/Farinotti-based reconstructions (H_0).

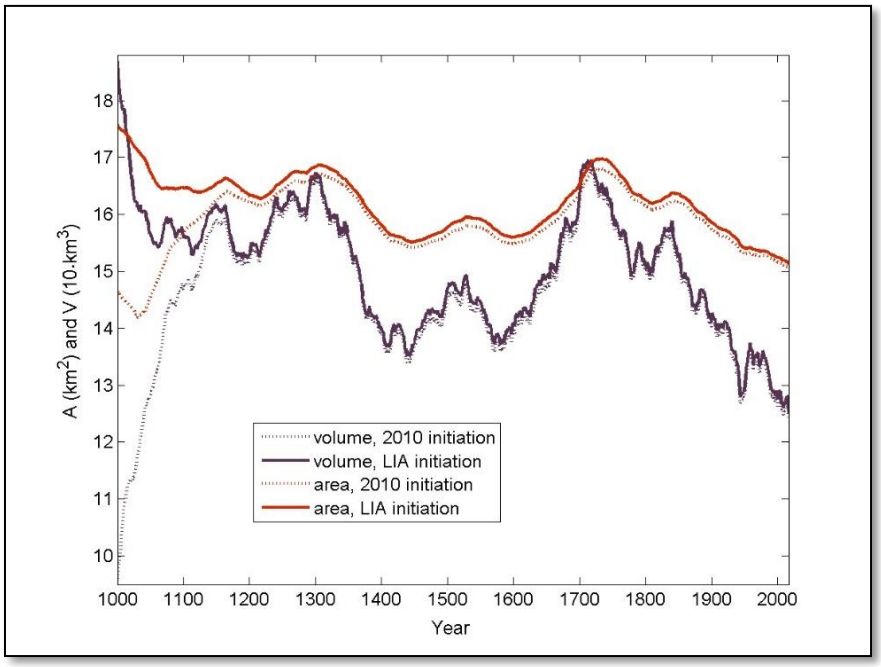

Figure 4. 16: Time series of modelled Athabasca Glacier evolution over the last millennium. Red lines show the glacier area (km^2) and dark purple lines plot glacier volume ($10 \cdot km^3$), with the dashed lines from the 2009 initial model and solid lines from the Little Ice Age spinup.

It is also important to consider the effects of initial conditions on the transient glacier simulation. Figure 4.16 shows the millennial simulation at Athabasca Glacier for two different initial conditions: (i) the LIA spinup simulation of Section 4.5 and (ii) the 2009 glacier geometry, with ice thickness estimates from the Farinotti method.

Climate mass balance forcing is the same in these two scenarios. It requires about 170 years of transient evolution before these simulations converge. After about 1200 AD the two simulations track each other closely, with slightly greater area and volume persisting for the LIA initial model.

Scientifically, it is interesting to note that four or five periods of glacial advance are predicted over the last millennium, at ~1150, 1300, 1550, 1720, and 1840. The maximum glacier extent is in the early 1700s, following a relatively strong recession between 1400 and 1600. The 20th century glacier retreat is stronger than this earlier recession, however. Another important point is that with the transient climate forcing, Athabasca Glacier does not reach an equilibrium in this millennial simulation. The maximum modelled ice extent, around 1720 AD, is less than that of the equilibrium LIA simulation.

Chapter 5: Discussion and Recommendation

5.1. Summary of Research

The purpose of this thesis was to develop a flowband model for glacier reconstructions in the Canadian Rockies, as a new modelling tool for examining glacier history and glacier response to climate change. As part of this process, I needed to map the present day (2009) extent of Athabasca Glacier in the Canadian Rockies, using a single SPOT 5 image and a digital elevation model (DEM) with the help of an ArcMap tool (ArcHydro). To develop a model for Athabasca Glacier mass balance, I examined the mass balance record of nearby Peyto Glacier. I apply the Peyto mass balance gradient to Athabasca and found that a bivariate model based on Jasper summer temperature and the winter PDO give a good reconstruction of interannual mass balance variability for the period 1966-2017. Based on tree-ring proxy data for summer temperature and the PDO, this mass-balance reconstruction was extended to the period 1000 AD to present. Using these forcings, a numerical flowband model was applied to simulate the changes in Athabasca Glacier over the last millennium.

In this final chapter, the primary aim is to discuss the conclusions obtained from the results of this thesis.

5.2. Evaluation of the method

The method that has been developed here has several merits over traditional methods. An automated method has been developed here for estimating the volume loss, based on flow-line modelling propounded by Nye. The newest inclusion in this modelling is the longitudinal stress and the basal sliding, which Nye considered to be negligible. In this method, the impact of valley morphology to glacier discharge is fully considered, including allowance for changing valley shape along the flowline. Based on the Farinotti et al. (2009) method, ice thickness has been calculated, which is an advanced form of the classical method. Each of these methods used in my modelling is physically based and simple to use, but is an advancement on conventional flowline modelling.

I chose methods in this thesis that are designed to make it most suitable for estimating glacier change over large glacier systems or multiple outlet glaciers on an icefield,

without needing 2D or 3D models that are more complex and may be inappropriate, given the lack of detailed knowledge of topographic and climate conditions.

I examined two methods of calculating ice thickness in this thesis, the classical method based on an inversion of the local ice surface slope and a method developed by Farinotti et al. (2010). These are similar but offer some flexibility in reconstructing centreline ice thickness from the surface digital elevation model (DEM). DEMs are now readily available through governmental and non-governmental agencies, and are good-quality sources of data for this type research work, where resolutions of order 25 to 100 m are appropriate to describe mountain glacier dynamics. The overall time for data collection is very much reduced with the easy availability of the DEM. Identification of the glacier central flowline was also possible through the ArcMap tool skeleton, after delineating the glacier boundary. The use of remote sensing image and GIS tools was also relatively straightforward and objective, particularly the use of ArcHydro tool to delineate the glacier flowshed. Remote sensing images make it easier to access the remote areas, and are also increasingly available.

One disadvantage of my approach is that it is difficult to automate. I had originally intended to develop a flowband model that could be applied to the whole Columbia Icefield or to other glaciers in the Rockies, but the datasets for ice geometry are mixed and it is not easy to generate the glacier flowline position, widths, and thicknesses automatically. This makes it difficult to model large ensembles of glaciers.

There are few errors in my approach too. The catchment area calculated by Tennant and Menounos is different from the one I have calculated in my study. This was simply because of the method that has been used in my research, which is using Arc Hydro tool for the delineation of the catchment area.

5.3. Evaluation of Results

Chapter 4 summarizes glacier characteristics measured and modelled using different methods, for the Little Ice Age maximum extent and for 2009. There are two main divisions of results: 1) estimating the LIA glacier extent, area, length, and volume using the spin-up simulations, and 2) transient simulations to study changes in Athabasca Glacier over the last millennium and compare the LIA extent with the present-day glacier extent, area, length, and volume.

The present-day (2009) glacier has an estimated volume of 1.0 km^3, but I do not have good error bounds on this estimate. Two different approaches to ice thickness reconstruction give similar ice thickness/volume estimates (within 10%), but the reality is not as accurate as this might indicate, due to structural uncertainties in the ice volume estimation. I have assumed a parabolic bed profile for the outlet glacier and a rectangular cross-section on the icefield plateau, and these idealized shapes may be far off; only the surface/flowband width is known with confidence. More importantly, the estimated present-day ice thickness seems too low compared to the observations of Paterson and Raymond. These observations are restricted to a few km of the outlet glacier and date to the 1960s, but they imply that present-day ice thicknesses in the outlet glacier should be 200-250 m, more than double the estimates from the slope- and Farinotti-based calculations. The glaciological model also wants to build thicker ice in the outlet glacier. This result speaks to a failure in the kinematic ice thickness estimates: some non-uniqueness in the estimates that are based on the surface slope. The Athabasca Glacier valley may be over-deepened, i.e., with a reverse bed slope due to centuries of erosion, without a surface expression of this. This may or may not be a problem on the icefield plateau. Overall, my present-day ice-volume value is probably a minimum estimate, and the actual ice volume may be up to 100% higher.

The LIA maximum extent of the glacier was determined using the terminal and lateral moraine as well as the vegetation trim lines, based on the SPOT5 imagery, with dates of the LIA maximum based on the findings of Luckman. The equilibrium (spin-up) simulations used the mapped LIA extent as a 'target'. The present day length is about 9 km, and the LIA length was 10.6 km, whereas the ice area declined from 17.6 km^2 to 14.6 km^2, from the LIA to present day.

In the spin-up simulations, for which all climatic conditions were held constant, the LIA ice volume is about 90% greater than at present-day: 1.87 ± 0.2 km^3, relative to the modern-day value of 1.0 km^3. The equilibrium ice volume is not very sensitive to the amount of sliding, changes in ice rheology, or the mass balance gradient, with changes of less than 10% for a wide range of plausible values. However, LIA reconstructions depend a great deal on the imposed cooling or the position of the ELA. The LIA ELA appears to have been close to 2650 m, based on the range of glacier reconstructions that

match the geologically-determined ice extent. The suite of acceptable experiments provides the basis for my error estimate of ±12%, but this again includes structural uncertainty associated with poor knowledge of the bedrock topography. Assuming substantially lower bed elevations in the outlet glacier valley, which is likely the case, the LIA glacier would also be much thicker. The estimated glacier volume loss of about 0.9 km^3 since the LIA may be the more robust result concerning ice volume.

The glacier thinned by about 35% since the LIA glacial maximum, from 106 to 69 m in the model reconstructions. These changes in glacier shape indicates that much of the ice loss in the past 140 years is due to thinning, but there are also important losses in volume associated with decreasing area and glacier recession. The glacier has retreated at a rate of about 9 m/yr from 1844 to present.

After reconstructing the mass balance for Athabasca glacier with PDO proxy and temperature tree ring data, it was seen that there were periods of advances and retreats of the glacier itself. For the Athabasca glacier. Heusser (1956) presented the evidence of first advance in 1714 A. D., whereas Luckman (1988) presented with details and claimed that 1840 witnessed the greatest advancement of the Athabasca glacier. Along with this Luckman (2000) mentioned about the sequences of glacial advances and retreats in the Canadian Rockies, which can be related with my 1000-year Athabasca's mass balance reconstruction. During 12th and 13th century, early 18th century and throughout 19th century witnessed glacial advances. This is mostly parallel with my graph showing reconstructed mass balance of the Athabasca glacier. As there is no proper data or studies done on this, it is hard to say the actual percentage of volume loss for the Athabasca glacier.

Since the LIA time period, the glacier has experienced a predominantly negative trend in mass balance which has been manifested in recession of the ice margin and a decrease in total glaciated area. One of the many likely causes for thus is an increase in summer temperature, as observed in Jasper and supported by the tree-ring temperature reconstruction data proximal to the icefield.

5.4. Recommendations for Future Research

Future research in the area should continue to add more precise techniques to collect data concerning subglacial bedrock topography in mountain glaciers and also to utilize high-resolution remote sensing and DEM technology in glacier studies. With new developments in these different technologies constantly becoming available, glaciologists should attempt to keep informed. While these new techniques should not be used simply for the sake of being current or updated, it is important to realize how they can be applied to the specific fields of glacier studies and mass balance study.

In this research, we have focused on the method development and tested it with only a single glacier. A next step would be to assess its applicability for a set of glaciers, in order to estimate their thicknesses and volumes. Also, it would be valuable to compare the performance of the methods with more complete 2D or 3D models of glacier dynamics. The flowband method shows promise for efficient numerical solutions that have the capability of including 3d flow influences and higher-order ice stresses. This model can be calibrated against historical glacier extent to improve projections of future change, which would be a logical next step in my work.

There is a great deal of speculations on the future of the Earth's climate, but a number of facts stands out. Within the past years a huge number of extreme weather events occurred which evidently have modified the climate surroundings. These, again affected the glaciers worldwide, and made them to lose their volume. These increased level of climatic disturbances are affected by greenhouse gas emissions and global warming (Mooney, et al., 1993). Oerlemans (1992, 1994) noted that glacier fluctuations already provide the most important evidence of post-industrial global warming. As we progress through the 21st century, the study of the glacier fluctuations and changes in mass, volume will continue to be documented in order to understand the relationships between human and environment, and better quantitative tools are needed to understand how glacier changes will affect global sea level and regional water resources.

References

Adhikari, S., and Marshall, S. J. 2011. Improvements to shear-deformational models of glacier dynamics through a longitudinal stress factor. *Journal of Glaciology.* Vol. 57 (206). 1003-1016.

Adhikari, S., and Marshall, S. J. 2012. Parameterization of lateral drag in flowline models of glacier dynamics. *Journal of Glaciology*. Vol. 58 (212). 1119-1132.

Ahlmann, H. W. 1953. *Glacier Variations and Climatic Fluctuations.* American Geographical Society., Bowman memorial Lectures, Series Three, 51 pages.

AntarcticGlaciers.org, ND. *Glaciers and Climate.* http://www.antarcticglaciers.org/glaciers-and-climate/ Accessed on 2-2-2017.

Arendt, A. A., Echelmeyer, K. A., Harrison, W. D., Lingle, C. S., and Valentine, V. B. 2002. Rapid wastage of Alaska glaciers and their contribution to rising sea level. *Science.* Vol. 297. 382-386.

Bahr, D. B., Meier, M. F., and Peckham, S. D. 1997. The physical basis of glacier volume-area scaling. *Journal of Geophysical Research.* Vol. 102 (B9). 20,355-20,362.

Bahr, D. B., Pfeffer, W. T., and Kaser, G. 2015. A review of volume-area scaling of glaciers. *Review of Geophysics.* Vol. 53. 95-140.

Benn, D. I., and Evans, D. J. A. 1998. *Glaciers and Glaciation.* Arnold Publishers, London. 734 pages.

Biondi, F., Gershunov, A., and Cayan, D. R. 2001. North Pacific decadal climate variability since 1661. *American Meteorological Society.* Vol. 14. 5-10.

Bitz, C. M. and Battissti, D. S. 1999. Interannual to decadal variability in climate and the glacier mass balance in Washington, Western Canada, and Alaska. *Journal of Climate*. American Meteorological Society. Vol. 12. 3181-3196.

Bjornsson, H., Aoalgeirsdottir, G., Guomundsson, S., Johannwsson, T., Sigurdsson, O., and Palsson, F. 2006. Climate change response of Vatnajokull, Hofsjokull and Langjokull ice caps, Iceland. *In: European Conference on Impacts of Climate Change on Renewable Energy Sources. Reykjavik* June 5-9, Iceland.

Bolch, T., Menounos, B., and Wheate, R. 2010. Landsat-based inventory of glaciers in western Canada, 1985-2005. *Remote Sensing of Environment.* Vol. 114. 127-137.

Bonsal, B. R., Shabbar, A., and Higuchi, K. 2001. Impacts of low frequency variability modes on Canadian water temperature. *International Journal of Climatology.* Vol. 21. 95-108.

Budd, W. F., and Jenssen, D. 1971. Numerical modelling of glacier systems. *Snow and Ice symposium (Proceedings of the Moscow Symposium): IAHS-AISH Publ.* No. 104. 257- 291.

Chen, J., and Ohmura, A. 1990. Estimation of alpine glacier water resources and their change since the 1840s. *Hydrology in Mountainous regions.* Proceedings of two Lausanne Symposia. Publ. no, 193. 127-135.

Cogley, J. G. 2009. A more complete version of the World Glacier Inventory. *Annals of Glaciology*. Vol. 50 (53). 32-38.

Cogley, J. G., Hock, R., Rasmussen, B., Arendt, A., Bauder, A., Braithwaite, R. J., Jansson, P., Kaser, G., Moller, M., Nicholson, L., and Zemp., M. 2011. *Glossary of Glacier Mass Balance and related Terms.* Paris: IHP-VII Technical Documents in Hydrology No. 86, IACS Contribution No. 2, UNESCO-IHP. 124.

Cuffey, K. M. and Paterson, W. S. B. 2010. *The Physics of Glacier.* 4th Edition. Elsevier. 704 pages.

Davis, W. M. 1900. Glacial erosion in France, Switzerland, and Norway. *Proceedings of Boston Soc. Nat. Hist.* Vol. 29. 273-322.

Demuth, M., Pinard, V., Pietroniro, A., Luckman, B., Hopkinson, C., Dornes, P. and Comeau, L. 2008. Recent and past-century variations in the glcier resources of the Canadian Rocky Mountains: Nelson River System. *Terra Glacialis.* Vol. 11. 27-52.

Duval, P., Montagnat, M., Grennerat, F., Weiss, J., Meyssonnier, J., and Philip, A. 2010. Creep and plasticity of glacier ice: a material science perspective. *Journal of glaciology*. Vol. 56 (200). 1059-1068.

Dyurgerov, M., and Meier, M. F. 1997. Year-to-Year fluctuations of global mass balance of small glaciers and their contribution to sea-level changes. *Arctic and Alpine Research.* Vol. 29 (4). 392-402.

Dyurgerov, M., and Meier, M. F. 2000. Twentieth century climate change: evidence from small glaciers. *Proceedings of the National Academy of Sciences.* Vol. 97 (4). 1406-1411.

Dyurgerov, M. 2002. Glacier Mass Balance and Regime: Data of Measurements and Analysis. Occasional Paper No. 55. *INSTAAR, University of Colorado at Boulder, Colorado.* Institute of Arctic and Alpine research, University of Colorado, Boulder.

Dyurgerov, M., and Meier, M. F. 2005. Glaciers and the changing Earth system: A 2004 Snapshot. *INSTAAR, University of Colorado at Boulder, Colorado.* Occasional Paper No. 58. Institute of Arctic and Alpine Research, University of Colorado.

Farinotti, D., Huss, M., Bauder, A., Funk, M., and Truffer, M. 2009. A method to estimate the ice volume and ice-thickness distribution of alpine glaciers. *Journal of Glaciology*, Vol. 55 (191). 422-430.

Farinotti, D., Huss, M., Bauder, A., and Funk, M. 2009. An estimate of the glacier ice volume in the Swiss Alps. *Global and Planetary Change.* Vol. 68. 225-231.

Farinotti, D. 2010. *Simple methods for inferring glacier ice-thickness and snow-accumulation distribution*. Ph.D. dissertation. *ETH Zurich,* Switzerland.

Fleming, S. W., and Whitfield, P. H. 2010. Spatiotemporal mapping of ENSO and PDO surface meteorological signals in British Columbia, Yukon, and southeast Alaska. *Atmosphere- Ocean.* Vol. 48 (2). 122-131.

Frey, H, Machguth, H., Huss, M., Huggel, C., Bajracharya, S., Bolch, T., Kulkarni, A., Linsbauer, A., Salzmann, N., and Stoffel, M. 2014. Estimating the volume of glaciers in the Himalayan-Karakoram region using different methods. *The Cryosphere.* Vol. 8. 2312-2333.

Gershunov, A., and Barnett, T. P. 1998. Interdecadal modulation of ENSO teleconnections. *Bulletin of the American Meteorological Society.* 2715-2726.

Glen, J. W. 1952. Experiments on the deformation of ice. *Journal of Glaciology.* Vol. 2 (12). 111-114.

Glen, J. W. 1955. The creep of polycrystalline ice. *Proceedings of the Royal Society,* Series A. Vol. 228. (1175). 519-538.

Glen, J. W. 1958. The flow law of ice. A discussion of the assumptions made in glacier theory, their experimental foundations and consequences. *Symposium Chamonix, Int. Asso.of Sci. Hydrol./ Int. Union Geod. Geophys., IASH Publ*. Vol. 47. 171-183.

Greuell, W. 1992. Hintereisferner, Austria: mass-balance reconstruction and numerical modelling of the historical length variations. *Journal of Glaciology.* Vol. 38 (129). 233-244.

Grove, J. M. 1988. *The little ice age*. London. Routledge. 498 pages.

Haeberli, W, Cihlar, J., and Barry, R. 2000. Glacier monitoring within the global climate observing system. *Annals of Glaciology.* Vol 31. 241-246.

Haeberli, W., and Holzhauser, H. 2003. Alpine glacier mass changes during the past two millennia. *Pages News.* Vol 11 (1). 13-15.

Hamlet, A. F, Mote, P.W., Clark, M. P. and Lettenmaier, D. P. 2005. Effects of temperature and precipitation variability on snowpack trends in the western United States. *American Meteorological Society.* Vol 18 (21). 4545-4561.

Hare, S. R. 1996. Low frequency climate variability and salmon production. Ph.D. Dissertation. *University of Washington, Seattle, WA.* 306 pages.

Heid, T., and Ka¨ab, A. 2012. Repeat optical satellite images reveal widespread and long term decrease in land-terminating glacier speeds. *The Cryosphere,* Vol. 6. 467–478.

Heusser, C. J. 1956. Postglacial environments in the Canadian Rocky Mountains. *Ecological Monograohs.* Vol 26 (4). 264-302.

Hirose, J. M. R. and Marshall, S. J. 2013. Glacier meltwater contributions and glaciometeorological regime of the Illecillewaet River, British Columbia, Canada. *Atmosphere-Ocean*. 1-20.

Hock, R. 2010. Glacier Mass Balance. *Handout from Summer School in Glaciology*. Fairbanks/McCarthy 7-17 June.

Hubbard, A., Blatter, H., Nienow, P., Mair, D., and Hubbard, B. 1998. Comparison of a three-dimensional model for glacier flow with field data from Haut glacier d'Arolla, Swizerland. *Journal of Glaciology,* Vol. 44(147). 368-378.

Huss, M., Farinotti, D., Bauder, A., and Funk, M. 2008. Modelling runoff from highly glaciarized alpine drainage basins in a changing climate. *Hydrological Processes*. Vol. 22 (19). 3888-3902.

Huss, M., and Farinotti, D. 2012. Distributed ice thickness and volume of all glaciers around the globe. *Journal of Geophysical Research.* Vol. 117.

Huybrechts, Ph., Nooze, P. de., and Decleir, H. 1989. Numerical modelling of glacier d'Argentiere and its historic front variations. In Oerlemans, J. (ed.). *Glacier Fluctuations and Climate Change.* Kluwar Academic Publishers, London. 353-371.

Intergovernmental Panel on Climate Change (IPCC). 2014. Climate change 2014: Impacts, Adaptation, and vulnerability. Part B: Regional aspects. *Contribution of*

Working Group II to the Fifth Assessment Report of the Intergovernmental Panel on climate Change (Barros, V.R., Field, C.B, Donken, D.J., Mastrandrea, M.D., Mach, K.J., Bilir, T.E., Chatterjee, M., Ebi, K. L., Estranda, Y.D., Genova, R.C., Girma, B., Kissel, E. S., Levy, A. N., MacCracken, S., Mastrandrea, P. R.,and White, L. L. (eds.)). Cambridge University Press, Cambridge, United Kingdom and New York, NY, USA. 688.

Kaab, A., Huggel,C., Paul, F., Wessels, R., Raup, B., Kieffer, H., and Kargel, J. 2002. Glacier monitoring from ASTER Imagery: Accuracy and Applications. *Proceedings of EARSeL-LISSIG-Workshop Observing our Cryosphere from Space, Bern*. 43-53.

Kienholz, C., Rich, J. L., Arendt, A. A., and Hock, R. 2014. A new method for deriving glacier centerlines applied to glaciers in Alaska and northwest Canada. *The Cryosphere.* Vol. 8. 503-519.

Kite, G. W., and Reid, I. A. 1977. Volumetric change of the Athabasca glacier over the last 100 years. *Journal of Hydrology.* Vol 32. 279-294.

Kucera, R. E. 1978. *Probing the Athabasca Glacier*. Evergreen Press, Vancouver. 32 pages.

Kucera, R. E. 1981. *Exploring the Columbia Icefield*. Canmore, Alberta, High Country Press. 64 pages.

Kucera, R. E., and Henock, W. E. S. 1978. Glacier and Landform features in the Columbia Icefield Area, Banff and Jasper National Parks, Alberta, Calgary, Canada. Glaciology division Inland Waters Directorate, Environment Canada.

Leclercq, P. W., and Oerlemans, J. 2012. Global and hemispheric temperature reconstruction from glacier length fluctuations. *Climate dynamics.* Vol. 38. 1065-1079.

Letreguilly, A., 1988. Relation between the mass balance of western Canadian mountain glaciers and meteorological data. *Journal of Glaciology.* Vol- 34 (116). 11-18.

Li, H., Li, Z., Zhang, M., and Li, W. 2011. An improved method based on shallow ice approximation to calculate ice thickness along flow-line and volume of mountain glaciers. *Journal of earth Science.* Vol. 22 (4). 441-448.

Lillesand, T. M., Kiefer, R. M., and Chipman, J. W. 2004. *Remote Sensing and Image Interpretation.* Fifth Edition. Wiley.

Longley, P. A., Goodchild, M. F., Maguire, D. J., and Rhind, D. W. 2005. *Geographical information systems: Principles, Techniques, Management and Applications*. 2nd Edition. Wiley. 404 pages.

Luckman, B. H. and Osborn, G. D. 1979. Holocene glacier fluctuations in the middle Canadian Rocky Mountains. *Quaternary Research.* Vol. 11. 52-77.

Luckman, B. H., 1986. Reconstruction of Little Ice Age Events in the Canadian Rocky Mountains. *Geographie Physique et Quaternaire*. Vol. 40 (1). 17-28.

Luckman, B. H. 1988. Dating the moraines and recession of Athabasca and Dome Glaciers, Alberta, Canada. *Arctic and Alpine Research.* Vol. 20 (1). 40-54.

Luckman, B. H., Holdsworth, G., and Osborn, G. D. 1993. Neoglacial glacier fluctuations in the Canadian Rockies. *Quaternary Research.* Vol. 39. 144-153.

Luckman, B. H., Briffa, K. R., Jones, P. D., and Schweingruber, F. H. 1997. Tree-ring based reconstruction of summer temperatures at the Columbia Icefield, Alberta, Canada, AD 1073-1983. *The Holocene.* Vol. 7 (4), 375-389.

Luckman, B. H., Kavanagh, T. A., Craig, I., and Scott, R. 1999. Earliest photograph of Athabasca and Dome glaciers, Alberta. *Geographic physique et Quaternaire*, Vol. 53 (3). 401-405.

Luckman, B. 2000. The Little Ice Age in the Canadian Rockies. *Geomorphology.* Vol. 32. 357-384.

Luckman, B. H., and Wilson, R. J. S. 2006. Canadian Rockies Summer Temperature Reconstruction. *IGBP PAGES/World Data Center for Paleoclimatology. Data Contribution series # 2006-011.* NOAA/NCDC Paleoclimatology Program, Boulder CO, USA. ftp://ftp.ncdc.noaa.gov/pub/data/paleo/treering/reconstructions/canada/icefields-summer-maxt.txt

MacDonald, G. M., and Case, R. A. 2005. Variations in the Pacific Decadal Oscillation over the past millennium. *Geophysical Research Letters.* Vol. 32. L08703. ftp://ftp.ncdc.noaa.gov/pub/data/paleo/treering/reconstructions/pdo-macdonald2005.txt

Mantua, N. J., Hare, S. R., Zhang, Y., Wallace, J. M., and Francis, R. C. 1997. A Pacific interdecadal climate oscillation with impacts on salmon production. *Bulletin of the American Meteorological Society.* 1069-1080.

Mantua, N. J., and Hare, S, R. 2002. The Pacific Decadal Oscillation. *Journal of Oceanography.* Vol. 58. 35-44.

Marshall, S. J., and White, E. 2010. Alberta glacier inventory and ice volume estimation. *Crowfoot Ice Research and Consulting.* 54 pages.

Marshall, S. J. 2011. *The Cryosphere.* Princeton Primers in Climate. 304 pages.

Marshall, S. J., White, E. C., Demuth, M. N., Bolch, T, Wheate, R., Menounos, B., Beedle M. J., and Shea, J. M. 2011. Glacier water resources on the eastern slopes of the Canadian Rocky Mountains. *Canadian Water Resources Journal.* Vol. 36 (2). 109-134.

Marshall, S. J. 2014. Meltwater run-off from Haig Glacier, Canadian Rocky Mountains, 2002-2013. *Hydrological Earth System Science*. Vol. 18. 5181-5200.

Marzeion, B., Cogley, J. G., Richter, K., and Parkes, D. 2014. Attribution of global glacier mass loss to anthropogenic and natural causes. *Science.* Vol. 345 (6199). 919-921.

Matthes, F. E. 1939. Report of the committee on glaciers. *Transactions of the American Geophysical Union.* Vol. 20. 518-523.

Mayer, C., and Siegert, M. J. 2000. Numerical modelling of ice-sheet dynamics across the Vostok subglacial lake, central East Antarctica. *Journal of Glaciology.* Vol. 46 (153). 197-205.

McCabe, G. J., and Fountain, A. G. 1995. Relations between atmospheric circulation and mass balance of South Cascade glacier, Washington, U. S. A. *INSTAAR, University of Colorado.* Vol. 27 (3). 226-233.

McGee, W. J. 1883. Glacial canons. *The Journal of Geology.* Vol. 2 (4). 350-364.

Melkonian, A.K., Willis, M. J., Pritchard, M. E., Rivera, A., Bown, F., and. Bernstein, S. A. Satellite-derived volume loss rates and glacier speeds for the Cordillera Darwin Icefield, Chile. *The Cryosphere*. Vol. 7. 823–839.

Merriam-Webster. 2018. *Definition of Conservation of Mass*. https://www.merriam-webster.com/dictionary/conservation%20of%20mass

Molg, T. and Hardy, D. R. 2004. Ablation and associated energy balance of a horizontal glacier surface on Kilimanjaro. *Journal of Geophysical Research.* Vol. 109.

Mote, P. W. 2003. Trends in snow water equivalent in the Pacific Northwest and their climatic causes. *Geophysical Research Letters*. Vol. 30 (12). 1601-1605.

Mooney, H. A., Fuentes, E. R and Kronberg, B. I. 1993. Earth system responses to global change. Contrasts between North and South America. *Academic Press, Inc.* Toronto, Canada.

National Post. 2016. *Breathtaking views: Take a snowcoach ride onto the Columbia Icefield's Athabasca glacier.* Postmedia Network Inc. http://nationalpost.com/travel/breathtaking-views-take-a-snowcoach-ride-onto-the-columbia-icefields-athabasca-glacier Accessed on 1.5.2017.

Nye, J. F. 1952. The mechanics of glacier flow. *Journal of Glaciology*. Vol. 2 (12). 82-93.

Nye, J. F. 1957. The distribution of stress and velocity in glaciers and ice-sheets. *Proceedings of the Royal Society, Series A.* Vol. 239. (1216). 113-133.

Nye, J. F. 1965. The flow of a glacier in a channel of rectangular, elliptic or parabolic cross-section. *Journal of Glaciology.* Vol. 5 (41). 661-690.

Nuth, C., Kohler, J., König, M., Deschwanden, A. von, Hagen, J. O., Kääb, A., Moholdt, G. and Pettersson, R. 2013. Decadal changes from a multi-temporal glacier inventory of Svalbard. *The Cryosphere.* Vol. 7. 1603–1621.

Oerlemans, J. 1986. Glaciers as indicators of a carbon dioxide warming. *Nature*. Vol. 320. 607-609.

Oerlemans, J. 1989. A projection of future sea level. *Climatic Change*. Vol 15. 151-174.

Oerlemans, J., and Fortuin, J. P. F. 1992. Sensitivity of glaciers and small ice caps to greenhouse warming. *Science.* Vol. 258. 115-117.

Oerlemans, J. 1994. Quantifying global warming from the retreat of glaciers. *Science.* Vol. 243-245.

Oerlemans, J. 1997a. Climate sensitivity of Franz Josef glacier, New Zealand, as revealed by numerical modeling. *Arctic and Alpine Research.* Vol. 29 (2). 233-239.

Oerlemans, J. 1997b. A flowline model for Nigardsbreen, Norway: projection of future glacier length based on dynamic calibration with the historic record. *Annals of Glaciology.* Vol. 24. 382-389.

Oerlemans, J. Anderson, B., Hubbard., and Huybrechts. Ph., 1998. Modelling the response of glaciers to climate warming. *Climate dynamics*. Vol 14. 267-274.

Oerlemans, J. 2001. *Glaciers and Climate Change.* A. A. Balkema Publishers, Rotterdam. 148 pages.

Oerlemans, J. 2005. Extracting a climate signal from 169 glacier records. *Science*. Vol. 308 (29).

Oerlemans, J., Giesen, R. H., and Broeke, M. R. V. D. 2009. Retreating alpine glaciers: increased melt rates due to accumulation of dust (Vadret da Morteratsch, Switzerland). *Journal of Glaciology.* Vol. 55 (192). 729-736.

Osborn, G. and Luckman, B. 1988. Holocene glacier fluctuations in the Canadian Cordillera (Alberta and British Columbia). *Quaternary Science Review*. Vol. 7 (2). 115-128.

Osborn, G. D., Robinson, B. J., and Luckman, B. H. 2001. Holocene and latest Pleistocene fluctuations of Stutfield glacier, Canadian Rockies. *Canadian Journal of Earth Science.* Vol. 38. 1141-1155.

Paterson, W. S. B and Savage, J. C. 1963a. Geometry and movement of the Athabasca glacier. *Journal of Geophysical Research.* Vol. 68 (15). 4513-4520.

Paterson, W. S. B and Savage, J. C. 1963b. Measurements on Athabasca Glacier relating to the flow law of ice. *Journal of Geophysical Research*. Vol. 68 (15). 4537-4543.

Paterson, W. S. B. 1964. Variations in velocity of Athabasca glacier with time. *Journal of Glaciology.* Vol. 5 (39). 277 – 285.

Paterson, W. S. B. 1970. The sliding velocity of Athabasca Glacier, Canada. *Journal of Glaciology.* Vol. 9 (55). 55-63.

Paterson, W. S. B. 1971. Temperature measurements in Athabasca glacier, Alberta, Canada. *Journal of Glaciology.* Vol. 10 (60). 339-349.

Paterson, W. S. B. 1972. Temperature distribution in the upper layers of the ablation area of Athabasca glacier, Alberta, Canada. *Journal of Glaciology.* Vol. 11 (61). 31-41.

Paterson, W. S. B. 1981. *The Physics of Glacier.* 2nd edition. Pergamon International Library of science, technology, engineering and social studies. 380 pages.

Pattyn, F. 2003. A new three-dimensional higher order thermomechanical ice sheet model: Basic sensitivity, ice stream development, and ice flow across subglacial lakes. *Journal of Geophysical Research*. Vol. 108 (B8).

Pellikka, P. K. E. and Rees, W. G. 2010. *Remote Sensing of Glaciers: Techniques for Topographic, spatial and thematic Mapping of Glaciers.* CRC Press/Taylor & Francis. 340 pages.

Pfeffer, W. T., Arendt, A. A., Bliss, A., Bolch, T., Cogley, J. G., Gardner, A.S., Hagen, J., Hock, R., Kaser, G., Kienholz, C., Miles, E. S., Moholdt, G., Molg, N., Paul, F., Radic, V., Rastner, P., Raup, B. H., Rich, J., and Sharp, M. J. 2014. The Randolph Glacier Inventory: a globally complete inventory of glaciers. *Journal of Glaciology.* Vol. 60 (221). 537- 552.

PhysicalGeography.net 2014. Introduction to the Lithosphere. *Glacial Processes*. http://www.physicalgeography.net/fundamentals/10ae.html Accessed on 5-2-2017.

Plummer, M. A., and Phillips, F. M. A 2-D numerical model of snow/ice energy balance and ice flow for paleoclimatic interpretation of glacial geographic features. *Quaternary Science Reviews*. Vol. 22 (14). 1389-1406.

Porter, S. C. and Denton, G. H. 1967. Chronology of neoglciation in the North American cordillera. *American Journal of Science*. Vol. 265. 177-210.

Radic, V., Hock, R., and Oerlemans, J. 2007. Volume-area scaling vs. flowline modelling in glacier volume projections. *Annals of Glaciology.* Vol. 46. 234-240.

Radic, V., and Hock, R. 2010. Regional and global volumes of glaciers derived from statistical upscaling of glacier inventory data. *Journal of Geophysical Research.* Vol. 115.

Radic, V, and Hock, R. 2011. Regionally differentiated contribution of mountain glaciers and ice caps to future sea-level rise. *Nature Geoscience*. Vol. 4. 91-94.

Raymond, C. F. 1971. Flow in a transverse section of Athabasca glacier, Alberta, Canada. *Journal of Glaciology.* Vol. 10 (58). 55-84.

Rodenhuis, D. R., Bennett, K. E., Werner, A. T., Murdock, T. Q., and Bronaugh, D. 2007. Hydro-climatology and future climate impacts in British Columbia. *Pacific Climate Impacts Consortium*, University of Victoria, Victoria BC. 132 pages.

Rood, S. B., Samuelson, G. M., Braatne, J. H., Gourley, C. R., Hughes, F. MR., and Mohoney, J. M. 2005. Managing river flows to restore floodplain forests. *Front Ecological Environment.* Vol. 3 (4). 193-201.

Savage, J. C., and Paterson, W. S. B. 1963. Borehole measurements in the Athabasca glacier. *Journal of Geophysical Research.* Vol. 68 (15). 4521-4536.

Shabbar, A., and Khandekar, M. 1996. The impact of El-Nino-Southern Oscillation on the temperature field over Canada: Research note, A*tmosphere-Ocean.* Vol. 34 (2). 401-416.

Shabbar, A., Bonsal, B., and Khandekar, M. 1997. Canadian Precipitation patterns associated with the Southern Oscillation. *Journal of Climate.* Vol. 10. 3016-3027.

Sharp, R. P. 1960. *Glaciers*. Condon Lectures. University of Oregon Books. Oregon state system of higher education. Eugene, Oregon, 1960.

Shea, J. M., Anslow, F. S. and Marshall, S. J. 2005. Hydrometeorological relationships on Haig Glacier, Alberta, Canada. *Annals of Glaciology*. Vol. 40. 52-60.

Shea, J. M. and Marshall, S. J. 2007. Atmospheric flow indices, regional climate, and glacier mass balance in the Canadian Rocky Mountains. *International Journal of Climatology.* Vol. 27. 233-247.

Sugiyama, S., Bauder, A., Zahno, C., and Funk, M. 2007. Evolution of Rhonegletscher, Switzerland, over the past 125 years and in the future: application of an improved flowline model. *Annals of Glaciology*. Vol. 46. 268-274.

Svensson, H. 1959. Is the cross-section of a glacial valley a parabola? *Journal of Glaciology.* Vol. 3 (25). 362-363.

Stutfield, H. E. M., and Collie, N. F. 1903. *Climbs and Explorations in the Canadian Rockies.* Mountian Classics Collection. Rocky Mountain Books Ltd.

Tennant, C., Menounos, B., Ainslie, B., Shea, J., and Jackson, P. 2012. Comparison of modeled and geodetically-derived glacier mass balance for Tiedemann and Klinaklini glaciers, southern coast Mountains, British Columbia, Canada. *Global and Planetary Change.* Vol. 82. 74-85.

Tennant, C., and Menounos, B. 2013. Glacier change of the Columbia Icefield, Canadian Rocky Mountains, 1919-2009. *Journal of Glaciology.* Vol. 59 (216). 671-686.

Vaughan, D.G., Comiso, J.C., Allison, I., Carrasco, J., Kaser, G., Kwok, R., Mote, P., Murray, T., Paul, F., Ren, J., Rignot, E., Solomina, O., Steffen, K. and Zhang. T. 2013. Observations: Cryosphere. In: Climate Change 2013: *The Physical Science Basis. Contribution of Working Group I to the Fifth Assessment Report of the*

Intergovernmental Panel on Climate Change. Cambridge University Press, Cambridge, United Kingdom and New York, NY, USA.

Waddington, E. D. 1981. *Accurate modelling of glacier flow*. Ph.D dissertation. University of British Columbia Library, Vancouver. https://open.library.ubc.ca/cIRcle/collections/ubctheses/831/items/1.0052458

Weertman, J. 1957. On the sliding of glaciers. *Journal of Glaciology.* Vol. 3 (21). 33-38.

WGMS (World Glacier Monitoring Service), 2012. *Fluctuations of Glaciers 2005-2010*. Zemp, X., Frey, M., Gartner-Roer, I., Nussbaumer, S. U., Hoelzle, M., Paul, F, and Haeberli, W. (eds.), Vol. 10. ICSU (WDS)/IUGG(IACS)/UNEP/UNESCO/WMO. Zurich, Switzerland. 336 pages.

WGMS (World Glacier Monitoring Service), 2013. *Glacier Mass Balance Bulletin No. 12 (2010-2011)*. Zemp, M., Nussbaumer, S. U., Naegeli, K., Gartner-Roer, I., Paul, F., Hoelzle, M., and Haeberli, W. (eds), ICSU(WDS)/IUGG(IACS)/UNEP/UNESCO/WMO, *World Glacier Monitoring Service*, Zurich, Switzerland. 106 pages.

Wiscombe, W. J. and Warren, S. G. 1980. A model for the spectral albedo of snow. I: Pure snow, *Journal of Atmospheric Science*. Vol.37. 2712-2733.

Whitfield, P. H., Moore, R. D. Fleming, S. W., and Zawadzki, A. 2010. Pacific Decadal Oscillation and the hydroclimatology of Western Canada-review and prospects. *Canadian Water Resources Journal.* Vol. 35(1). 1-28.

Zhang, Y, Wallace, J., and Battistti, D. 1996. ENSO-like interdecadal variability: 1900-93. *Journal of Climate.* Vol. 10. 1004- 1020.

Zhang, X., Vincent, L., Hogg, W., and Niitsoo, A. 2000. Temperature and precipitation trends in Canada during the 20th century. *Atmosphere-Ocean*. Vol. 38 (3). 395-429.

Zhang, T., Xiao, C., Colgan, W., Qin, X., Du, W., Sun, W., Liu, Y., and Ding, M. 2013. Observed and modelled ice temperature and velocity along the main flowline of East Rongbuk glacier, Qomolangma (Mount Everest), Himalaya. *Journal of Glaciology*. Vol. 59 (215). 438-448.